

Solar Powered Thermoelectric Distillation System

A thesis submitted to Cardiff University in the candidature for the degree of

Doctor of Philosophy

By

Hayder Sami Saleh Al-Madhhachi

B.Sc., PG Dip., M.Sc.

Institute of Energy
School of Engineering
Cardiff University
December 2017



Summary

An efficient thermoelectric distillation system was designed, constructed and tested. The unique aspect of this design is to use the waste heat from the hot side of thermoelectric module for heating of the feed water, to improve the evaporation while using the cold side of the module to cool the condenser and improve the condensation process. The developed thermoelectric distillation system produces 28.5 mL of distilled water (equivalent to 678 mL/m²) over a period of 1 hour. The corresponding electrical energy required for the water production is 0.0324 kWh, which gives a specific energy consumption of 0.00114 kWh/mL. The developed system in this research has significantly lower energy consumption than the existing thermoelectric distillation systems.

The transient to steady state behaviour of the developed thermoelectric distillation system was investigated. It was found that the system reaches steady state after approximately three hours of the system operation. The water temperature in evaporation chamber was increased from 22.3 °C to 47.8 °C. Similarly, the vapour temperature was increased moderately from 20.3 °C to 30.4 °C. The steady state water production, humidity, energy consumption and *COP* of the thermoelectric distillation system were 15.3 mL/h, 81%, 0.0324 kWh and 1.04, respectively.

Thermal models have been developed through water-vapour phase-change theory to interpret the evaporation and condensation processes involved in the fresh water production of the thermoelectric distillation system. The first model was related to the evaporation process to determine the vapour production in the system. A theoretical distillation ratio of 12% was obtained, with a predicted water temperature of 42.7 °C. This is in reasonable agreement with the 9.5% value experimentally obtained. The second

model has been developed for the water condensation process. The developed model can be used for determining the key parameters that control the condensation processes and the system thermal performance. This model shows that the rate of water condensation is dependent upon the convection heat transfer coefficient of the cold-side heat exchanger. The fitted value of the convection heat transfer coefficient in the thermoelectric distillation system is $8 \text{ W/m}^2\cdot\text{K}$.

Key factors that influence the total water production and water production rate have been investigated, including sample water temperature, vapour volume at sample water level, Peltier current and thermoelectric input power. The experimental data shows that an increase in sample water temperature from $30 \text{ }^\circ\text{C}$ to $60 \text{ }^\circ\text{C}$ gives a 47 % increase in total water production. Peltier current is demonstrated as a control factor in the design of an effective thermoelectric distillation system. The results show that the total water production increases by 61%, when the volume occupied by the vapour is reduced from 600 cm^3 to 400 cm^3 by increasing the sample water level from 10 mm to 30 mm in the system. The maximum water production is achieved by increasing sample water temperature and the corresponding optimised input power.

Measurements of the distilled water show that it has similar quality to drinkable tap water in terms of pH, total dissolved solids and electrical conductivity values. Photovoltaic Geographical Information System was used to estimate the global irradiation per square meter and the solar electricity generation in kWh received by a solar panel in a specific region. Using the experimental prototype, the maximum monthly average water production is 4023.3 mL when using 8.52 kWh of electricity produced during March at the University of Kufa. The minimum average monthly water production is 2970.3 mL using 6.29 kWh of electricity produced during November.

Declaration and Statements

Declaration

This work has not been submitted in substance for any other degree or award at this on any other university or place of learning, nor is being submitted concurrently in candidature for any degree or other award.

Signed..... (Hayder Sami Saleh Al-Madhhachi), Date.....

Statement 1

This thesis is being submitted in partial fulfilment of the requirements for the degree of Doctor of Philosophy (PhD).

Signed..... (Hayder Sami Saleh Al-Madhhachi), Date.....

Statement 2

This thesis is the result of my own independent work/investigation, except where otherwise stated, and the thesis has not been edited by a third party beyond what is permitted by Cardiff University's Policy on the Use of Third Party Editors by Research Degree Students. Other sources are acknowledged by explicit references. The views expressed are my own.

Signed..... (Hayder Sami Saleh Al-Madhhachi), Date.....

Statement 3

I hereby give consent for my thesis, if accepted, to be available online in the University's Open Access repository and for inter-library loan, and for the title and summary to be made available to outside organisations.

Signed..... (Hayder Sami Saleh Al-Madhhachi), Date.....

Acknowledgements

First and foremost I am thankful to my God for providing me with the patience and strength to go on and complete this task.

I would like to thank my supervisor, Professor Gao Min, for the continuous help and guidance he gave me during my PhD; I am sincerely grateful to him. His invaluable guidance, excellent research attitude and knowledge about the field of study always encouraged me.

I would also like to thank the Republic of Iraq, especially the Ministry of Higher Education and Scientific Research (MOHESR) for providing the moral and financial support.

My deepest appreciation goes to my beloved wife, Elham Al ateya, for her constant care, love and support, and for always standing beside me during happy and sad moments. Thanks also to my lovely daughters Arwa and Raya. They have suffered the most from my absence during their most difficult times.

My acknowledgment goes also to my parents, brothers and sister. This thesis would have been simply impossible to complete without their support.

Special thanks go to Dr Jorge García-Cañadas, Dr Tracy Sweet, Dr Matthew Phillips, Dr Martin Prest and Dr Tanuj Singh for their feedback and comments on the thesis chapters.

Lastly, I offer my regards and gratitude to all of those who supported me in any aspect during the completion of this thesis, in particular, my colleagues in the department of mechanical engineering in University of Kufa.

Publications

1. Al-Madhhachi, H. and Min G., 2015, June. Experimental and theoretical study of evaporation and condensation processes in a water desalination unit using a thermoelectric cooling system. In 34th Annual International Conference on Thermoelectrics and 13th European Conference on Thermoelectrics; Poster presentation, Dresden, Germany.
2. Al-Madhhachi, H., Prest, M. and Min, G., 2016, October. Evaluation of the convection heat transfer coefficient in a thermoelectric distillation system. In *International Conference for Students on Applied Engineering (ICSAE)*, (pp. 213-217). IEEE.
3. Al-Madhhachi, H. and Min, G., 2017. Effective use of thermal energy at both hot and cold side of thermoelectric module for developing efficient thermoelectric water distillation system. *Energy Conversion and Management*, 133, pp.14-19.
4. Al-Madhhachi, H., Phillips, M. and Min, G., 2017, June. Validation of Vapour / Water Production in a Thermoelectric Distillation System. In *Proceedings of the 3rd World Congress on Mechanical, Chemical, and Material Engineering (MCM'17)*, 117, (pp.1-7).
5. Al-Madhhachi, H., Min, G., 2017. Key factors affecting water production rate in a thermoelectric distillation system. *Energy Conversion and Management*, (Under Review).

Contents

Summary	i
Declaration and Statements	iii
Acknowledgements	iv
Publications	v
Contents	vi
List of Symbols	xii
Abbreviations	xvi
List of Figures	xviii
List of Tables	xxv
Chapter One – Introduction	1
1.1 Background of water desalination technology	1
1.2 Benefits of the thermoelectric distillation system	3
1.3 Novelty of research	4
1.4 Aims and objectives	5
1.5 Thesis outline	6
Chapter Two – Literature Review	8
2.1 Introduction	8
2.2 The thermoelectric effects	8
2.2.1 Peltier effect	8

2.2.2 Seebeck effect	10
2.2.3 Thermoelectric module	11
2.3 Thermoelectric applications	12
2.3.1 Thermoelectric refrigeration	12
2.3.2 Thermoelectric generation	20
2.4 Desalination as a solution to the drinking –water problem	23
2.5 Water desalination technologies	24
2.5.1 Classifications of the desalination technologies	24
2.5.2 Conventional desalination processes	25
2.5.2.1 Multi-Stage Flash (MSF)	25
2.5.2.2 Multi-Effect Distillation (MED)	26
2.5.2.3 Vapour Compression (VC)	27
2.5.2.4 Still Distillation (SD)	28
2.5.2.5 Reverse Osmosis (RO)	28
2.5.2.6 Electro-Dialysis (ED)	29
2.5.3 Advantages and disadvantages of the desalination technologies	30
2.6 Thermal distillation technologies	31
2.6.1 Overview of thermal distillation system design	32
2.6.2 Integration of thermoelectric and water distillation systems	38
2.6.3 Performance analysis of thermoelectric distillation systems	45

2.7 Summary and conclusions.....	48
Chapter Three – Design and Construction of the Thermoelectric Distillation System.	50
3.1 Introduction	50
3.2 Novel thermoelectric distillation system	50
3.3 Theoretical outlines of the thermoelectric distillation processes	51
3.3.1 Thermal energy required for evaporation process	52
3.3.2 Rate of water condensation	59
3.3.3 Heating and cooling by thermoelectric module	66
3.4 Design of the thermoelectric distillation system	71
3.4.1 Sample water recirculation	73
3.4.2 The thermoelectric module	74
3.4.3 Evaporation/Condensation chamber	76
3.4.4 Hot side water heat exchanger for sample water heating	77
3.4.5 Cold heat sink for water condensation	78
3.5 Assembly of the thermoelectric distillation system	80
3.6 Summary of outcomes	82
Chapter Four – Experimental Investigations of Utilizing Hot and Cold Sides of a Thermoelectric Module for Water Distillation System	83
4.1 Introduction	83
4.2 System description	83

4.3 Instruments and sensors	84
4.4 Experimental setup	88
4.5 Experimental procedure	90
4.6 Results and discussions	91
4.6.1 Thermal behaviour of the system	91
4.6.2 Thermal behaviour of the thermoelectric module	94
4.6.3 Water productivity and energy consumption	97
4.6.4 Comparison with other technologies	98
4.6.5 Power generation after switching off	99
4.7 Conclusions	100
Chapter Five – Validation and Analysis of the Evaporation and the Condensation Processes in the Thermoelectric Distillation System	102
5.1 Introduction	102
5.2 Processes description in the thermoelectric distillation system	103
5.3 Theoretical models validation with the experimental results	104
5.3.1 Evaporation process at the water-vapour interface	104
5.3.2 Condensation process at the vertical fins	111
5.4 Water and vapour flows in the system	113
5.5 Overall energy losses at steady state	115
5.6 Conclusions	118

Chapter Six – Key Factors Affecting the Water Production Rate in the Thermoelectric Distillation System	120
6.1 Introduction	120
6.2 Factors affecting water productivity	120
6.3 System description	122
6.4 Modified experimental setup	123
6.5 Measurements procedure	124
6.6 Results and discussions	125
6.6.1 Effect of sample water temperature	126
6.6.2 Effect of cooling water flow rate	127
6.6.3 Effect of vapour volume	128
6.6.4 Effect of Peltier current	130
6.6.5 Optimisation of input power to the thermoelectric module.....	133
6.7 Conclusions	135
Chapter Seven – Water Production Analysis and Solar Panel Evaluation System.	136
7.1 Introduction	136
7.2 Water quality testing	137
7.3 Solar energy evaluation	142
7.4 Conclusions	145
Chapter Eight – Conclusions and Future Works	146

8.1 Conclusions	146
8.2 Future Works	149
8.2.1 Suggestions	150
8.2.2 Large scale unit	150
8.2.3 Other applications	151
Appendix	153
References	163

List of Symbols

Symbol	Definition	Unit
A	Area	m^2
A_c	Cross section area of fin	m^2
A_{leg}	Cross section area of thermoelectric leg	m^2
A_s	Surface area of condenser	m^2
dA_s	Surface area of differential element	m^2
E_d	Average daily electricity production	kWh
E_m	Average monthly electricity production	kWh
$E_{evap.}$	Energy required for evaporation	W
H	Latent energy	kJ/kg
H_d	Average daily sum of global irradiation	kWh/m ²
H_m	Average monthly sum of global irradiation	kWh/m ²
h_a	Ambient heat transfer coefficient	W/m ² .K
h_l	Local heat transfer coefficient	W/m ² .K
I	Current	Amp
J	Joule heating	W
k_{leg}	Thermal conductivity of thermoelectric leg	W/m. K
K_{TE}	Thermal conductance of thermoelectric module	W/ K

$L_{cond.}$	Latent heat of condensation	kJ/kg
$L_{evap.}$	Latent heat of evaporation	kJ/kg
L_{leg}	Length of thermoelectric leg	mm
L_T	Total thermal losses at steady state	W
m	Mass	kg
$\dot{m}_{cond.}$	Rate of water condensation	mL/s
$m_{distillate}$	Amount of water distillate	mL
m_f	Mass of liquid	Gram
$m_{initial}$	Initial mass of the water filled	Gram
m_g	Mass of gas	Gram
m_{mix}	Mass of mixture	Gram
m_{remain}	Mass of water remaining	Gram
n	Constant (equation 5.14)	
P	Electric power supply	W
P_{TE}	Thermoelectric power supply	W
P_{pump}	Water pump power supply	W
P_{system}	System power supply	W
P	Pressure	Pa
P_f	Fin Perimeter	m

Q	Heat transfer	W
$Q_{cond.}$	Heat transfer to condenser surface	W
Q_c	Absorbed heat at the cold side	W
Q_f	Heat transfer of fin	W
Q_H	Dissipated heat at the hot side	W
q_x	Heat transfer in x-direction along the fin	W
q_{x+dx}	Heat transfer in differential form along the fin	W
R	Resistance of thermoelectric module	Ohm
t	Time	Second
T	Temperature	°C
T_{amb}	Ambient temperature	°C
T_c	Cold side temperature of thermoelectric module	°C
T_{cp}	Peltier cold side temperature	K
T_f	Water film temperature	°C
T_H	Hot side temperature of thermoelectric module	°C
T_{hp}	Peltier hot side temperature	K
T_v	Vapour temperature	°C
T_s	Surface temperature of condenser	°C
T_w	Water temperature	°C

u_a	Air velocity	m/s
V	Volume	m^3
V_{total}	Total volume of water-vapour chamber	m^3
V	Voltage	Volt
x	Quality of vapour	
x	Distance	m
α_{leg}	Seebeck coefficient of a thermoelectric leg	V/K
θ	Angle of inclined condenser	Degree
$\theta(x)$	Temperature difference in differential form	$^{\circ}C$
ξ_{PV}	Photovoltaic efficiency	
ΔT	Temperature difference	K
Δm_g	Increase of vapour mass	Gram
\mathcal{V}	Specific volume	m^3/kg
\mathcal{V}_f	Specific volume of fluid	m^3/kg
\mathcal{V}_g	Specific volume of gas	m^3/kg
\mathcal{V}_{gf}	Difference of specific volume between gas and fluid	m^3/kg
\mathcal{V}_{mix}	Specific volume of mixture	m^3/kg
ρ_{actual}	Actual density of vapour	kg/m^3
$\rho_{saturation}$	Saturation density of vapour	kg/m^3

Abbreviations

Con	Convection
<i>COP</i>	Coefficient of performance
DC	Direct current
EC	Electric conductivity
ED	Electro-Dialysis
LED	Light emitting diode
MD	Membrane Desalination
MED	Multi Effect Distillation
MVC	Mechanical Vapour Compression
MSF	Multi Stage Flash
NASA	National Aeronautics and Space Administration
RH	Relative humidity
RO	Reverse Osmosis
pH	Potential of Hydrogen
PVC	Polymerizing Vinyl Chloride
PV	Photovoltaic
SD	Still Distillation
SEC	Specific energy consumption

TDS	Total dissolved solids
TE	Thermoelectric
TEC	Thermoelectric cooler
TEG	Thermoelectric generator
TVC	Thermal Vapour Compression
VC	Vapour Compression
WHO	World Health Organization
ZT	Figure of merit

List of Figures

Figure 1.1: Schematic diagram of the proposed thermoelectric distillation system	3
Figure 2.1: Schematic of thermoelectric module operation at Peltier mode	9
Figure 2.2: Schematic of thermoelectric module operation at Seebeck mode	11
Figure 2.3: ZT as a function of temperature for several thermoelectric materials	12
Figure 2.4: Schematic diagrams of multi-couple thermoelectric modules [13]	12
Figure 2.5: The working principle of the thermoelectric cooling and heating system in summer [45]	14
Figure 2.6: Cross-section view of a thermoelectric refrigerator [46]	15
Figure 2.7: Schematic of solar cell driven thermoelectric refrigerator [47]	16
Figure 2.8: Schematic diagram of a thermoelectric chiller [48]	17
Figure 2.9: Schematic diagram of the thermoelectric refrigerator [51]	19
Figure 2.10: Comparison of the COP numeric data with the experimental data [51]	19
Figure 2.11: Schematic diagram of the system [52].....	21
Figure 2.12: Model of a single module generator test rig [53]	21
Figure 2.13: Setup for natural convection operation [55]	23
Figure 2.14: Energy–water–environment relationship through desalination for the world [56]	24
Figure 2.15: Classifications of the desalination technologies	25
Figure 2.16: Schematic diagram of MSF unit [65]	26

Figure 2.17: Schematic diagram of MED unit [65]	27
Figure 2.18: Schematic diagram of VC (MVC and TVC) units [65]	27
Figure 2.19: Schematic diagram of a basic solar still design [66]	28
Figure 2.20: Schematic diagram of the reverse osmosis (RO) system [67]	29
Figure 2.21: Schematic diagram of ED unit [68]	29
Figure 2.22: A number of reported thermal distillation systems [69].....	33-34
Figure 2.23: Schematic of the weir-type distillation unit and its components [70]	36
Figure 2.24: Schematic diagram of an integrated hybrid PV active solar still [71]	37
Figure 2.25: Cross-sectional view of a single slope passive solar still [77]	38
Figure 2.26: Cross-sectional view of a double slope passive solar still [77]	38
Figure 2.27: Schematic diagram of the portable thermoelectric solar still [78]	39
Figure 2.28: a) schematic drawing of the distillation unit, b) photo of the unit and c) solar unit [79]	40
Figure 2.29: a) schematic drawing of the asymmetrical solar still and b) photo of the still [80]	41
Figure 2.30: Schematic of the air dehumidification process [81]	42
Figure 2.31: Schematic diagram of integrated photovoltaic-thermoelectric dehumidification system [82]	43
Figure 2.32: Diagram of the water condensation system [83]	44
Figure 2.33: Schematic diagram of experimental setup [84]	45

Figure 2.34: The specific energy consumption for various types of desalination systems using logarithmic scale [62-96].....	46
Figure 2.35: Diagram of the proposed system with the gaps identified in the literature.	48
Figure 3.1: Schematic diagram of thermal processes and design parameters of the model.....	52
Figure 3.2: T-v diagram of water and vapour phases in a system	54
Figure 3.3: The vapour quality and specific volume difference with increasing water temperature	57
Figure 3.4: The water-vapour mass with increasing water temperature	57
Figure 3.5: The evaporation energy as a function of the vapour mass and water temperature	58
Figure 3.6: The inclined and vertical surfaces of a condenser	59
Figure 3.7: Variation of the heat flux transfer to the cooling surface as a function of the temperature difference and the local heat transfer coefficient	61
Figure 3.8: Variation of the rate of the water condensate on the cooling surface as a function of the temperature difference and the local heat transfer coefficient	62
Figure 3.9: Schematic of the temperature profile in thermoelectric assisted condenser.	63
Figure 3.10: Heat balance of a straight fin of uniform cross section	64
Figure 3.11: The paths of the current and the heat through a thermoelectric leg	67
Figure 3.12: Length and width of one side of a leg of thermoelectric module	67
Figure 3.13: Schematic of the temperature profile in a TE module assisted condenser.	69

Figure 3.14: The difference between dissipated and absorbed heat as a function of temperature difference across the thermoelectric module for different input currents...	70
Figure 3.15: <i>COP</i> as a function of the temperature difference of the thermoelectric module for different input currents	71
Figure 3.16: The main parts of the thermoelectric distillation design	72
Figure 3.17: The main distances inside the system	74
Figure 3.18: A sketch of a thermoelectric module composed of P-type and N-type semiconductors [11]	75
Figure 3.19: The thermoelectric module used in the design	75
Figure 3.20: The thermoelectric cooling unit	76
Figure 3.21: Chamber's frame including the inclined cover	77
Figure 3.22: Schematic and photograph of the hot side water heat exchanger	78
Figure 3.23: The design drawing and a photograph of the aluminium condenser.....	79
Figure 3.24: A photograph of water drops on the surface of aluminium condenser.....	79
Figure 3.25: Assembly the thermoelectric module with the heat exchangers and the Plexiglas cover	80
Figure 3.26: The main components and assembly order of the developed thermoelectric distillation system	81
Figure 3.27: Design drawing of the assembled system (left) and cross-section views of the system (right)	81
Figure 3.28: A photograph of the actual system developed based on the above design.	82

Figure 4.1: Schematic diagram of the thermoelectric distillation system	84
Figure 4.2: Schematic diagram of the experimental set up	85
Figure 4.3: A photograph of the diaphragm pump used in the TE distillation system...	86
Figure 4.4: Positions of the thermocouples in the system	87
Figure 4.5: Photograph of a) K-type thermocouple and b) digital humidity sensor	87
Figure 4.6: TC-08 Serial thermocouple data logger by Pico technologies Ltd	88
Figure 4.7: A photograph of the experimental setup of the TE distillation system	89
Figure 4.8: The temperature variation of the system components	91
Figure 4.9: The temperature differences across the thermoelectric module (blue) and between the vapour and condenser (red)	92
Figure 4.10: The relative humidity in the chamber compared with that of ambient in the laboratory	93
Figure 4.11: The absorbed and released heat variation of the thermoelectric module ...	95
Figure 4.12: The <i>COP</i> of the TE module and the TE distillation system	96
Figure 4.13: The relationship between the ΔT and the <i>COP</i> of the TE module	96
Figure 4.14: The distillate water collected and total power input during more than three hours	97
Figure 4.15: The hourly water distillate and total power consumption during four hours operation	98
Figure 4.16: The temperatures profiles of the system after switching off	99
Figure 4.17: The output power and open circuit voltage of the system after switch off.	100

Figure 5.1: Schematic diagram of the heat transfer mechanism in the system	103
Figure 5.2: Two views of the pressure gauge connected to the thermoelectric distillation system	107
Figure 5.3: The water temperature and water production rate as a function of the hot side of the thermoelectric temperature	108
Figure 5.4: The experimental data of vapour temperature and humidity	108
Figure 5.5: The dew point and gauge pressure of the vapour produced	109
Figure 5.6: The validation of the vapour produced with two-hour system operation ...	110
Figure 5.7: The validation of the water mass remain with two hour system operation.	110
Figure 5.8: The temperature variation of the system components	112
Figure 5.9: The validation of the water condensation rate with the fitted h_c of $=8 \text{ W/m}^2\cdot\text{K}$	112
Figure 5.10: Water flow in the hot side heat exchanger at steady state	114
Figure 5.11: Vapour flow inside the chamber at steady state	114
Figure 5.12: Thermal losses from the thermoelectric distillation system to the ambient...	116
Figure 5.13: Diagram of the total losses of the system	118
Figure 6.1: Schematic diagram of a thermoelectric distillation system with independently controlled water circulations	122
Figure 6.2: A photograph of the modified experimental setup of the system	123
Figure 6.3: Total water production at different sample water temperatures	126
Figure 6.4: Vapour temperature at different sample water temperatures	127

Figure 6.5: Total water production at different cooling water flow rate	128
Figure 6.6: Total water production at different sample water levels	129
Figure 6.7: Water production rate vs. operation time for different Peltier currents from 10 A to 5 A	131
Figure 6.8: Water production rate vs. operation time for different Peltier currents from 5 A to 10 A	132
Figure 6.9: A photograph of ice formation on the condenser during an operation, in which the temperature of the sample water is 30 °C and the Peltier current is 9 A	132
Figure 6.10: Temperatures of the condenser and the cold side of the thermoelectric module as a function of the Peltier current	133
Figure 6.11: Total water production at different thermoelectric input powers and sample water temperatures	134
Figure 7.1: Hanna instruments HI-98129 for water quality analysis	137
Figure 7.2: The four locations of the seawater collected at Cardiff Bay	139
Figure 7.3: Average monthly water production from the thermoelectric distillation system versus electricity production from the PV solar panel	145

List of Tables

Table 2.1: Specifications of solar cell driven, storage battery and thermoelectric refrigerator [47]	15
Table 2.2: Several features of the desalination technologies	30
Table 2.3: Advantages and disadvantages of the desalination technologies	31
Table 2.4: Data collected from the literature survey	47
Table 2.5: Comparison of the SEC among various thermal distillation systems based on the data collected	47
Table 3.1: The two-phase system problem and the approach for solution	53
Table 3.2: Solution steps of the heat transfer problem	63
Table 3.3: The properties and the overall characteristics of the thermoelectric leg and the thermoelectric module	68
Table 3.4: Maximum and minimum allowable values of the thermal parameters	72
Table 4.1: The specifications of the diaphragm pump used in the TE distillation system.	85
Table 4.2: The specifications of the Digi Flow 6710M-34TM employed for this study.	86
Table 4.3: The specifications of K- thermocouple type used in the experiments	87
Table 4.4: Accuracies, ranges and standard uncertainty of the measuring instruments...	90
Table 5.1: Water production with and without thermoelectric module operation and water pump circulation	107
Table 5.2: The properties of the water and vapour in the system	113

Table 5.3: Mesh information of the thermoelectric system	114
Table 5.4: The output results of the water and vapour in the system	115
Table 5.5: Thermal losses calculations	117
Table 6.1: Constant geometric factors through the experiments	121
Table 6.2: Properties of the additional components used in the experiments	125
Table 6.3: Accuracies, ranges and standard uncertainty of the additional instruments.	125
Table 6.4: Average condenser temperature and humidity for different sample water temperatures.....	127
Table 6.5: Thermodynamic properties of the vapour at different sample water levels.	130
Table 6.6: Corresponding currents and voltages of the thermoelectric input power ...	134
Table 7.1: Specifications of the Hanna instruments HI-98129 pH water analysis meter.....	138
Table 7.2: pH levels before and after the distillation process	140
Table 7.3: TDS tests before and after the distillation process	141
Table 7.4: EC tests before and after the distillation process	141
Table 7.5: The input data to the PVGIS	143
Table 7.6: The output data (average electricity production E and the sum of global irradiation H) daily and monthly from the PVGIS	143
Table 7.7: Properties of some commercial solar panels can be used to power the TE system	145
Table 8.1: Specification for large scale application	151

Chapter 1

Introduction

1.1 Background of water desalination technology

Water shortage has become one of the major global challenges, which is linked to population growth. One-third of the world's population are already surviving in areas of middling to high levels of water stress; 1.5 billion people have poor access to drinkable water, with some 80 countries suffering from water shortage [1]. In much of the world, the health of river systems is at risk of overuse and pollution; rivers are often no longer able to supply and purify the amounts of water needed while the effect of pests and diseases is rising. With the establishment of deep underground pumping and piping across long distances, groundwater aquifers are progressively being depleted well beyond sustainable recovery levels; this also leads in many circumstances to brackish water with high concentrations of dangerous particulates and to resulting health problems [2].

The process of separating dissolved salts and other minerals from water is called desalination. Desalination has become a promising method of fresh water production from seawater and brackish water. [3]. Desalination technology involves two alternative processes, which currently lead the market; namely thermal distillation and membrane processes. Thermal distillation processes involve heating feed water for evaporation at the operating pressure to produce vapour and condensing the vapour molecules in a condenser unit to produce fresh water. It is called a phase change process. The technologies for this thermal process include: Multiple Effect Distillation (MED), Multi Stage Flash (MSF), Mechanical Vapour Compression (MVC) and Still Distillation (SD).

They generally have higher capital costs and consume more energy than membrane processes. However, they mostly produce a high quality distillate [4]. The membrane processes involve separation of dissolved salts from the feed water by mechanical, chemical or electrical methods using a membrane barrier between the feed water and the distilled water. Applications of this principle include Electro Dialysis (ED) and Reverse Osmosis (RO). They are called non phase-change processes. The technology is less suitable for high salinity or poor water quality. They have higher maintenance costs (pre-treatment costs and costs associated with membrane replacement) [5].

In general, the current desalination technologies are expensive, sensitive to increases in energy prices and result in high carbon emissions. The challenge is to design, construct and test a fresh water production system with low cost and low energy consumption which can be easily scaled up to any size. There are various integrated technologies for water distillation systems, one of these is thermoelectric technology. Thermoelectric modules have no moving parts and a long operational life. They are noiseless, easily controllable, and compact in size, environmentally friendly and so cause less pollution [6-8]. The key objective of the research is to design, construct and test an efficient water distillation system by appropriate incorporation of thermoelectric module. To ensure low energy consumption can be achieved, the unique design of the system will simultaneously use the heat from the hot side of the thermoelectric module for water evaporation and the cold side for vapour condensation. Figure 1.1 shows the main processes of the water distillation system which includes a thermoelectric module with a heat exchanger on both sides. The core of the thermoelectric distillation system is the thermoelectric module. The thermoelectric module has two sides, the hot side is mounted to a water heat exchanger and the cold side is attached to an aluminium heat sink.

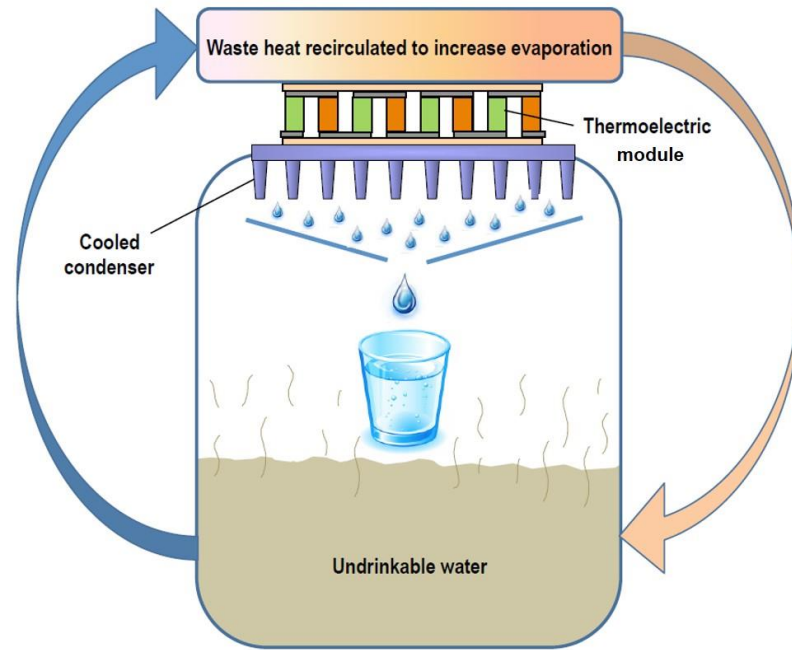


Figure1.1: Schematic diagram of the proposed thermoelectric distillation system.

1.2 Benefits of the thermoelectric distillation system

This research aims to demonstrate the benefits of the thermoelectric distillation system both to the scientific community and to industrial researchers. The design and construction of a feasible thermoelectric distillation system has required an investigation of the thermal performance of a thermoelectric concept for water distillation. This also highlighted the need for more specific investigation and analysis of the key factors that influence the evaporation and condensation processes in thermoelectric water distillation systems. A new technique of distillation is introduced which provides a more efficient process than other existing thermoelectric distillation systems (This is discussed in details in Chapter Four). The heat removed during condensation is then used for water heating by recirculating the sample water through the hot side of the thermoelectric module, improving the efficiency. This leads to enhance the water production rate at a lower energy consumption. Another benefit of using the thermoelectric module is the precise

temperature control of the cold and hot exchangers connected to the cold and hot sides of the thermoelectric module to investigate the key factors that control the evaporation and condensation processes (This is discussed in details in Chapter Six).

One of the benefits of the thermoelectric distillation system is the easy integration with other technologies such as the photovoltaic solar panel. The integrated system would allow solar energy to power the thermoelectric distillation system. As the availability and quality of the produced water is related to health and economy, this research will demonstrate the benefits to water quality by testing various samples of sea water from different regions in Cardiff Bay (This is discussed in details in Chapter Seven).

1.3 Novelty of research

The innovative aspects of the research include the following

- Design verified by construction and testing of a novel thermoelectric distillation system employing a thermoelectric module to enhance the evaporation and condensation processes. The design of the system utilises the rejected waste heat from the thermoelectric to heat the sample water for evaporation, resulting in a thermal energy requirement which is lower than conventional thermal distillation systems. The thermoelectric distillation system could also be operated as a low power generator after switch off under Seebeck mode.
- Development of theoretical models of the thermoelectric distillation system which can predict the thermal behaviour of the system based on water-vapour phase-change phenomena of the evaporation and condensation processes. The theoretical models validates with the experimental results obtained under controlled conditions in the thermoelectric distillation system.

- Understanding of the key factors that influence the water production rate, including; the effects of sample water temperature, vapour volume at sample water level, Peltier current and thermoelectric input power and temperatures of the hot and cold sides of the thermoelectric module.

1.4 Aims and objectives

The main objective of this research was to design, construct and test a novel thermoelectric distillation system with low energy consumption to produce fresh water. The developed system utilises a novel technique to enhance the rate of water evaporation and vapour condensation by employing a thermoelectric module. Specific objectives were as follows:

- Characterisation of the performance of specific thermal distillation systems in terms of water production and energy consumption.
- Development of theoretical models to support the interpretation of the processes involved in the water and vapour production of a thermoelectric distillation system.
- Understanding of the thermal behaviour of the thermoelectric distillation system experimentally in steady and transient states.
- Identify and qualify the key factors that control the evaporation and condensation processes in the thermoelectric distillation system.
- Verification of the quality of the produced water, to determine whether it is drinkable in terms of pH levels, total dissolved solids and electrical conductivity values.
- Evaluation of a capable and competent solar panel to power the thermoelectric distillation system in a selected area.

1.5 Thesis outline

The research was carried out in different stages and covered a number of tasks as reported in different chapters and sections of this thesis. The thesis consists of eight chapters. A brief outline of these chapters is given below:

- *Chapter One* gives background information which introduces the proposed research. It describes the aims and objectives of the research, and further breaks down the objectives into specific tasks. The chapter describes the novelty of the research and the potential benefits of using thermoelectric technologies in thermal distillation systems. It concludes with the outline of the thesis.
- *Chapter Two* presents a literature review on desalination and thermoelectric technologies in order to understand the types, processes and applications of these technologies. Major desalination technologies are reviewed with advantages and disadvantages. A review of thermoelectric refrigeration and power generation is undertaken. The integration of a thermoelectric module into a thermal distillation system is presented with analysis of the thermal performance of these technologies.
- *Chapter Three* explains the design and construction of the thermoelectric distillation system and the major challenges faced during the design. These challenges presented an opportunity to investigate the technical side of distillation and thermoelectric technologies working together in one system. Theoretical foundations associated with the evaporation and condensation processes were outlined to provide insights and guidelines for the design of the proposed thermoelectric distillation system.
- *Chapter Four* explores the experimental set up and procedure for the designed thermoelectric distillation system. It describes the individual components of the system, system instrumentation and measuring devices with their accuracies, ranges and standard uncertainty. The thermal performance of the system includes the

temperature distributions of the system components, humidity, water production and the energy consumed by the system. The results are analysed under steady state and transient state operating conditions. This is followed by comparison of the specific energy consumption with a number of systems using thermoelectric technology for water production.

- *Chapter Five* develops the theoretical models of the thermoelectric distillation system. The models are validated by comparing the theoretically obtained water and vapour production with those obtained experimentally during the evaporation and the condensation processes. The models include heat transfer analysis of the condenser fins and phase-change theory at the water-vapour interface in order to interpret the thermal behaviour of the processes.
- *Chapter Six* identifies the key factors affecting the total and the rate of the water production in the thermoelectric distillation system. The factors include: sample water temperature, volume occupied by the vapour, Peltier current, thermoelectric input power and the hot and the cold side temperatures of the thermoelectric module.
- *Chapter Seven* describes the measurements undertaken to assess the quality of the water produced by the developed thermoelectric distillation system in terms of pH levels, total dissolved solids and electrical conductivity values. The possibility of using a solar panel to power the developed thermoelectric distillation system is also evaluated, based on the solar irradiation and electricity generation at a specific location.
- *Chapter Eight* summarises the conclusions of the thesis and describes recommended future work.

Chapter 2

Literature Review

2.1 Introduction

In order to establish a firm foundation to the research presented, the literature survey begins with an introduction to thermoelectric technology including a discussion on the thermoelectric effect and the applications of thermoelectric modules. This is followed by classification of water desalination technologies, the advantages and disadvantages of these technologies in terms of water production rate, energy consumption, environmental aspects and water quality. Finally the literature review focusses on designs, investigations and improvements to water distillation systems integrated with thermoelectric modules.

2.2 The thermoelectric effects

2.2.1 Peltier effect

Thermoelectric phenomena describes the interaction between heat and electricity in solids and liquids. The principle of a thermoelectric device is based on the Peltier, Seebeck and Thomson effects. The thermoelectric devices can be employed for refrigeration (cooling), power generation and temperature sensing [9-13]. The practical applications of thermoelectric cooling or power generation became possible with discovery of suitable semiconductor materials. Figure 2.1 is a schematic diagram of a thermocouple consisting of n-type and p-type semiconductor materials. In the cooling mode, direct current passes from the n-type semiconductor, through a metal contact, to a p-type semiconductor material.

As a result, the heat is pumped from the top junction to the bottom junction. Consequently, the temperature at the top junction, T_C , decreases and the temperature at the bottom junction, T_H , increases. This phenomenon is called the Peltier effect [14]. Practically, the net amount of heat moved from the cold side to the hot side is reduced due to the Peltier effect by heat conduction and Joule heating J . The heat conduction flow is due to thermal transport by moving electrons and phonons (heat carries), and is dependent on the temperature difference between the cold and hot sides of the semiconductor material. Hence, heat will be conducted through the semiconductor material from the hot to the cold side. As the current is increased, the temperature difference, and thus the heat conduction, increases because the Peltier cooling effect increases. However, Joule heating is proportional to the square of the current [15, 16].

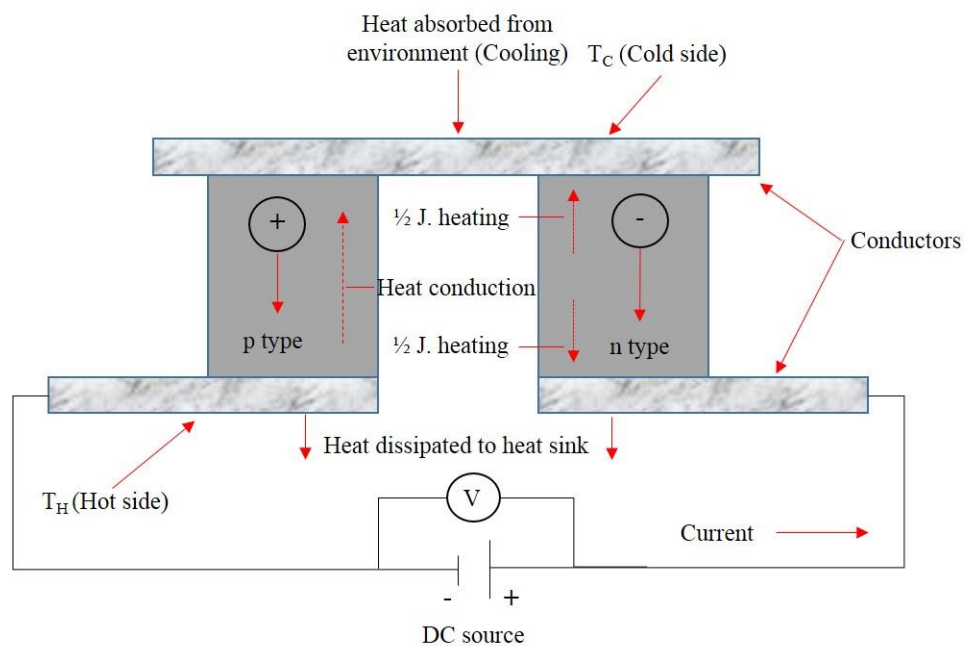


Figure 2.1: Schematic of thermoelectric module operation at Peltier mode.

In the Peltier mode, the amount of heat absorbed at the cold side and heat dissipated at the hot side are dependent on the Peltier coefficient, thermal conductivity, resistance of the module and the current flowing through the module. At any given current, thermal equilibrium is established at the cold side when the Peltier effect at the cold side is equal

to the sum of the conducted heat plus 50 % of the Joule heat. The other 50 % of the Joule heat goes to the hot side. As the current continues to increase and Joule heating becomes the controlling factor, the net heat dissipated at the hot side is the sum of the net heat absorbed at the cold side plus the applied electric power. The coefficient of performance (*COP*), used to define the cooling efficiency, is defined as the heat absorbed at the cold side divided by the applied electric power. The refrigeration capability of a semiconductor material is dependent on a combined effect of the material's Seebeck coefficient, electrical resistivity, and thermal conductivity over the operational temperature range between the cold and hot sides [17, 18].

2.2.2 Seebeck effect

The thermoelectric phenomenon can also be employed for power generation. When a temperature difference is established between the hot and cold sides of the semiconductor material, a voltage is created across the terminals of the material. This voltage is called the Seebeck voltage, and it is directly proportional to the temperature difference. As shown in Figure 2.2, if heat is supplied at one junction, this causes an electric current to flow in the circuit and when there is a load on the circuit, electrical power is delivered. The ratio of the Seebeck voltage to the temperature difference is referred to as the Seebeck coefficient. There is a link between the Seebeck and Peltier coefficients, the Peltier coefficient is the product of the Seebeck coefficient of the semiconductor material and the absolute temperature. Actually, the Seebeck effect is an inverse effect of the Peltier effect [19-23]. In the Seebeck mode, the amount of heat absorbed at the hot side and heat dissipated at the cold side are dependent on the Seebeck coefficient, thermal conductivity, resistance of the thermoelectric module and the current flowing through the semiconductor material.

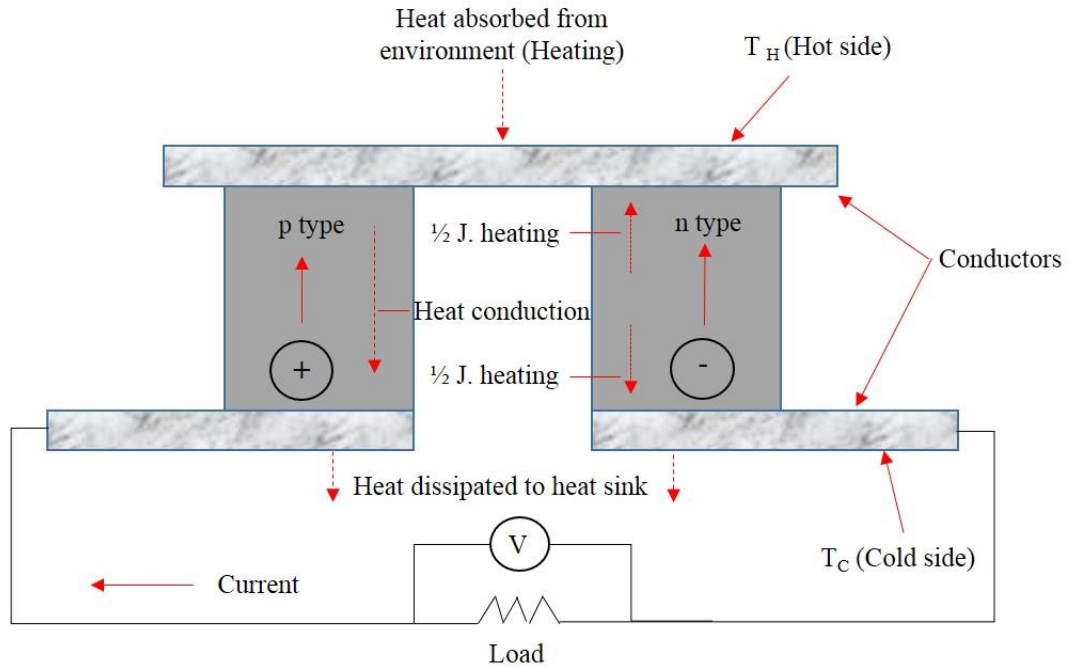


Figure 2.2: Schematic of thermoelectric module operation at Seebeck mode.

2.2.3 Thermoelectric module

In practice, a large number of thermocouples are put together to form a module. Within the module each semiconductor leg is called a thermoelement, and a pair of thermoelements is called a thermocouple. Thermoelectric module is formed by a group of thermocouples. Bismuth telluride (Bi_2Te_3) thermoelectric is particularly suited to this application because the figure of merit (ZT) was higher than other alloys over the temperature range of 0 – 400 K as shown in Figure 2.3. However, the thermoelectric properties of this material are particularly favourable above room temperature [6]. A typical thermoelectric module is shown in Figure 2.4, which usually utilises p-type and n-type bismuth telluride thermoelements connected electrically in series and thermally in parallel and sandwiched between ceramic substrates. In practical operation, thermoelectric modules should be connected to heat exchangers to obtain or dissipate heat. Thermoelectric modules can be viewed as a solid state heat pumps or generators.

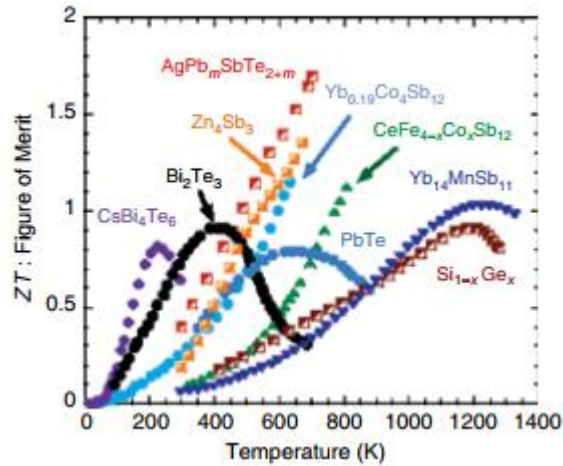


Figure 2.3: ZT as a function of temperature for several thermoelectric materials [6].

The modules follow the laws of thermodynamics in the same manner as mechanical heat pumps, or vapour compressors (conventional refrigerators) based on the operating modes. Therefore, the thermoelectric modules can be employed as coolers (or heaters), power generators and temperature sensors [24, 25].

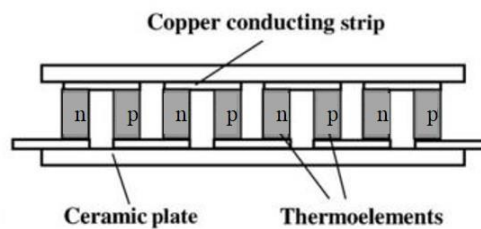


Figure 2.4: Schematic diagrams of multi-couple thermoelectric modules [13].

2.3 Thermoelectric applications

2.3.1 Thermoelectric refrigeration

Thermoelectric refrigerators made from semiconductors have no moving parts, therefore, they have a very long life-time. They are noiseless, simple, compact in size and easy to control. These coolers can operate in any position and they don't have any potential fluid leakage issues. Thermoelectric refrigerators can efficiently work with

photovoltaic PV panels because of the low DC voltage requirement and they can take the voltage directly from a PV panel. The experimental investigation and analysis of a thermoelectric refrigerator driven by solar cells has been previously investigated [26-29]. The performance of a thermoelectric refrigerator is dependent on the volume to be cooled by the refrigerator. They have a number of advantages for cooling small enclosures. Many factories use thermoelectric refrigerators for cooling cold boxes with a low power source. They are also insensitive to movement, so they can be used for portable purposes [30-32]. Practically, thermoelectric refrigerators have been used in many applications, and the number of applications is growing with the development of new thermoelectric materials with higher thermoelectric figure-of-merit and coefficient of performance values [33-37]. Thermoelectric refrigerators can also be integrated with electronic devices as an active cooling technology which is possibly the only solution that could satisfy such industrial requirements (thermal management and reliability) [38, 39]. Many recent efforts have focused on improving the coefficient of performance of the thermoelectric refrigeration by developing effective heat absorption and rejection methods [40-44].

He et al. [45] investigated theoretically and experimentally a thermoelectric cooling and heating system in buildings to cool in summer and heat rooms in winter. The thermoelectric module was driven by solar cells. In summer, the module was operated as a Peltier cooler powered by solar panel as shown in Figure 2.5. The bottom of a heat pipe (1) is welded on the back of solar cells, while the top is inserted in the heat exchanger. The bottom of thermoelectric module in the experimental room was connected to radiator whose material was aluminium, and the top was connected to the evaporator end of heat pipe (2) whose condenser end was inserted into the outside heat exchanger. The cold side of thermoelectric module absorbed heat from the room to reduce its temperature. The experiments were performed in a model room with 0.125 m^3 volume, solar cells of 0.5 m^2

area and 23 °C ambient temperature. The model of thermoelectric module used in the test was TE-127-03 whose rated voltage was 12 V and rated current was 3 A.

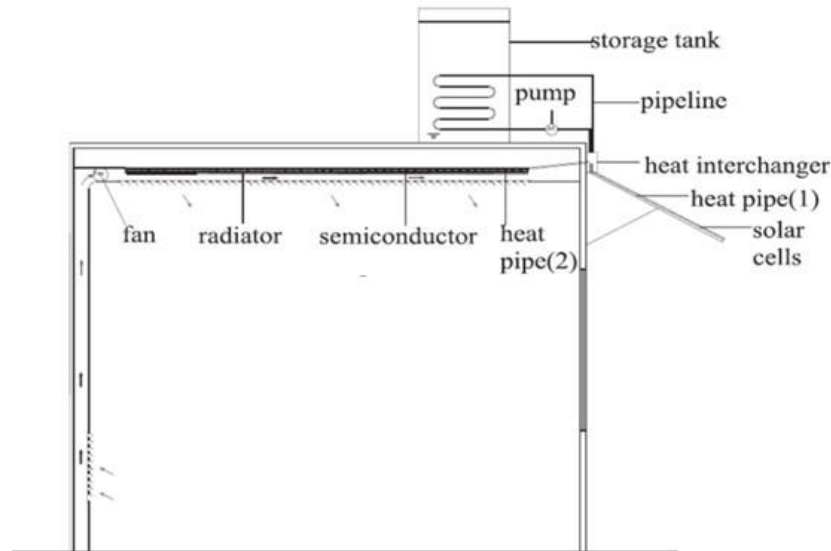


Figure 2.5: The working principle of the thermoelectric cooling and heating system in summer [45].

The results of this research showed that the minimum temperature in the model room was 17 °C, the coefficient of performance of the thermoelectric device was 0.45, the temperature of water in the storage tank with a volume of 18.5 L had risen about 9 °C and the thermal efficiency of the system (Heat flow of the storage tank divided by the solar power) was 12.06 %.

Abdul-Wahab et al. [46] manufactured a solar thermoelectric refrigerator for people living in remote areas without electricity. The schematic diagram of the solar refrigerator is shown in Figure 2.6. The refrigerator cabinet (0.5 L capacity) was designed with a cooling heat exchanger system involving six heat sinks to increase the amount of heat transfer from the hot side of the thermoelectric module (15 mm x 15 mm x 4.3 mm) and six cooling fans to discard the heat to the atmosphere. The results showed that the temperature of the cabinet decreased from 27 °C to 5 °C in less than 45 minutes. The total power provided by the 64 solar cells (32 solar cells from each side) was 115.2 W. The *COP* of the thermoelectric refrigerator was 0.16.

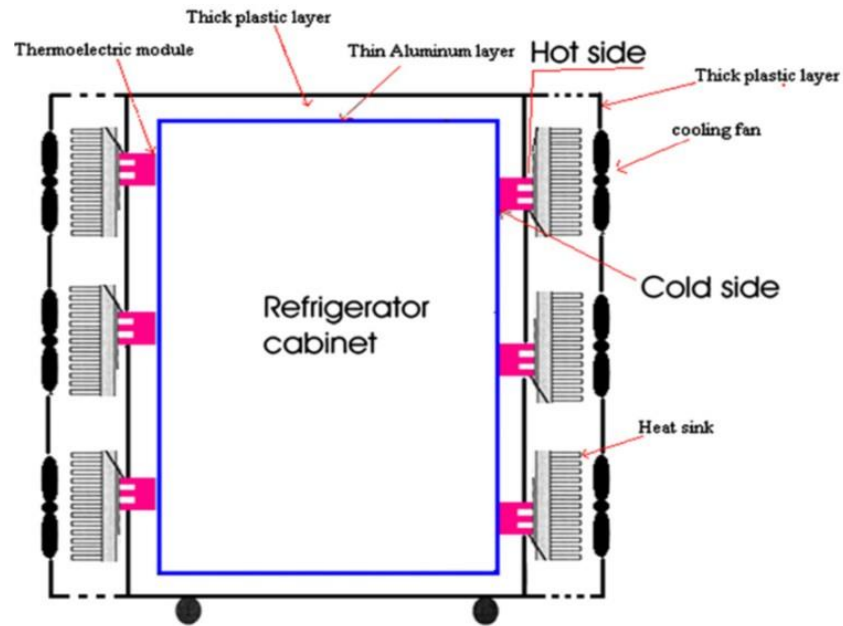


Figure 2.6: Cross-section view of a thermoelectric refrigerator [46].

Dai et al. [47] conducted an experimental investigation and analysis on a thermoelectric refrigerator powered by solar energy. The refrigerator was operated in daytime and night time and was designed as a portable device. The thermoelectric refrigerator consisted of an array of solar cells, controller device, storage battery, rectifier device and thermoelectric module as shown in Figure 2.7. The battery was used to power the thermoelectric refrigerator when electric PV power production was inadequate. The important part in the refrigerator is the thermoelectric cooling module, the cold side of it was located inside the refrigerator and the hot side set outside. About 500 ml of water was put into the refrigerator for testing. Cost of the unit is fundamental in the design. Specifications of the solar cells, storage battery and thermoelectric refrigerator are shown in Table 2.1.

Table 2.1: Specifications of solar cell driven, storage battery and thermoelectric refrigerator [47].

Array of solar cells		Storage battery		TE element	
Area	0.8 m ²	Storage capacity	75.7 Ah	α	0.0444 V/K
PV efficiency	0.13	P consumption	22 Ah/day	R	2.545 Ω
		No. of days	2	K	0.495 W/K
		Efficiency	0.85	Figure of merit	1.6e ⁻³

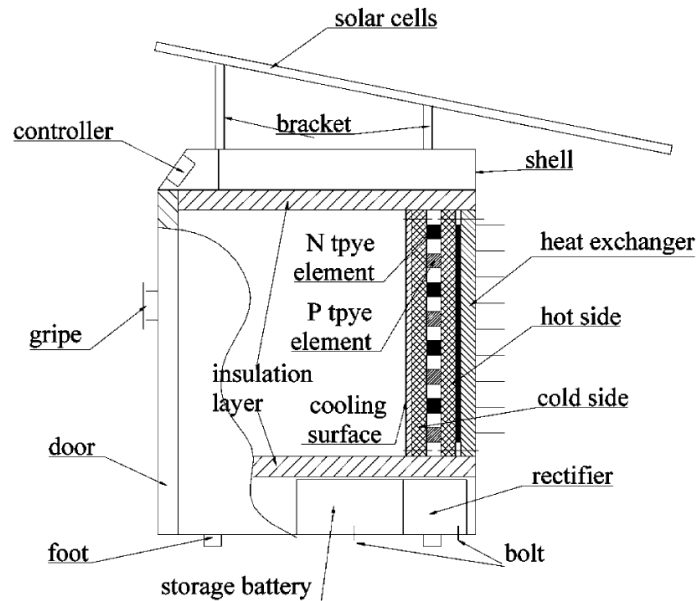


Figure 2.7: Schematic of solar cell driven thermoelectric refrigerator [47].

It was noted that the solar insolation rate dropped from 880 to 770 W/m^2 in one and a half hours with a constant voltage level about 12 V to 12.4 V and the cooling production dropped from 26 W to about 12 W at the end of the operation. The value of the thermoelectric current was required from 1.5 A to 4 A when the cold side temperature was 5 °C. Experimental results showed that the unit could maintain the temperature in the refrigerator between 5 - 10 °C, and the *COP* of the refrigerator was about 0.3 . The thermoelectric refrigerator could be used for cold storage of vaccine, foodstuffs, and drink in remote areas.

Chen et al. [48] carried out experimental investigations on cooling performance of a thermoelectric chiller driven by solar cells in daytime and fixed direct current in cloudy days or at night time. It used solar cells to power the thermoelectric chiller, where the cold side was connected to the water tank and the hot side of the thermoelectric module was connected to a heat exchanger to provide more cooling efficiency, as shown in Figure 2.8.

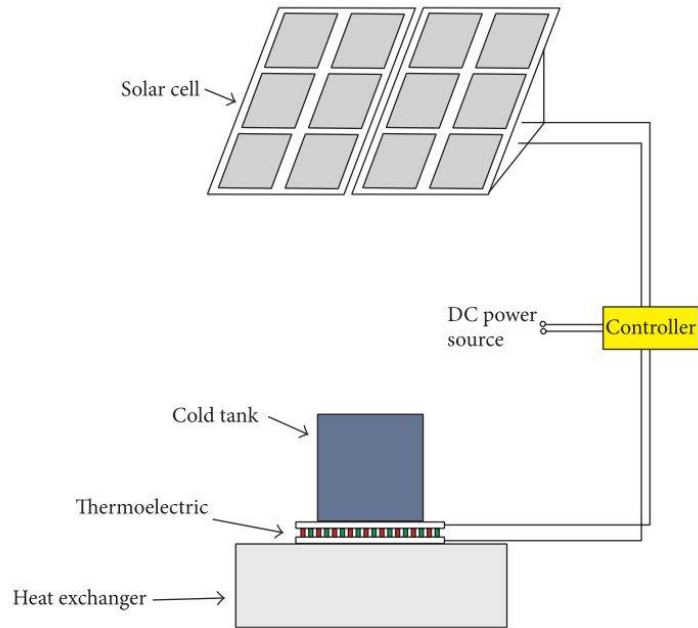


Figure 2.8: Schematic diagram of a thermoelectric chiller [48].

The solar panel had a maximum voltage of 17.6 V, maximum current 7.39 A, an area of 0.89 m^2 and a conversion efficiency of 11 %. The size of the thermoelectric module was $40 \text{ mm} \times 40 \text{ mm} \times 4.2 \text{ mm}$ and it was able to cool a volume of 250 ml of water from $18.5 \text{ }^\circ\text{C}$ to $13 \text{ }^\circ\text{C}$. The coefficient of performance of the system varied from 0.55 to 1.05 when solar irradiation changed between 450 W/m^2 and 1000 W/m^2 because of the input electric power of the thermoelectric system varied from 5.5 W to 26 W.

Xi et al. [49] presented a survey of thermoelectric technologies, which are powered by solar energy. Since 1954, the thermoelectric technology has become an attractive research topic in USA, Europe and Japan. Its applications were explored by big organizations including National Aeronautics and Space Administration (NASA) and the World Health Organization (WHO). The study illustrated a brief review of the environmental problems related to the use of conventional technologies and the benefits and drawbacks of the solar powered thermoelectric systems. The review takes into consideration some typical applications, such as a solar powered thermoelectric

refrigerator and thermoelectric power generation. The results of the survey showed that these systems could be used in various applications for refrigeration, air conditioning and power generation. However, these technologies have limited applications because of the small value of *COP* and conversion efficiency.

Pridasawas, and Lundqvist, [50] compared the performance of solar PV/battery thermoelectric refrigeration with other solar driven refrigeration systems. The analysis is based on the following conditions: a solar radiation of 700 W/m^2 , a cooling element temperature of $10 \text{ }^\circ\text{C}$, a cooling capacity of 5 kW , butane as the refrigerant in the non-thermoelectric system and an ambient temperature of $30 \text{ }^\circ\text{C}$ as the reference temperature. The comparison between these systems revealed the advantages of the thermoelectric system as follows: no working fluid and no moving parts, quiet, small size and light-weight. Disadvantages are low coefficient of performance, difficult to reach a low refrigeration temperature and not reliable when the power supply fluctuates. The study concluded that photovoltaic powered thermoelectric cooling systems are suitable for small refrigeration purposes such as cooling boxes. The efficiency of a photovoltaic powered thermoelectric cooling system depends on the photovoltaic efficiency and the coefficient of performance of the refrigerator. The coefficient of performance of thermoelectric refrigerators increases when the thermal resistance in the heat exchanger of the thermoelectric device decreases because the geometry of the refrigerator decreased.

Astrain et al. [51] developed a computational model to investigate how thermoelectric refrigerators compete against traditional vapour compression cooling systems. The model inputs were: refrigerator material and geometry, dimensions and materials of thermoelectric module, electrical voltage supplied to the module and the hot / cold side thermal resistances. The model outputs from the simulation were: internal temperatures, heat flows, electrical power consumption and *COP* of the refrigerator. In

this work, the researchers designed, built and tested a thermoelectric refrigerator prototype with an inner volume of 0.0055 m^3 as shown in Figure 2.9.

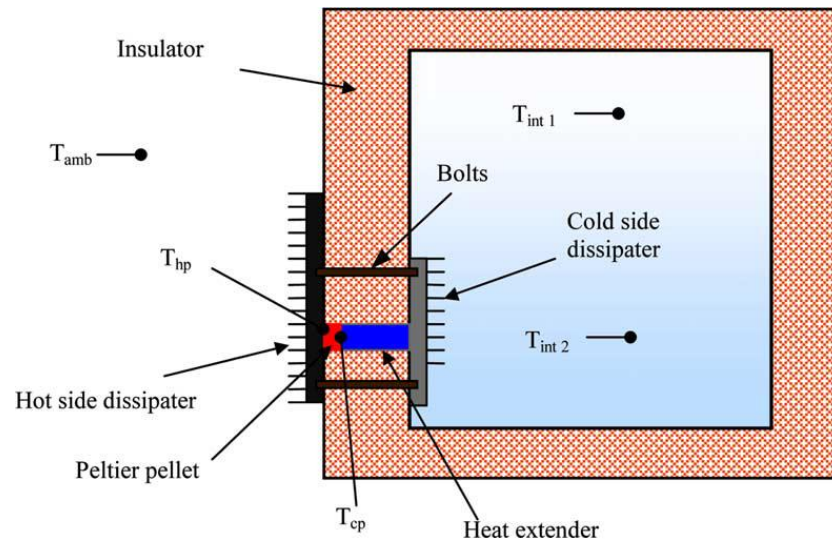


Figure 2.9: Schematic diagram of the thermoelectric refrigerator [51].

The thermoelectric module employed has a power rating of 50 W and dimensions of 40 mm x 40 mm x 4 mm. Two fin-type heat sinks were connected to the hot and cold sides, respectively. A comparative analysis of the experimental *COP* and the one obtained with the model also carried out as shown in Figure 2.10.

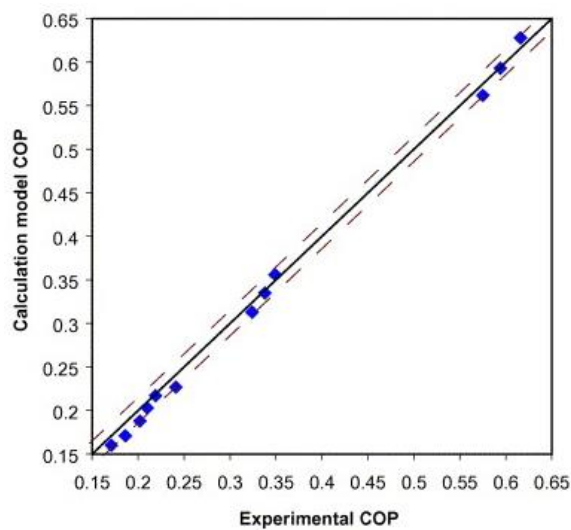


Figure 2.10: Comparison of the *COP* numeric data with the experimental data [51].

The study demonstrated the following advantages of a thermoelectric refrigeration in comparison with vapour compression: The system is environmentally friendly because it does not use refrigerants and relatively silent and robust because it does not need a compressor.

2.3.2 Thermoelectric generation

Waste heat in manufacturing is generated from particular industrial systems distributed throughout a plant. The main sources of waste heat for most industries are exhaust, flue gases and heated air from heating systems and processes such as high-temperature gases from burners in process heating, lower temperature gases from heat treating furnaces, several types of dryers and heat from heat exchangers. When a thermoelectric module converts thermal energy into electricity, it is said that it is operating in Seebeck mode and it is called a generator. One of the most common applications of thermoelectric generator is used to recover waste heat from processes with high exhaust streams. Demir and Dincer [52] designed a waste heat recovery system based on the thermoelectric generator. The system was located after the exhaust manifold of the automobile for using the recovered heat and it consists of a shell, tube heat exchanger and pipes covered by thermoelectric generators. In Figure 2.11, the exhaust gas (red arrow) of the automobile provides the heat for the thermoelectric generators, while the incoming air from the front grill (blue arrow) maintains the temperature difference for the thermoelectric generators. The shell and tube heat exchanger consist of 37 tubes and four baffles. Three different thermoelectric modules used in this study. The temperature difference between hot and cold streams generated electricity employing thermoelectric module operated under Seebeck mode. The maximum generated power from waste heat was 158 W corresponding to a 0.51 % thermal efficiency. The energy conversion

efficiency was calculated based on the heat transfer rate from the hot stream to the thermoelectric generators and the generated power.

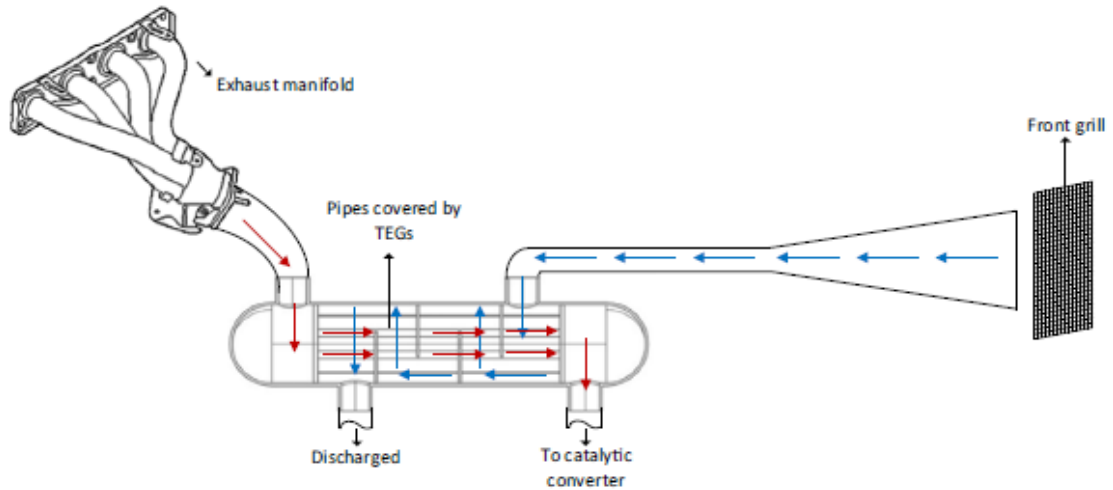


Figure 2.11: Schematic diagram of the system [52].

A thermoelectric generator for stove-tops has been studied because additional power could be obtained from heating stoves in winter months. Nuwayhid et al. [53] modelled a simplified generator using a 2-dimensional heat transfer model. A half-section of the generator model is shown in Figure 2.12.

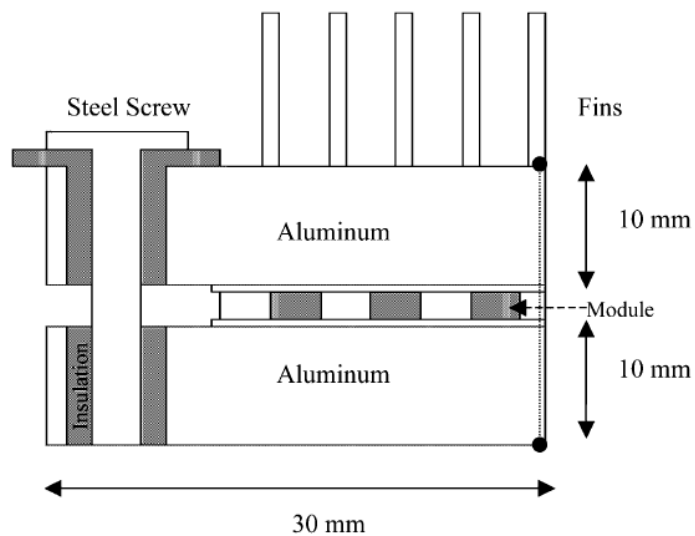


Figure 2.12: Model of a single module generator test rig [53].

Typical materials were used such as aluminium, insulator, steel screws, bismuth telluride and alumina. The fixing screws show a significant thermal bridge, leading to a higher cold-side temperature and a lower temperature difference. Some commonly available commercial Bi_2Te_3 modules (40 mm x 40 mm) were examined with hot side temperatures of 100–300 °C. The module HT6-12-40 (Melcor, USA) and the module TEC1-12708 (Taihuaxing, China) were selected for the study based on the price. Fifteen modules are required to produce maximum power of 100 W in a cheap manner using existing technology for domestic use.

Lertsatitthanakorn, [54] added a commercial thermoelectric module to the side-wall of a stove and created a biomass stove thermoelectric generator using a proportion of the stove's waste heat. The stove weighs about 12 kg. The system is composed of a thermoelectric module (Taihuaxing model TEP1-1264–3.4), a metal sheet wall that acts as one side of the stove's structure and the hot side of the module and a rectangular heat sink at the cold side of the thermoelectric module (No. of thermoelements = 126, active area = 1.96 mm² and thickness = 0.8 mm). The system generated approximately 2.4 W with a temperature difference of 150 °C. The results show that the payback period of the system was 0.74 year, when compared with batteries supplying power to a 1.8 W load with an annual operating time of 365 h.

To improve the cooling performance using natural convection only, an alternative was considered by Mastbergen and Willson [55] that uses additional draft from the chimney of the stove. The design is shown in Figure 2.13. To maintain a large temperature difference between hot and cold sides of the module, two heat exchangers are required on each side. The fluid on both sides of the module was air. Maximum temperature was operated with the hot side temperature up to 250 °C. The air was used to cool the cold side of the thermoelectric module to the ambient air temperature using natural convection.

The cold air travels up the chimney after passing through the cold sink and was further heated by the chimney. A fan 1.3 W was used to increase the power output of the system (forced convection).

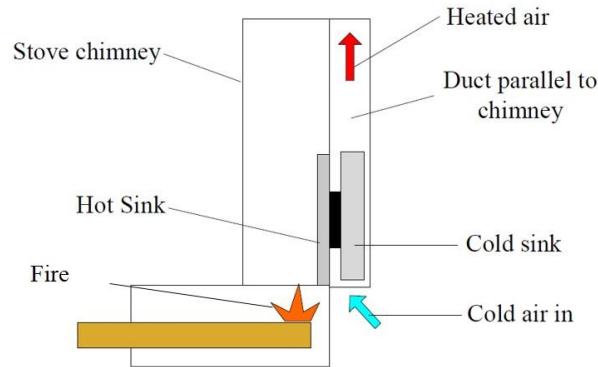


Figure 2.13: Setup for natural convection operation [55].

Natural convection alone on a heat sink was not sufficient for the size of the system. Even with the larger extrusion heat sinks available, the thermal resistance is still too high to achieve the target system power. The best performance was achieved when the fan was attached, with an output power of at least 3.8 W and was used to power a high intensity light emitting diode (LED).

2.4 Desalination as a solution to the drinking-water problem

Energy consumption is one of the biggest difficulties that desalination faces. Although it has been around for hundreds of years, desalination still consumes too much energy as shown in illustration Figure 2.14. Desalination is a process that separates dissolved solids (generally salts) from a saline water source to produce fresh water, driven by an evaporative process (thermal distillation) or a mechanical filtration (membrane separation) process [56-58]. The number of desalination systems has increased continuously in recent years with a worldwide daily production totalling 66.4 million m³ of desalinated water in 2010, 71.9 million m³ in 2011, 320 million m³ in 2014 and 1800 million m³ in 2016 [59]. Water conservation is a crucial part of the overall global water

strategy. Desalination is the most promising solution to supply some remote regions with fresh water [60]. Production of fresh water requires energy, which is currently being provided by 84% fossil fuels (55% petroleum products and 29% coal).

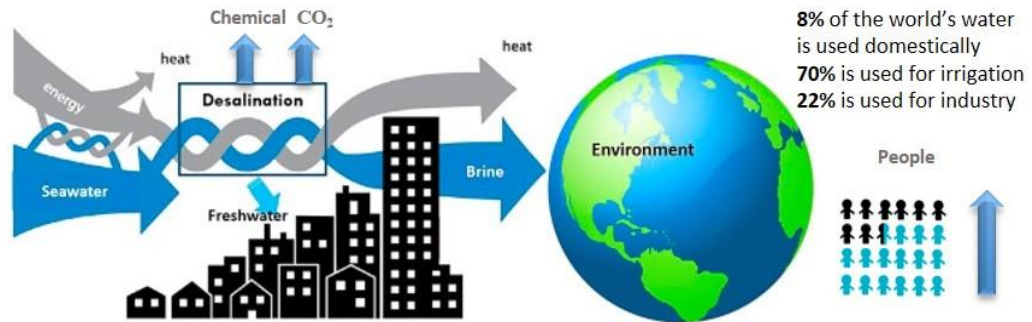


Figure 2.14: Energy–water–environment relationship through desalination for the world [56].

2.5 Water desalination technologies

A seawater desalination process separates saline seawater into two streams: a fresh water stream containing a low concentration of dissolved solids and a concentrated brine stream. This process requires specific forms of energy to desalinate, and utilizes several different technologies for separation. A variety of desalination technologies have been developed over the years on the basis of phase change and non-phase-change techniques [61]. The classifications of the desalination technologies used in the industry are described below.

2.5.1 Classifications of the desalination technologies

Desalination technologies are grouped as thermal distillation (phase-change) and membrane desalination (non-phase-change). These are further divided into subgroups. The main thermal distillation technologies are multi-stage flash (MSF), multi-effect distillation (MED), vapour compression (VC) and still distillation (SD). The main membrane technologies are reverse osmosis (RO) and electro-dialysis (ED) as shown in

Figure 2.15. The principles of these desalination technologies are described briefly as follows:

- Thermal distillation (phase-change) processes involve heating the feed water at the operating pressure to produce water-vapour, and condensing the vapour to fresh water.
- Non phase-change processes involve separation of dissolved salts from the feed waters by mechanical, or electrical or chemical means such as using a membrane as a barrier to stop the dissolved salts but filter through the fresh water.
- Hybrid processes involve a combination of thermal and membrane processes. Examples include: membrane distillation (MD); reverse osmosis combined with MSF or MED processes [62-64].

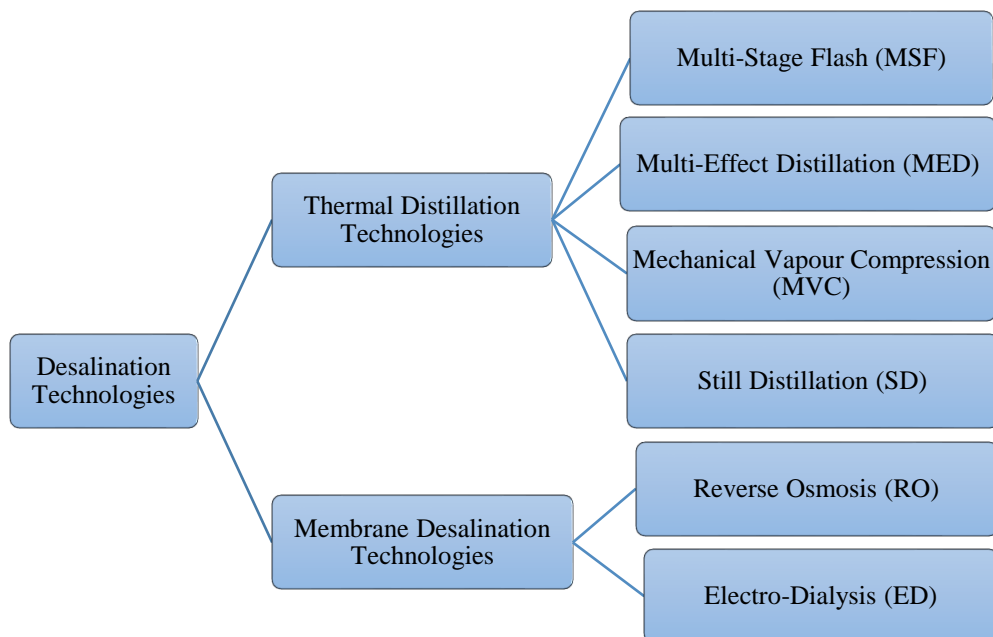


Figure 2.15: Classifications of the desalination technologies.

2.5.2 Conventional desalination processes

2.5.2.1 Multi-Stage Flash (MSF)

The MSF distillation is an energy-intensive process that requires both thermal and electrical energy. The thermal energy is in the form of low-pressure drain steam (1 to 3

bar) for the feed-brine heating, and medium-pressure steam for the ejectors to generate the required vacuum in different sections of the unit. MSF consists of a series of spaces called stages. Each stage has different pressure corresponding to the boiling point of water. The brine enters at a temperature above the boiling point of the stage and a small fraction of the brine water boils (flashes) to steam to decrease the temperature until an equilibrium is reached. The total energy consumption of the MSF ranges between 19.6×10^{-6} and 27.3×10^{-6} kWh/mL of distilled water. MSF processes are used for desalination of seawater. Figure 2.16 shows a schematic diagram of the MSF unit [65].

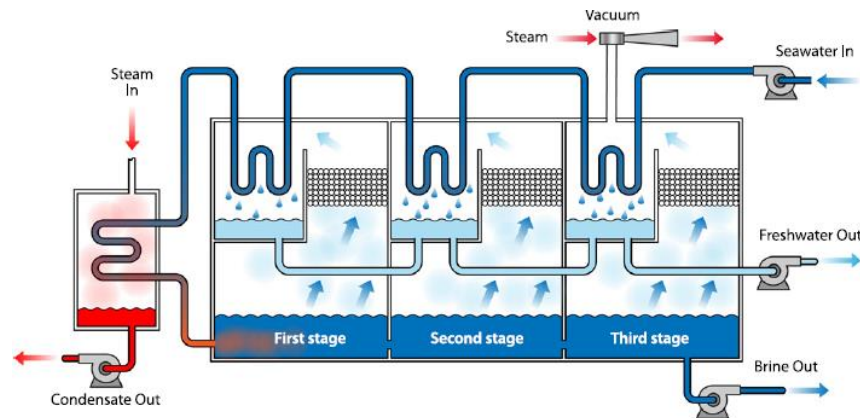


Figure 2.16: Schematic diagram of MSF unit [65].

2.5.2.2 Multi-Effect Distillation (MED)

The MED process consists of a series of stages or effects (usually from 2 to 16) that are maintained at decreasing levels of pressure and temperature from the first hot stage to the last cold stage. Each stage consists of a horizontal tubes bundle. The top of the bundle is sprayed with the sea water and flows down from the tubes by gravity. Thermal energy comes from a fossil-fuel boiler, power-plant waste heat, solar, or other sources to increase the brine temperature of the first stage to around 70 °C. This evaporates some of the brine inside the stage that is kept at low pressure. The total energy consumption of the MED units ranges between 14.5×10^{-6} and 21.5×10^{-6} kWh/mL of distilled water. Figure 2.17 shows a schematic diagram of the MED unit [65].

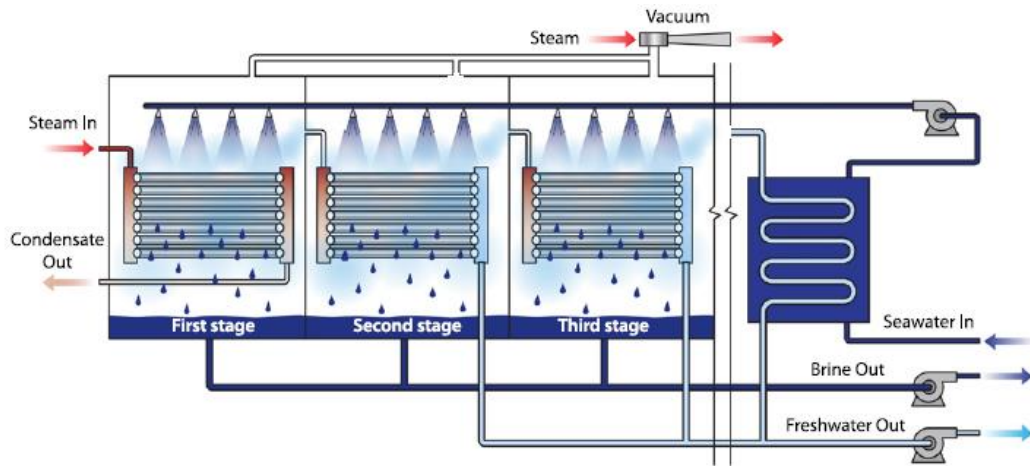


Figure 2.17: Schematic diagram of MED unit [65].

2.5.2.3 Vapour Compression (VC)

Distillation plants using vapour compression rely on the heat generated by the compression of water vapour to evaporate salt water, and two methods are employed mechanical vapour compression (MVC) and thermal vapour compression (TVC). The feed water enters the VC process through a heat exchanger, and vapour is generated in the evaporator and is compressed by mechanical (MVC) or thermal (TVC) means. The total energy consumption of the MVC and TVC units are $14.5 \times 10^{-6} - 21.5 \times 10^{-6}$ kWh/mL and 16.3×10^{-6} kWh/mL of distilled water, respectively. Figure 2.18 shows both types [65].

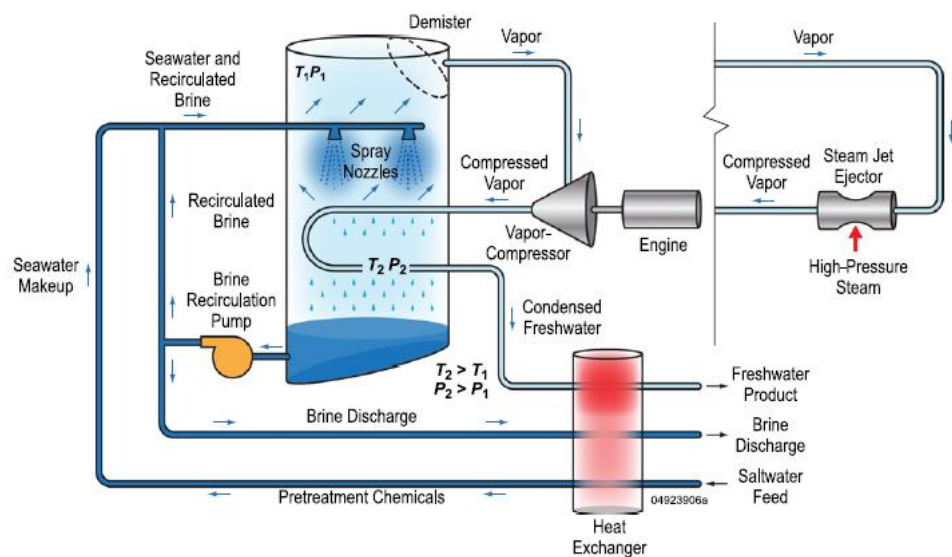


Figure 2.18: Schematic diagram of VC (MVC and TVC) units [65].

2.5.2.4 Still Distillation (SD)

Still distillation (SD) is a process of separating component or substance from a liquid mixture by evaporation and condensation. SD have been used to produce perfume, medicine, ethanol for pharmaceutical use and fresh water, generally to separate and purify different chemicals to produce distillate. The simplest standard distillation apparatus is commonly known as a solar still. Solar stills can be used for low capacity and self-reliance water supply since they can produce drinkable water by using only the solar energy. [66]. Figure 2.19 shows a schematic diagram of a basic design of a solar still.

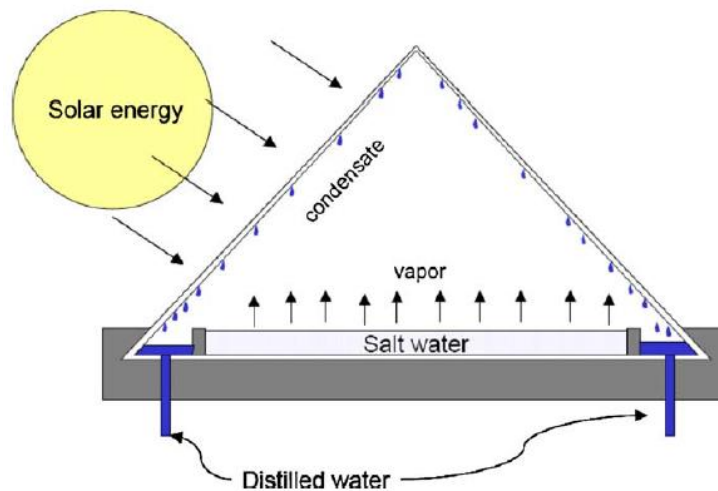


Figure 2.19: Schematic diagram of a basic solar still design [66].

2.5.2.5 Reverse Osmosis (RO)

Reverse osmosis (RO) is a form of pressurized filtration in which the filter is a semi-permeable membrane that allows water, but not salt, to pass through. This yields permeated fresh water and leaves a concentrated solution on the high-pressure side of the membrane. It has four subsystems: (1) pre-treatment, (2) high-pressure pump, (3) membrane, and (4) post-treatment. The total energy consumption of the RO units ranges between 5×10^{-6} – 15×10^{-6} kWh/mL of distilled water. Figure 2.20 is a schematic diagram of an RO system [67].

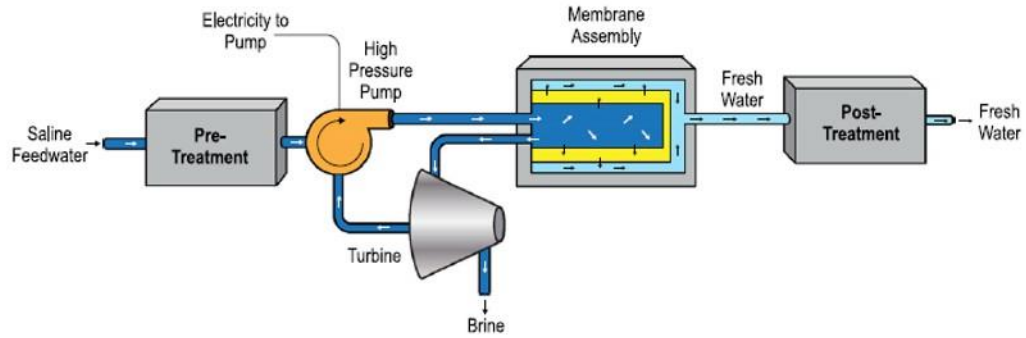


Figure 2.20: Schematic diagram of the reverse osmosis (RO) system [67].

2.5.2.6 Electro-Dialysis (ED)

Electro-dialysis (ED) is an electrochemical separation process that operates at atmospheric pressure and uses direct electrical current to move salt ions through a membrane, leaving fresh-water behind. The ED unit consists of the following sections: pre-treatment system, membranes, low-pressure circulation pump, direct current supply and post-treatment system. Figure 2.21 shows the schematic diagram of an ED unit [68].

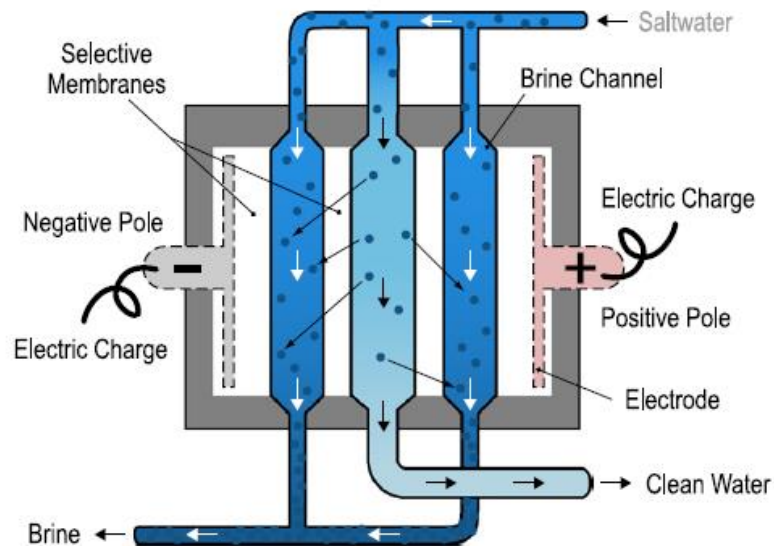


Figure 2.21: Schematic diagram of ED unit [68].

The operational principle of the ED is as follows: electrodes are connected to a direct current in a container of salt water containing a parallel membrane connected in

parallel channels. Once the salt water flows between the channels, and electricity is charging the electrodes, positive salt ions move through the cation-permeable membrane toward negative electrodes, and negative salt ions move through the anion-permeable membrane to the positive electrode, which causes to remove the salinity from the salt water and produce a clean water. The total energy consumption of the ED units ranges between $1.5 \times 10^{-6} - 7.5 \times 10^{-6}$ kWh/mL of distilled water.

2.5.3 Advantages and disadvantages of the desalination technologies

Different technologies have been used to desalinate seawater and brackish water with various performance characteristics. This section outlines current desalination technologies and compares their performance in terms of high water quality, long operation life, high energy consumption, high environmental impact and the possibility to design a system for a portable size as shown in Table 2.2.

Table 2.2: Several features of the desalination technologies.

Feature	MSF	MED	VC	SD	RO	ED
High water quality	✓	✓	✓	✓	✗	✗
Long operation life	✓	✓	✗	✓	✗	✗
High energy consumption	✓	✓	✓	✗	✗	✗
High environmental impact	✓	✓	✓	✗	✓	✓
Portable size	✗	✗	✗	✓	✓	✓

The advantages and disadvantages of the desalination technologies described above are summarised in Table 2.3 [62-68]. It is important to weigh these technologies to determine attractive process to research and investigate for development.

Table 2.3: Advantages and disadvantages of the desalination technologies.

Type	Advantages	Disadvantages
MSF	<ul style="list-style-type: none"> • High water productivity • High water quality • Leading technology for large-scale seawater distillation • Reliable technology with long operating life • Minimal pre-treatment of feed water required 	<ul style="list-style-type: none"> • Large space needed • High energy input • Inefficient with PV panel (high –voltage requirement) • High maintenance (corrosions problems) • High greenhouse gas emissions • Large amount of water needed for cooling.
MED	<ul style="list-style-type: none"> • High water productivity • High water quality • The quality of the feed water is not as important as for a reverse osmosis system • Heat energy can be sourced by combining with power generation 	<ul style="list-style-type: none"> • Large space needed • High energy consumption • Inefficient with PV panel (high voltage requirement) • High maintenance • High greenhouse gas emissions • High capital and operational costs • High water temperatures increase corrosion of the system
VC	<ul style="list-style-type: none"> • High water productivity • High water quality • The operating costs are low compared to MSF or MED especially with high salinity • The system is smaller than MSF or MED 	<ul style="list-style-type: none"> • Smaller system but not portable • Energy consumption is high • Inefficient with PV panel (high –voltage requirement) • High maintenance (Compressor) • Requires a heating source to generate vapour
SD	<ul style="list-style-type: none"> • No pollution • Low cost • Portable • Efficient with solar module • High water quality • Almost maintenance free 	<ul style="list-style-type: none"> • Low water production • A distillation process can take between two to five hours to purify one litre of water • Large glass area cover might be an attraction to bugs and insects
RO	<ul style="list-style-type: none"> • No thermal energy • Potable • Reduced energy costs compared to MSF, MED and VC systems • Automation feasible • High water productivity • No cooling water flow 	<ul style="list-style-type: none"> • Higher costs for chemical and membrane replacement • Different chemicals are used for cleaning • Mechanical failure due to high pressure operation possible • High combustion of electric energy • Complicated feed water pre-treatment • Wastes a portion of the water that runs through its system.
ED	<ul style="list-style-type: none"> • High water productivity • Very effective process to remove and purify salt concentrate as a valuable product • Applications in many commercial industries • Operational at low to moderate pressures • Low energy consumption compared with RO 	<ul style="list-style-type: none"> • Not portable • Pre-treatment and post-treatment are required to remove bacteria • Works most efficiently in low-salinity applications • Periodic cleaning of membrane required

2.6 Thermal distillation technologies

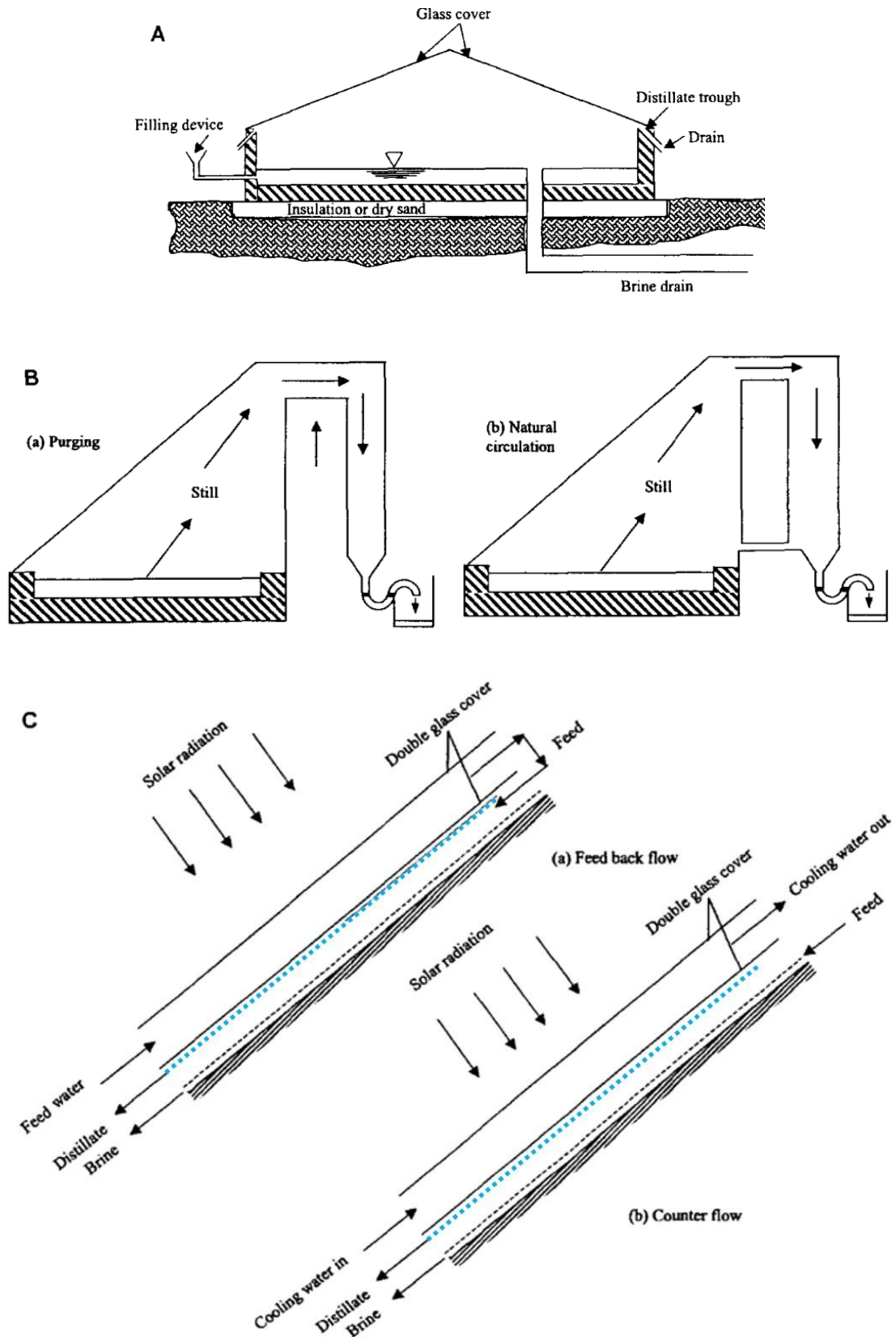
Distillation remains one of the most important thermal separation methods in the chemical processing industry. This section focuses on the aspects of design and construction of these systems. Most of them are already applied at domestic scale, while

others are at least at the stage of prototypes. The second part of this section reviews the distillation systems that combined thermal distillation with thermoelectricity. The performance of these systems is analysed in terms of water production rate and energy consumption.

2.6.1 Overview of thermal distillation system design

With no pollution and being almost maintenance free, the most common thermal process for desalination is still-based distillation. A variety of technologies are used to purify saline and brackish water in the thermal distillation systems such as using heat pipe heat exchangers with water as a working fluid, thermoelectric modules, dehumidification systems (these systems are used to remove moisture from the air and control humidity) and solar cell technologies. Several types of the thermal distillation systems employed these technologies and will be described in detail in this section.

Solar methods are well-suited for the arid and sunny regions of the world, such as the Arabian Gulf countries, the southwestern region of the US, and the southwest coast of South America. A number of thermal distillation systems have been developed as shown Figure 2.22. These include: A) Single basin still (double sloped); B) Single-sloped still with passive condenser; C) Cooling of glass cover by (a) feed water in feedback flow, or (b) cooling water in counter flow; D) Single and double-basin solar stills (single sloped); E) Directly heated still coupled with flat plate collector by forced circulation or natural circulation [69].



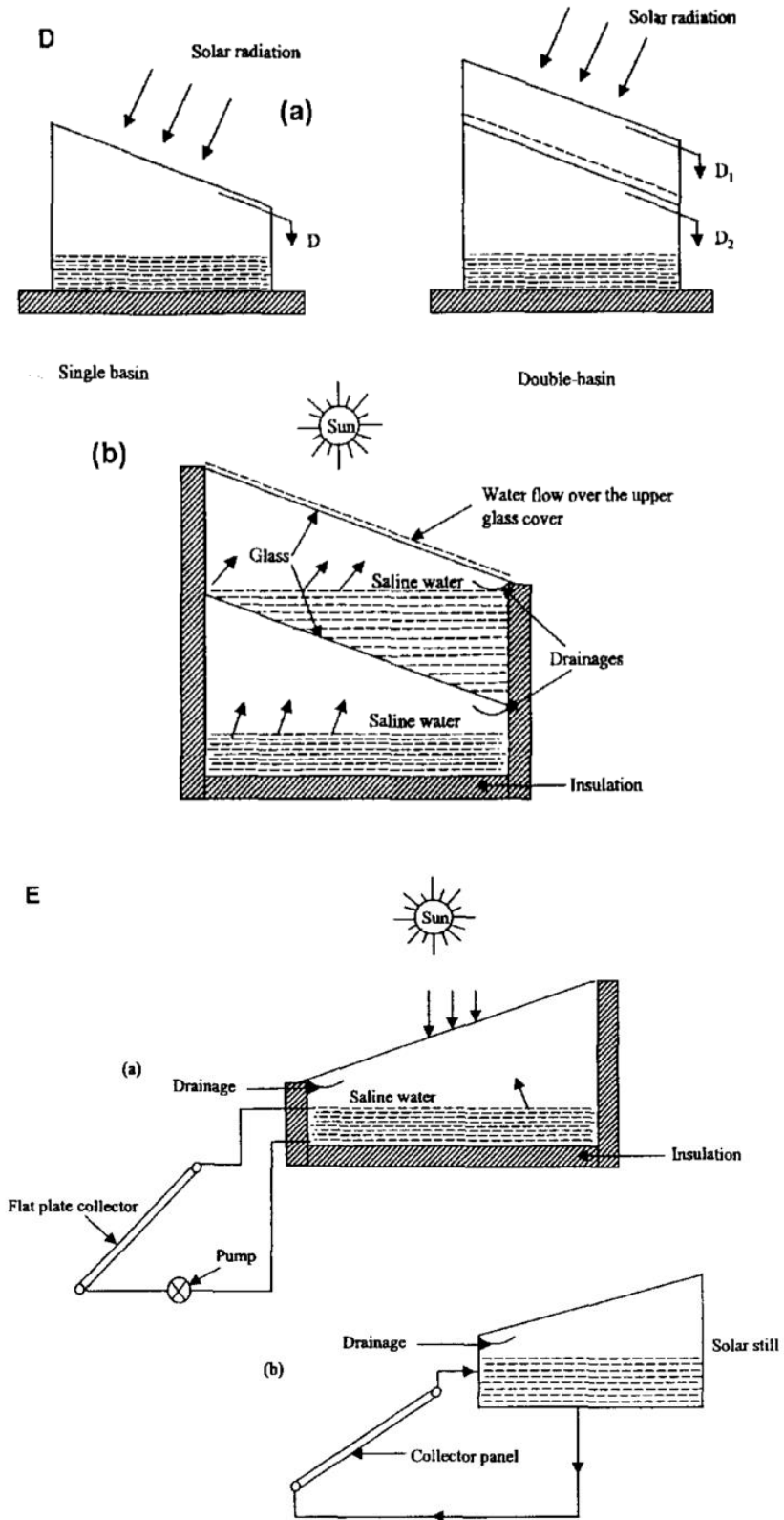


Figure 2.22: A number of reported thermal distillation systems [69].

The design of these thermal distillation systems needs to consider the following factors:

- Material and shape of the unit frame.
- Amount of sample water in the basin.
- Water surface area and the depth.
- Inclination of the cooling surface.
- Volume and surface area of heat exchanger.
- Condensing area and its material.
- Volume of evaporation / condensation chamber.
- Heating and cooling methods for evaporation and condensation processes.
- Sample water feeding and freshwater collecting techniques.

Sadineni, et al. [70] designed a weir-type solar distillation unit. The aim of the design is to increase the water surface area which is exposed to the solar irradiation and to reuse unevaporated water for water production. The weir-type unit was designed and built to test under Las Vegas weather conditions and is shown in Figure 2.23. It was an inclined type still, which consists of a weir-shaped absorber plate, cover condensing glass, distillate collection trough and water circulation system. The weir-type unit was insulated to minimize any heat loss from the bottom and sides of the unit. A small pump was also used to return the unevaporated water to the top tank. The water productivity with the double and single pane glass covers was approximately 2.2 L/m² and 5.5 L/m² per day respectively, measured in the months of August and September. Mathematical models were devised for hourly productivity both single and double pane glass covers and these were compared with the experimental results. The measured values of electrical conductivity and pH at 25 °C of water temperature were 300 μS/cm and 7.08 respectively.

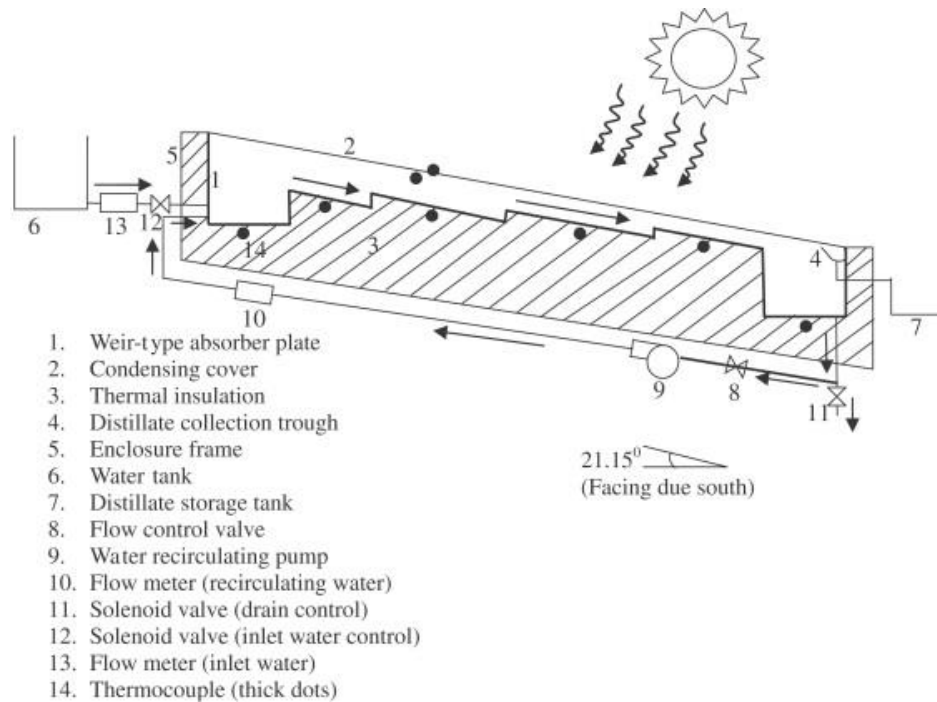


Figure 2.23: Schematic of the weir-type distillation unit and its components [70].

Kumar and Tiwari [71] designed and tested a new hybrid photovoltaic/ thermal distillation system. A photovoltaic system is used to generate electricity to power a pump and to increase water temperature in the basin, enabling the system to be self-sustainable. They considered two methods of water-heating: 1) a passive solar still where the sample water is heated directly by solar irradiation and 2) a hybrid active solar still where the sample water is heated directly by solar irradiation and indirectly by heat dissipation from the back of photovoltaic panel. The active solar still uses the otherwise wasted thermal energy of the photovoltaic system for water heating as shown in Figure 2.24. The experiments were conducted with different water depths for various running duration of the pump. The results obtained from this work show that the daily water production of the hybrid active solar still is 3.5 times that of the passive one. The power consumption is reduced by 43% when the running period of the pump was reduced from 9 to 5 hours daily. The maximum distillation yield of the hybrid active solar still was 0.68 L/m²h.

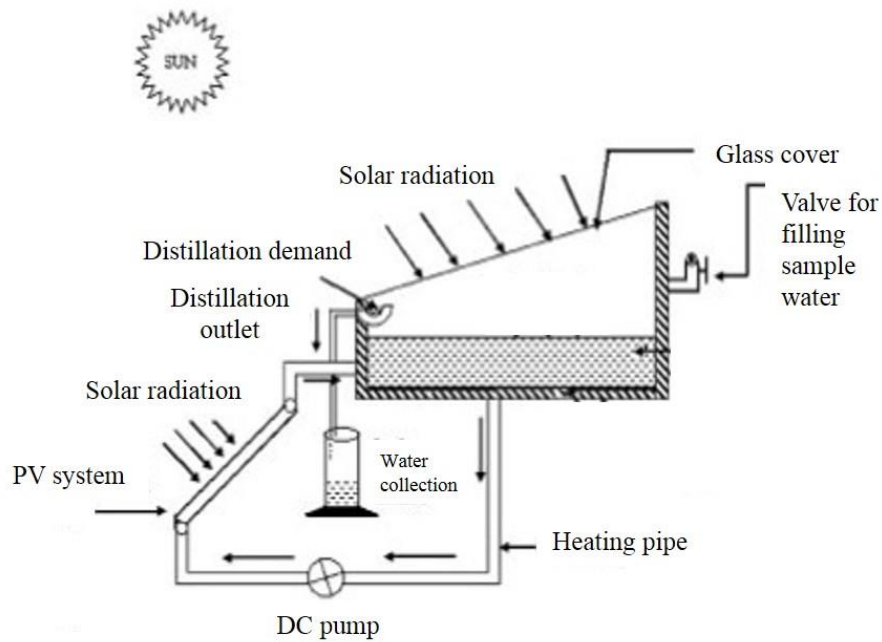


Figure 2.24: Schematic diagram of an integrated hybrid PV active solar still [71].

In thermodynamics, the thermal distillation systems depend on evaporation and condensation processes, the rates of which mainly rely on convective heat transfer. The rate of these processes change with the type of fluid, interface area, heat transfer coefficient and temperature difference between the fluids [72 - 76].

Dwivedi and Tiwari [77] evaluated the internal heat transfer coefficient of single and double slope passive solar stills in summer as well as winter seasons for three different water depths 0.01 m, 0.02 m and 0.03 m using various thermal models. The experimental validation of water distillation using different thermal models was carried out for a composite climate. The composite climate is a hot and dry climate that covers the central part of India (New Delhi). The cross sectional view of single and double slope passive solar stills are shown in Figures 2.25 and 2.26. The authors concluded that the average annual value of the internal heat transfer coefficient for single and double slope solar stills is $8.837 \text{ W/m}^2\text{K}$ and $8.19 \text{ W/m}^2\text{K}$, respectively. The annual output of the single slope solar still is 499.41 L/y , compared to the double slope solar still of 464.68 L/y .

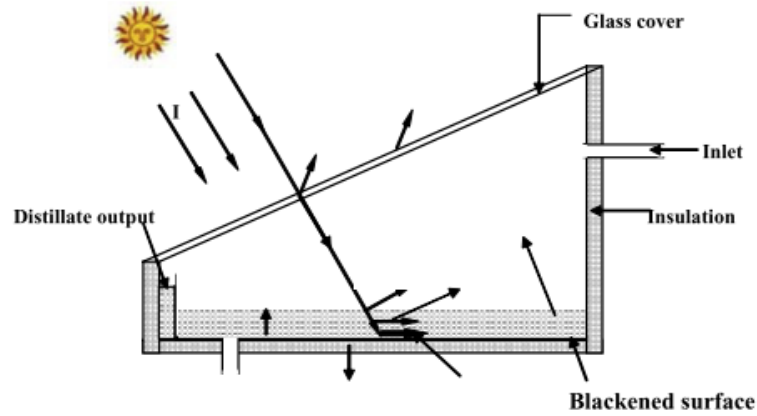


Figure 2.25: Cross-sectional view of a single slope passive solar still [77].

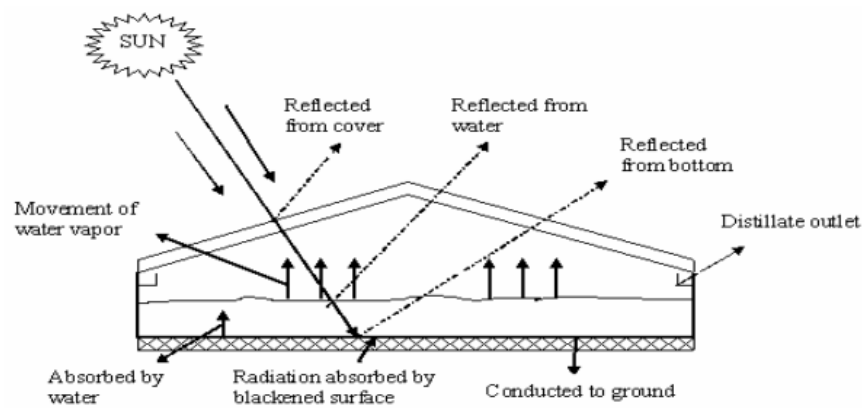


Figure 2.26: Cross-sectional view of a double slope passive solar still [77].

2.6.2 Integration of thermoelectric and water distillation systems

Recently, many research [78-103] have been made to enhance the performance and productivity of thermal distillation systems using thermoelectric devices. They reported the benefits of integration of thermoelectric technology with distillation systems for water production.

Rahbar and Esfahani [78] designed a portable thermoelectric solar still. A thermoelectric module was used to enhance the temperature difference between the evaporating and condensing zones. A schematic diagram of the still is shown in Figure 2.27. The bottom side of the solar still was made from black Plexiglas to maximise the absorption of solar radiation. The condensing part consisted of an inclined and horizontal

region. The inclined region uses the clear Plexiglas with thickness of 6 mm and was positioned at a 40° angle to the horizontal plane. In the horizontal roof region, there was an aluminium plate cooled by a thermoelectric module. The heat from the hot side of the thermoelectric module is dissipated through a heat-pipe enhanced heat exchanger, which is cooled by forced air from a fan of 1.9 W. A PV panel was used to drive the fan and the thermoelectric module. Measurements of solar intensity, wind velocity, ambient temperature, water production and temperature of the thermoelectric module, water, walls and heat pipe were investigated in the climate conditions of Semnan in Iran which were almost constant for 5 days. The results show that the temperature of the cold side of thermoelectric module was lower than wall temperature. So by using a thermoelectric module, a higher temperature difference was achieved. The integration between the heat pipe and the thermoelectric module was used to increase the water production. The maximum water productivity was $280 \text{ mL/m}^2/\text{day}$ and the maximum daily efficiency of the still (The solar still daily efficiency is the ratio of the summation of energy used for water production to the summation of total solar radiation rate fall on the still) was 7 %.

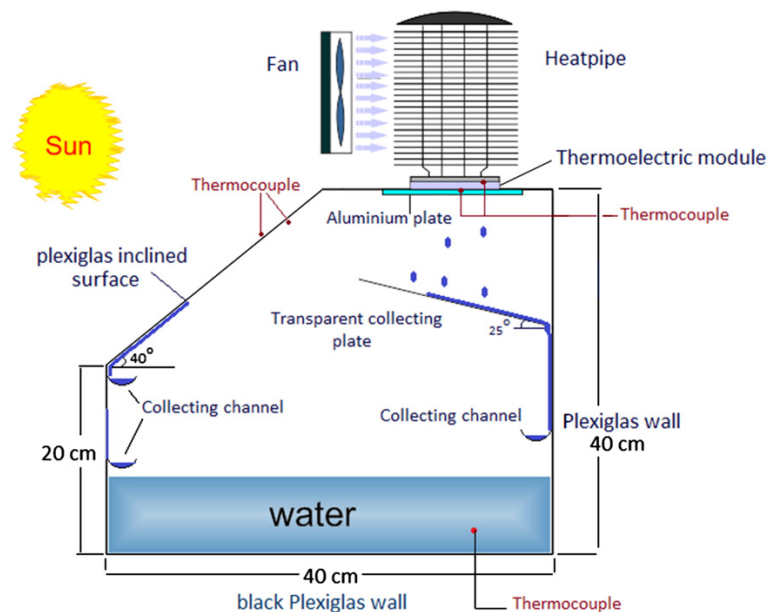


Figure 2.27: Schematic diagram of the portable thermoelectric solar still [78].

Esfahani, et al. [79] constructed a portable active distillation unit for water production. In this study, several approaches were employed in order to increase the water evaporation rate including a solar collector, black wool and water sprinkling system. A thermoelectric cooling device was used to enhance water condensation. The solar unit, a portable parabolic solar collector (40 cm × 24 cm plane area), was made from Plexiglas of 10 mm thick. The distillation unit consisted of evaporating and condensing zones and a small DC pump was fixed at the bottom of the evaporating zone. The pump delivered water to a portable parabolic solar collector which focused the solar radiation on to a copper tube frame in the collector as shown in Figure 2.28 b and c. The results of the study concluded; 1) the maximum efficiency of the unit was 13% in the winter season, 2) the cost of adding a thermoelectric cooler was low, but using Plexiglas material increased the cost of the whole unit and 3) the rate of daily productivity of the unit in 9 days of experiments was 1.2 L/m².

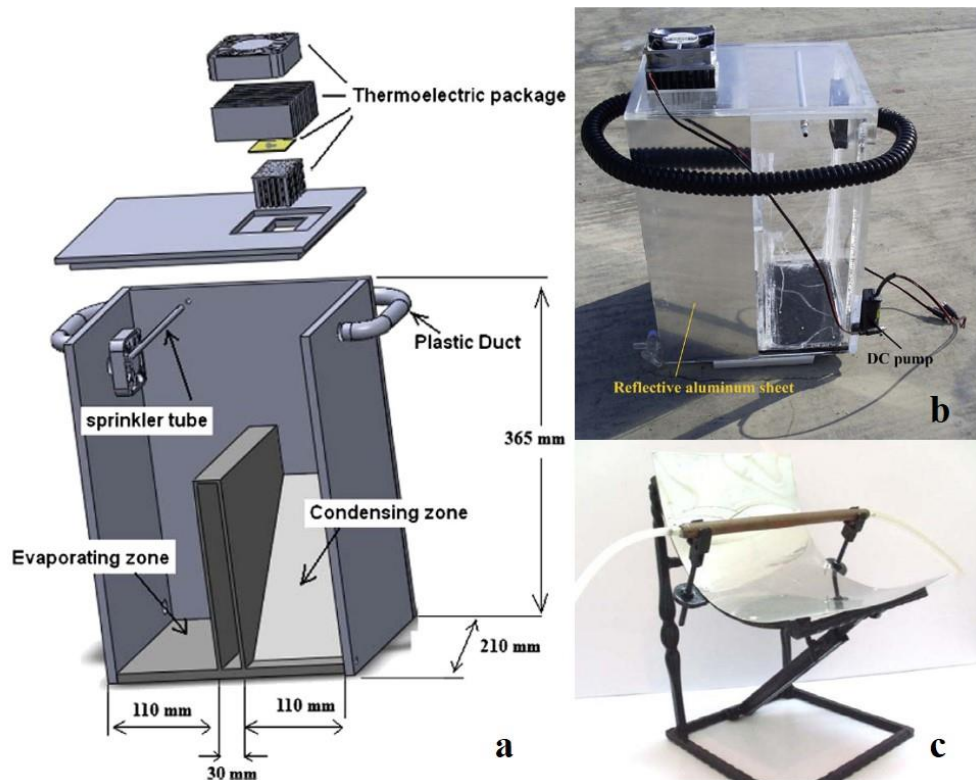


Figure 2.28: a) schematic drawing of the distillation unit, b) photo of the still and c) solar unit [79].

Rahbar, et al. [80] designed, fabricated and tested a novel asymmetrical solar still utilizing a thermoelectric cooler. The study was a further investigation of the authors' previous work on evaluating the productivity of portable solar stills using thermoelectric modules [78, 79]. Three thermoelectric modules (TEC-12708) were mounted on an aluminium plate, which serves as a condenser and was cooled by the thermoelectric modules. Thermal silicone paste was used to reduce the thermal contact resistance between the aluminium plate and the thermoelectric modules. The hot side of the thermoelectric modules were attached to a heat sink to dissipate heat through forced air convection by three fans of approximate 2 W each, which were located outside of the solar still (see Figure 2.29 a and b). The minimum and maximum daily rates of water production of the system were approximately 225 and 500 ml for solar intensities of 20,500 and 25,500 J/m², respectively.

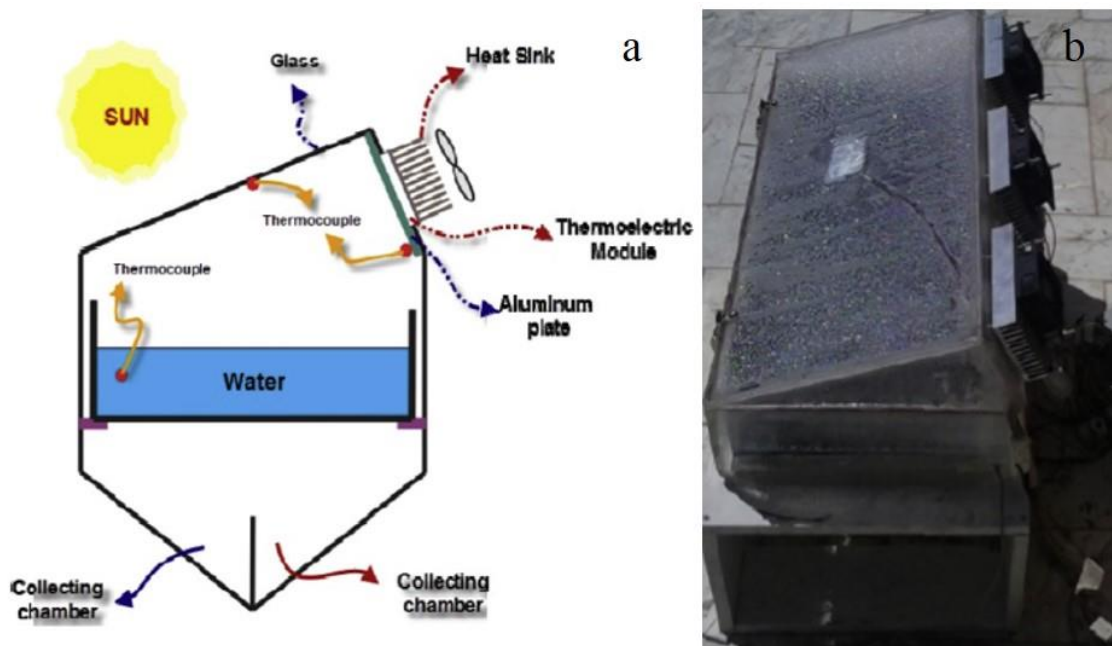


Figure 2.29: a) schematic drawing of the asymmetrical solar still and b) photo of the still [80].

Milani et al. [81] investigated theoretically the capability of using thermoelectric coolers in a dehumidification system to condense air in high humidity conditions and

provide fresh water. The calculations were represented using a psychrometric chart (A psychrometric chart is a graphical representation of the physical and thermodynamic properties of air such as dry bulb temperature, wet bulb temperature, humidity RH , enthalpy, and air density) at the inlet and outlet air-flow of the thermoelectric dehumidification system as shown in Figure 2.30. The amount of condensed water, the power required and the total cost were estimated. The effects of differences in relative humidities on saturation temperature, power consumption, water productivity and the cost of generated water were also investigated. The key results of this study show that the cost of generated water was estimated to be approximately 82 $\$/\text{m}^3$, which depends on climate conditions and energy cost (the price of energy was fixed at 0.1 $\$/\text{kWh}$) and responsible for more than 95% of the total cost per m^3 .

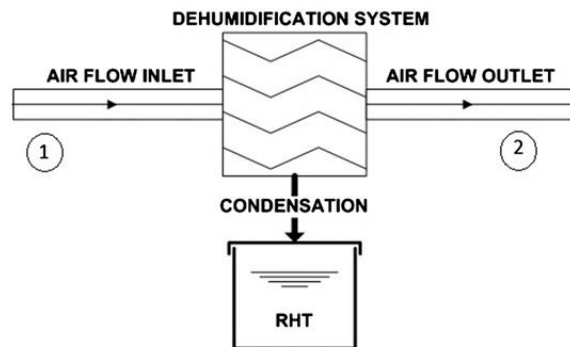


Figure 2.30: Schematic of the air dehumidification process [81].

Jradi et al. [82] studied the integration of thermoelectric and photovoltaic systems for air dehumidification and fresh water production. Integration between thermoelectric and photovoltaic systems are efficient for conversion solar energy into electric energy. Figure 2.31 shows a solar distiller that has a thermoelectrically cooled channel powered by a photovoltaic panel.

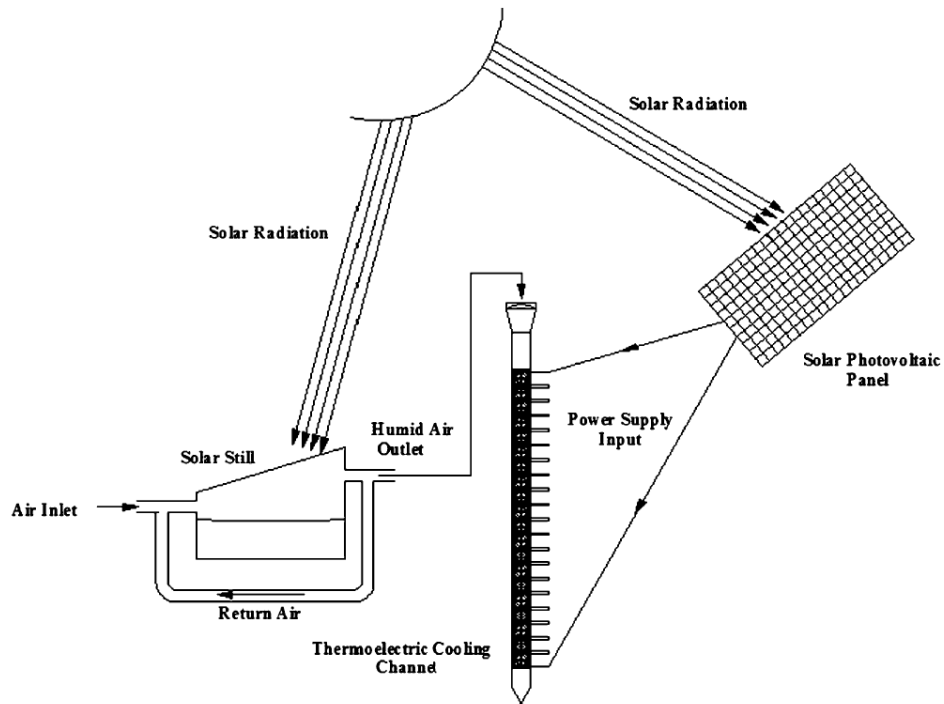


Figure 2.31: Schematic diagram of integrated photovoltaic-thermoelectric dehumidification system [82].

The unit consists of three key components: thermoelectrically cooled channel, solar panel and solar distiller. The water production of this integrated system was 10 L/day, using five thermoelectric cooling channels, which have a length of 1.2 m and an area of $(0.07 \times 0.5) \text{ m}^2$. The area of the solar distiller is 1.2 m^2 that recirculates the air at a constant mass flow rate of 0.15 kg/s. The optimal electrical current input to the thermoelectric modules varies depending on the months and it was 2.2 A in June, 2.1 A in July and 2 A from August to October.

Atta [83] built and tested a solar water condenser using thermoelectric coolers for high humidity environments such as places close to the sea, where water can be condensed from the ambient air. The system consisted of cooling elements, a heat exchanger and an air circulation unit as shown in Figure 2.32. A solar panel configured for high current output powers the cooling elements by means of a controlling circuit.

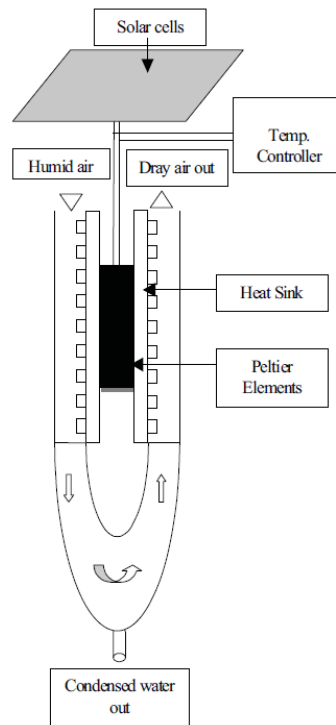


Figure 2.32: Diagram of the water condensation system [83].

The solar cells used in this system have an output voltage of 12 V with a maximum output power of 120 W, which is able to supply enough power to three 40 W Peltier modules connected in parallel. Each Peltier module has a dimension of 4 cm x 4 cm x 0.8 cm, a maximum current of 3.6 A and a maximum temperature difference of 87 °C. Applying this system in a high humidity region such as Yanbu, which is a major Red Sea port in the Al Madinah province of western Saudi Arabia, it produced almost 1 litre of water per hour during day-light which can be used for irrigation.

Yıldırım et al. [84] investigated experimentally the possible use of a novel portable desalination system. The system is based on a humidification–dehumidification principle on small-scale systems. The principle of the humidification–dehumidification processes is to produce a vapour by heating feed water then condensed it on a cold surface. The humidification–dehumidification technique has been used in many studies recently, because of the low-temperature energy use (geothermal, solar, waste energy), simplicity,

and low cost in installation and operation. This type of system also works at atmospheric pressure; hence it requires a small amount of energy input for circulation pumps and fans. A thermoelectric cooler (TEC) was integrated into the system to enhance the process of both humidification and dehumidification. The TEC (TEC1-12709) has a dimension of 40 mm x 40 mm x 3.4 mm. A prototype was fabricated as shown in Figure 2.33 and its performance was tested for various working conditions.

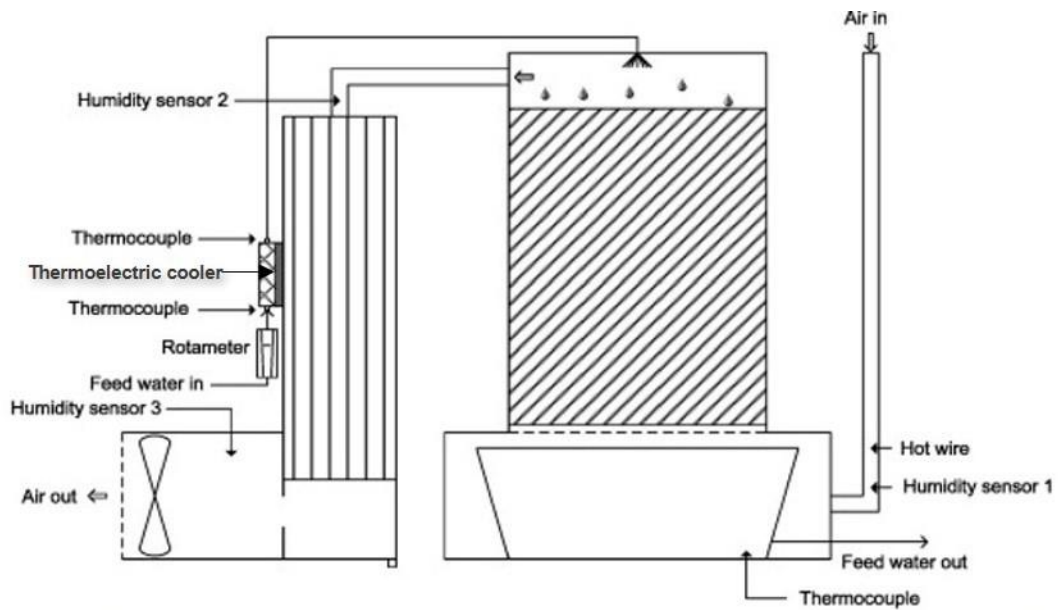


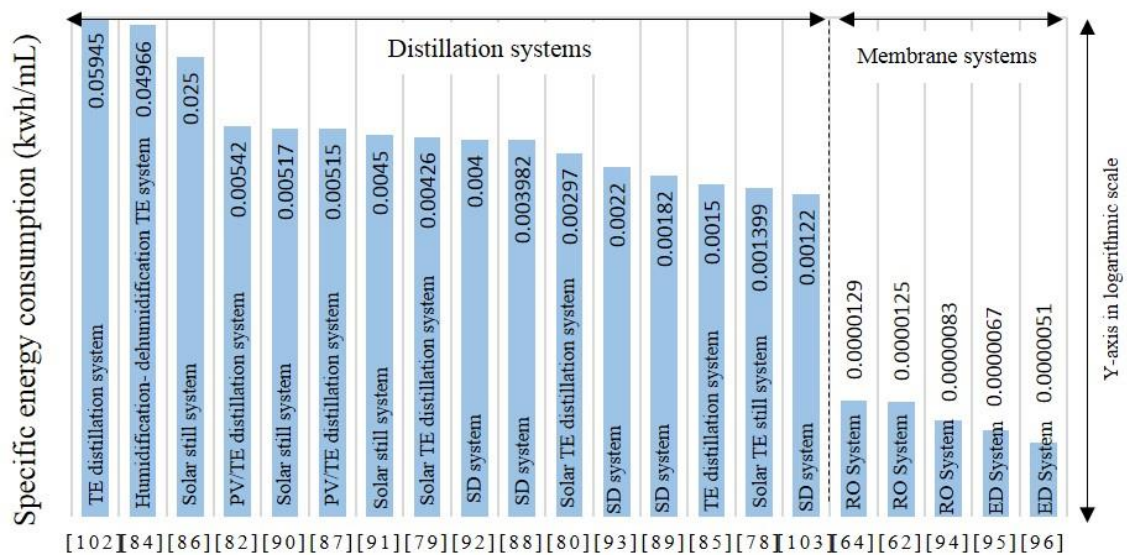
Figure 2.33: Schematic diagram of the experimental setup [84].

The effect of feed water mass flow rate and air-flow velocity on the *COP* of the thermoelectric cooler and clean water production of the system were examined. The maximum daily yield of the system and the *COP* of the thermoelectric cooler were recorded as 143.6 ml and 0.78, respectively.

2.6.3 Performance analysis of thermoelectric distillation systems

The parameters that affect the performance of the desalination systems include water productivity, energy consumption, operational and maintenance cost and environmental impact. In the design of a desalination system, the primary parameters to be considered

are water productivity and the energy consumption. A useful parameter that is directly associated with the system's economic viability is the specific energy consumption (SEC) defined as the mechanical or electrical energy required for producing one millilitre of desalinated water (kWh/mL). Figure 2.34 displays the specific energy consumption for various types of the desalination systems reviewed in this chapter. The SEC values of several systems were collected from the literature survey and converted from kWh/m³ to kWh/mL [62, 64, 85-89 and 90-96]. It can be seen that the membrane systems generally requires less mechanical or electrical energy than that of the distillation systems because both evaporation and condensation processes requires more energy.



The type of water desalination system for different references

Figure 2.34: The specific energy consumption for various types of desalination systems using logarithmic scale [62-96].

Due to high energy consumption, it is necessary to improve the efficiency of desalination processes. RO, ED, and VC systems use electricity as a main source of energy, whereas MSF, MED, and TVC systems use thermal energy as a main source and electricity as a minor source to drive the pumps. Electricity could be generated from fossil

fuel (coal, oil and gas), renewable energy, or nuclear sources. Thermal energy could be produced from fossil-fuel fired boilers, power-plant waste heat, renewable energy sources, or industrial-waste heat sources [97-101].

The comparisons among various thermal distillation systems were carried out using the data collected from this literature survey, which were normalised to an operation period of one hour and the surface area of 1 m², assuming linear scalability of these distillation processes. The results are displayed in Tables 2.4 and 2.5 [78-103].

Table 2.4: Data collected from the literature survey.

Ref.	Type of system	Experiments (hours) per day *	Max. solar radiation (W/m ²) *	Surface area (m ²) *	Daily productivity (L/m ²) *
[78]	Solar TE still	7	1000	0.034	0.5
[79]	Solar TE distillation	7	728	0.024	1.2
[80]	Solar TE distillation	11	810	0.167	3
[82]	PV/TE distillation	9	No solar	0.3	15.5
[84]	Humidification TE still	8	No solar	0.192	0.74
[87]	PV/TE distillation	12	1000	0.4375	2.33
[102]	TE distillation	24	No solar	0.036	26.91
[103]	Solar distillation	7	732	0.71	4.2

Table 2.5: Comparison of the SEC among various thermal distillation systems based on Data collected.

Ref.	Energy consumption (kWh)	Max. water production (mL)	SEC (kWh/mL)
[78]	0.034	2.43	0.01399
[79]	0.0175	4.11	0.00426
[80]	0.135	45.45	0.00297
[82]	2.8 *	516.7	0.00542
[84]	0.882 *	17.76	0.04966
[87]	0.4375	84.95	0.00515
[102]	2.4 *	40.37	0.05945
[103]	0.519	426	0.00122

The mark (*) means the data were obtained directly from the literature data. The energy consumption in (kWh) and the water production in (mL) were converted based on the solar radiation (W/m^2) and the daily productivity (mL/m^2), respectively. The specific energy consumption (SEC) in (kWh/mL) was calculated based on the corresponding energy consumption divided by the water production.

According to the valuable information provided in this chapter, Figure 2.35 illustrates the diagram of the proposed system with the gaps identified in the literature survey.

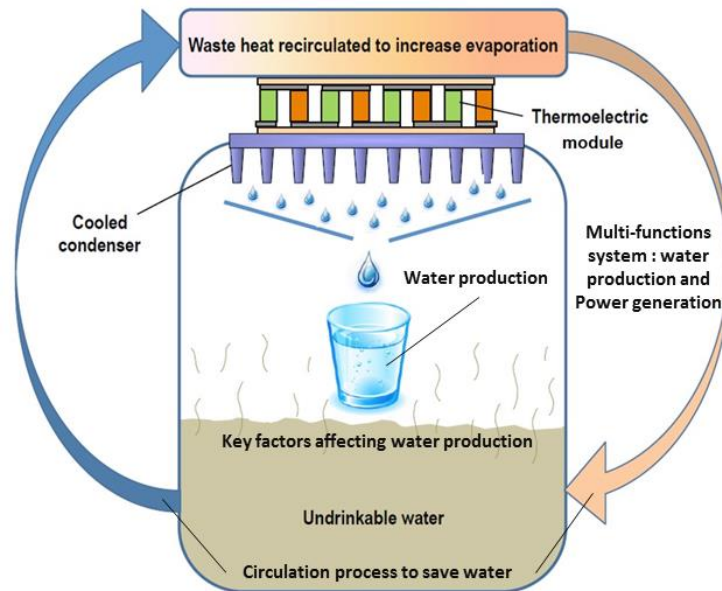


Figure 2.35: Diagram of the proposed system with the gaps identified in the literature survey.

2.7 Summary and conclusions

In order to establish a firm foundation to the present research, a literature review was conducted with a focus on the design, testing and improvement of the water desalination systems and, the potential benefits of integrating these technologies with

thermoelectricity. The applications of thermoelectric modules for refrigeration and power generation were reviewed. Previous studies showed that the geometry of the thermoelectric module, (active area, thickness and number of the thermoelements) as well as the heat exchangers on the hot and cold sides are the most important factors that determine the thermal performance of the thermoelectric module. The literature review on the water desalination systems covers their classification as well as the advantages and disadvantages of these systems. The important parameters include: water productivity, water quality, energy consumption, maintenance requirements and system portability. The data obtained from this literature survey enables the comparison of the water productivity and the energy consumption among various existing water desalination systems.

The literature survey provided valuable information on the design and construction of various water desalination systems, which are currently employed or being investigated. The thermoelectric distillation systems reviewed in this literature survey appear to only focus on improving the water productivity by using the cold side of the thermoelectric module to enhance the condensation process. The reviewed research suggested that the water productivity can be improved at lower energy consumption by using hot and cold sides of the thermoelectric module for evaporation and condensation processes.

Chapter 3

Design and Construction of the Thermoelectric Distillation System

3.1 Introduction

This chapter begins with an introduction to a proposed concept of a novel thermoelectric distillation system, followed by providing essential theoretical outlines of evaporation and condensation processes to offer insights and guidelines for design and optimisation of the proposed thermoelectric distillation system. The second part of this chapter focuses on the design and construction of the proposed thermoelectric distillation system.

3.2 Novel thermoelectric distillation system

The key design objective is to ensure that the desirable energy flow in the evaporation-condensation processes can be achieved by the appropriate incorporation of a thermoelectric module in a water distillation system. The unique feature of the thermoelectric distillation system is a novel design that utilises the heat at the hot side of the thermoelectric module which can be circulated back to the water tank to enhance water evaporation, while simultaneously using the cold side of the thermoelectric module to lower the temperature of the condenser to improve water condensation. The novel design leads to an improvement in the system performance by increasing the water productivity and significantly reduces energy consumption because the developed system doesn't require any type of heater for evaporation process. Another function of this design is to investigate the key factors that control the evaporation and condensation processes.

In order to design and construct the novel water distillation system employing a thermoelectric module, there are several requirements that should be considered:

1. *Factors affecting the distillation system*: the system will be used to study the key factors controlling the evaporation and condensation processes. The design will consider the suitability and flexibility to investigate these factors.
2. *Size of the system*: the system is likely to be used in remote areas where no electricity is available (e.g. southern Iraq). The size of the system should be portable and the power requirement could be met by using solar energy.
3. *Water quality*: fresh water produced by the thermal distillation technology is of higher quality than the membrane technology [104, 105]. Therefore, the thermal distillation technology is preferred for producing high quality water without chemical addition, which is used for cleaning in membrane technology.
4. *Heating and cooling heat exchangers*: a thermoelectric module will be used to precisely control the heating and cooling of the heat exchangers, which are connected to the hot and cold sides of the module, in order to maintain the desirable temperatures of the fluids for experimental investigations.
5. *Energy consumption*: the thermal distillation technologies require energy to heat the sample water for evaporation. The design should be aimed at reducing energy consumption and hence, lower the running cost of the system.
6. *Simplicity of operation and maintenance*: the system should be easy to use and to maintain. Maintenance is needed in order to keep the system components clean after running for long durations.

3.3 Theoretical outlines of the thermoelectric distillation processes

A theoretical model of the thermoelectric distillation system proposed in this study was developed in order to assist the design and study of optimisation of key

parameters of the thermoelectric distillation system. The model is based on a set of equations that can be used to describe the thermal distillation processes involving evaporation and condensation, heat conduction, convective heat transfer and phase change. In addition, the knowledge about the thermoelectric module for cooling and heating applications is also crucial. Figure 3.1 shows a schematic diagram of the main components, thermal processes, boundaries conditions and key design parameters of the model. The model developed will be validated in the next chapters using the experimental data of the constructed thermoelectric distillation prototype system under the steady state and transient state operation.

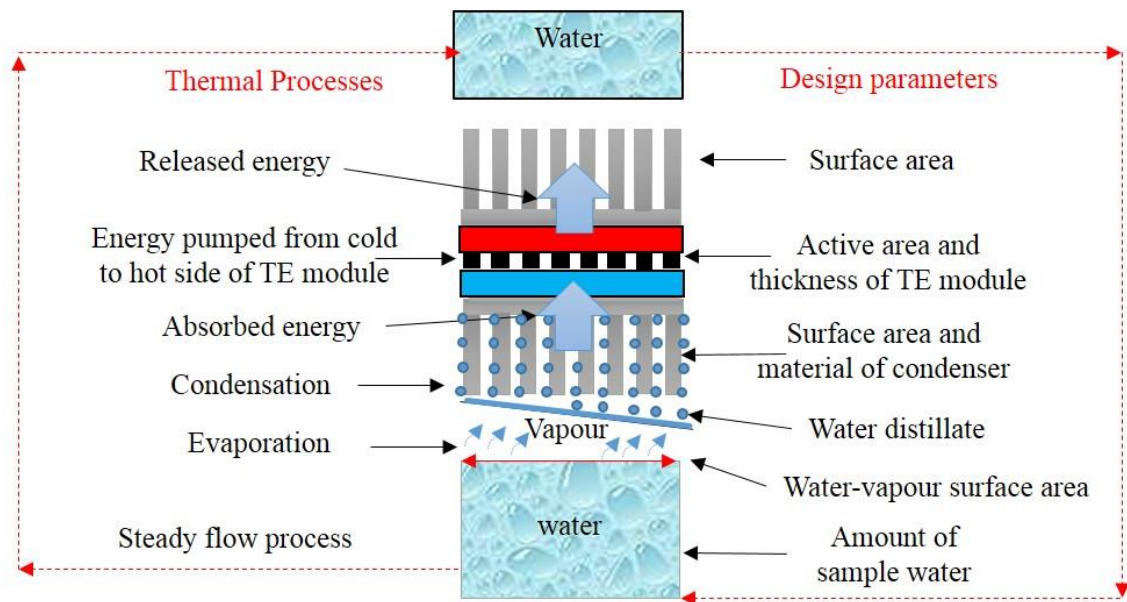


Figure 3.1: Schematic diagram of thermal processes and design parameters of the model.

3.3.1 Thermal energy required for evaporation process

In a phase – change phenomena, some molecules in the water are evaporated into the gas state when the water is heated. In order for water molecules to become gaseous, they must have enough energy to overcome attractions to their neighbouring molecules in the water. Even when water is not hot, a small number of molecules can still acquire sufficient energy to escape from the water and become a gas. Each of these phases has different thermodynamic properties such as mass, volume, temperature, pressure and

specific volume. As the water temperature increases, a larger fraction of the water molecules will be able to escape from the water-vapour interface and form a vapour. In this study, it is very important to calculate the amount of heat required for the evaporation process. The amount of heat required can be determined by estimating the mass of the produced vapour at a specific water temperature. Table 3.1 show the two-phase system problem and the solution steps to calculate the mass of each phase.

Table 3.1: The two-phase system problem and the approach for solution.

No.	Steps of the two-phase system problem and the approach for solution
1	Problem of two-phase system (calculate the mass of water and vapour under evaporation process)
2	Mathematical formulation (calculate mass fraction of each phase based on specific volume)
3	Calculate the initial properties of the system (total volume, initial mass and surface area)
4	Using the Steam Tables under specific temperature and pressure to find the properties of each phase
5	Solution of the problem (calculate the mass of vapour and water in grams)

In a system that has two phases in an equilibrium state, the mass of the vapour is increased while the mass of the water is decreased during an evaporation process in constant volume under saturation pressure. In order to determine the mass of the produced vapour and the mass of water remaining in the system, the concept of the specific volume of the phase change (water – vapour) is employed. The principle of this method is based on the Temperature – specific volume (T - v) diagram that relates the temperature of the fluid to the change of the substance's specific volume (see Figure 3.2). The T - v diagram shows the phase change at any temperature. The peak on the diagram is referred to as the critical point, which represents the critical saturation temperature. At the critical point, the liquid will instantly change to a vapour. When the temperature goes above the critical point, there will be no further phase change and all substance will become vapour. The T - v diagram can also show the mixture of liquid and vapour phases at any temperature. To find the thermodynamic properties of each phase (water and vapour), the quality mass

fraction is calculated at the specific temperature using lever rule tool. The quality defines the proportions of the water and vapour phases in the mixture. Specific volume of the two phases can be represented at the atmospheric pressure by the thermodynamic properties of water including gas, liquid and solid phases in the Steam Tables [106].

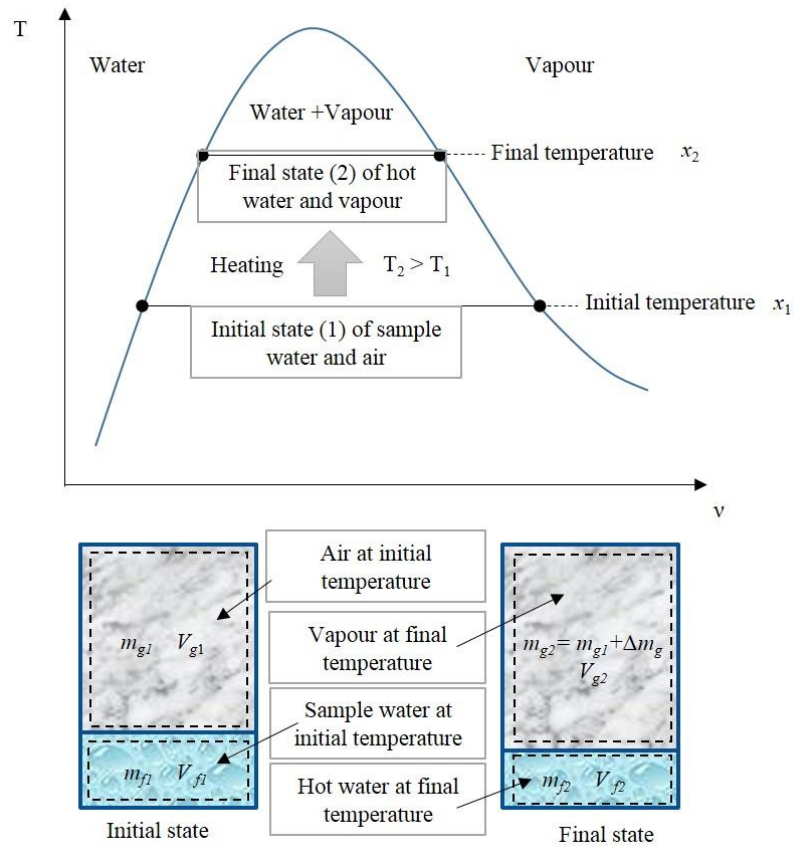


Figure 3.2: T - v diagram of water and vapour phases in a system.

Specific volume is the volume per unit mass of the water vapour (m^3/kg). At specific saturation temperature, v_f is the specific volume of the liquid, v_g is the specific volume of the vapour and v_{gf} is the difference between the specific volume of the vapour and the liquid. States 1 and 2 are defined by the values of mass m and volume V of the liquid and vapour at saturation water temperatures T_1 and T_2 respectively, where $T_2 > T_1$ since this describes a heating process.

$$v = \frac{V}{m} \tag{3.1}$$

In a closed system; mass, volume and specific volume of the mixture (*total*) are constant.

$$m_{total} = m_f + m_g \quad 3.2$$

$$V_{total} = V_f + V_g \quad 3.3$$

$$v_{total} = \frac{V_{total}}{m_{total}} = \frac{V_f + V_g}{m_f + m_g} \quad 3.4$$

The quality of the vapour x is the vapour mass fraction, which is the ratio of the vapour mass to the total mass of the mixture (liquid and gas) [107].

$$x = \frac{m_g}{m_{total}} \quad 3.5$$

This fraction can be represented as a relative humidity (RH) of vapour – water mixture, which is the ratio of the partial pressure of vapour to the equilibrium vapour pressure of water ($RH = \frac{P_v}{P_s}$). Relative humidity is normally expressed as a percentage, a higher percentage means that the air–water mixture is more humid.

Sub. (3.5) in (3.2)

$$m_{total} = m_f + x \cdot m_{total}$$

$$x = 1 - \frac{m_f}{m_{total}} \quad 3.6$$

To find v_{total} in terms of m_f and m_g , sub (3.1) into (3.3)

$$v_{total} \cdot m_{total} = v_f \cdot m_f + v_g \cdot m_g$$

$$v_{total} = \frac{v_f \cdot m_f}{m_{total}} + \frac{v_g \cdot m_g}{m_{total}} \quad 3.7$$

Rewrite equation (3.7) to read

$$v_{total} = v_f + x (v_g - v_f) \quad 3.8$$

The vapour quality can be expressed by rearranging equation (3.8)

$$x = \frac{v_{total} - v_f}{v_g - v_f} = \frac{v_{total} - v_f}{v_{gf}} \quad 3.9$$

The vapour quality and mass of the initial state (State 1) are

$$x_1 = \frac{v_{total} - v_{f1}}{v_{g1} - v_{f1}} \quad 3.10$$

$$m_{g1} = x_1 \cdot m_{total} \quad 3.11$$

When the water is heated at constant volume from T_1 to T_2 , v_{g2} and v_{f2} values are required to calculate x_2 and m_{g2} .

$$x_2 = \frac{v_{total} - v_{f2}}{v_{g2} - v_{f2}} \quad 3.12$$

$$m_{g2} = x_2 \cdot m_{total} \quad 3.13$$

The increase of the vapour mass due to the heating process is

$$\Delta m_g = m_{g2} - m_{g1} \quad 3.14$$

In water-vapour equilibrium, the specific volume increases through more liquid evaporating and more vapour being produced. During this process, heat is transferred to the system, the mass of the water is decreased while the mass of the vapour is increased. Based on the Steam Tables [106], there is a direct relationship between water temperature and specific volume of each phase at the atmospheric pressure. The mass of the produced vapour and the mass of the water remaining in the system were determined at the water temperature range 20 °C - 60 °C. The initial mass of the water is 300 grams. The vapour quality is increased when the water temperature is increased due to the evaporation process. According to equation 3.9, the increasing in the vapour quality leads to decrease in the specific volume difference between the water and the vapour (see Figure 3.3). It might be expected that the water temperature increases in the thermoelectric distillation system from $T_1 = 20$ °C to $T_2 = 40$ °C within one hour of water heating, the vapour quality

also increases from $x_1 = 0.07$ to $x_2 = 0.15$. That means the amount of water remaining in the system is 270 grams and the amount of vapour produced is 32.7 grams (based on equations 3.5 and 3.6, see Figure 3.4). Water temperature can be increased from $T_2 = 40$ °C to $T_3 = 60$ °C within further one hour of water heating. By two hours water heating, the mass fraction of the water and the vapour are expected about 63% and 37%, respectively. The amount of water remaining in the system and the amount of produced vapour will be compared with experimental data of the circulation system in Chapter Five.

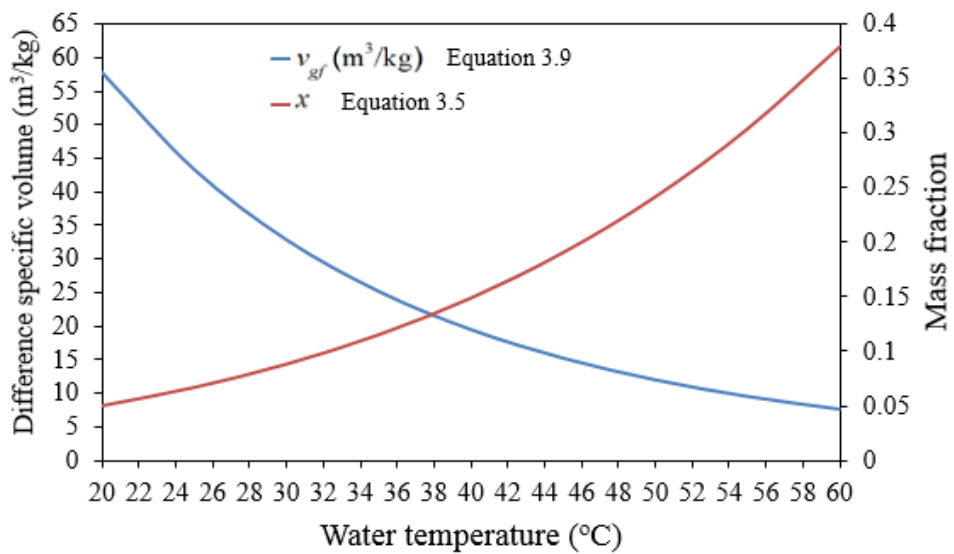


Figure 3.3: The vapour quality and specific volume difference with increasing water temperature.

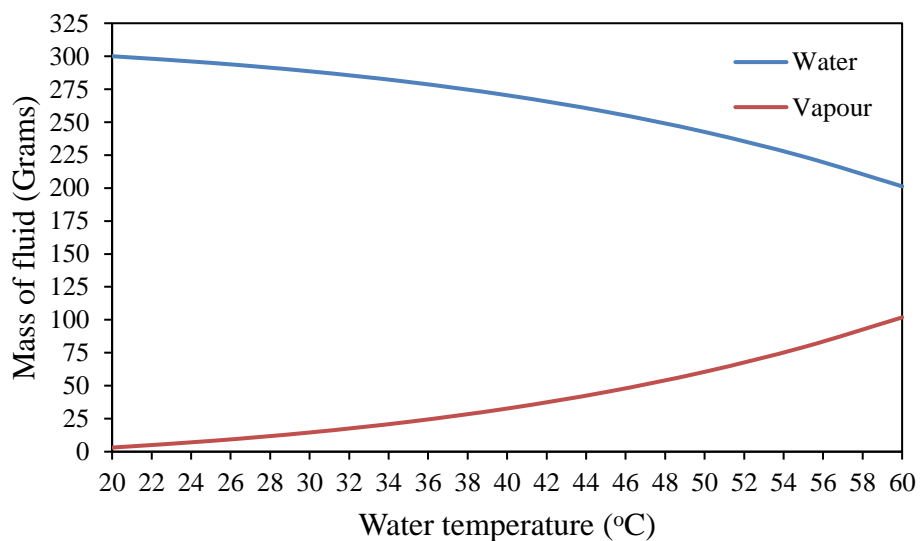


Figure 3.4: The water-vapour mass with increasing water temperature.

In evaporation – condensation processes, pressure increases due to evaporation whereas with condensation, pressure decreases [108]. However, the vapour pressure in the distillation system is assumed to be in equilibrium and equal to the atmospheric pressure. The evaporation process takes place across the water surface interface by free convection, which is caused by the effect of the density variation and temperature difference between the water and the vapour [109]. In the steady state condition, the energy required for evaporation $E_{evap.}$ is expressed as

$$E_{evap.} = \Delta m_g L_{evap.} \quad 3.15$$

Where Δm_g is the increase of the vapour mass from state 1 to state 2 in (Grams) and $L_{evap.}$ is the latent heat of evaporation (kJ/kg). The latent heat for a given water temperature is obtained from Steam Tables (for details, see Appendix A.1: thermodynamic properties of water). Using equation 3.15, the energy required to produce an amount of vapour at given water temperature is shown in Figure 3.5. Both the evaporation energy and mass of the vapour increase as water temperature increases.

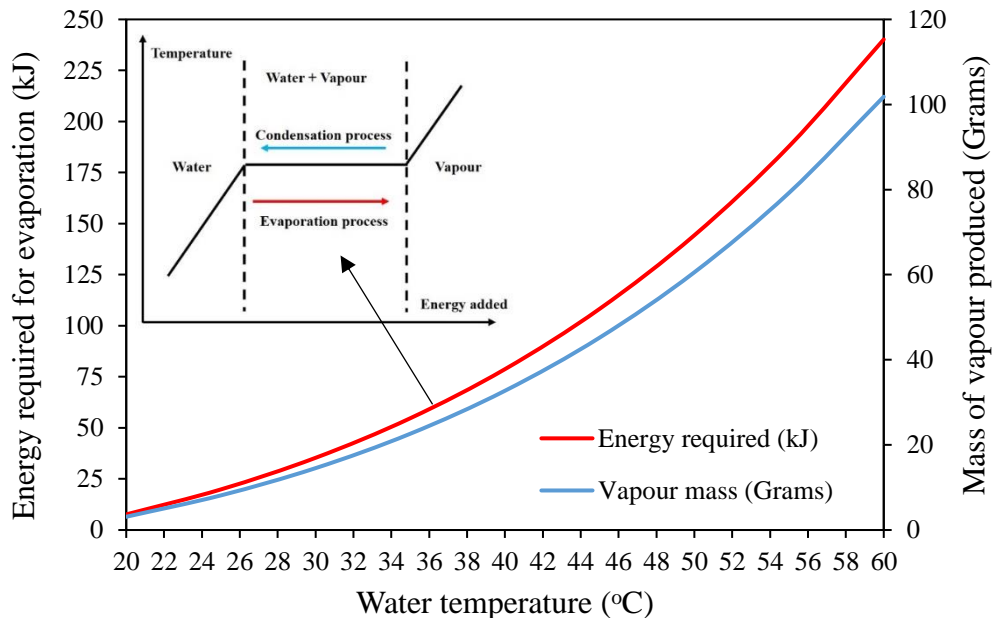


Figure 3.5: The evaporation energy as a function of the vapour mass and water temperature.

3.3.2 Rate of water condensation

Condensation occurs when the temperature of the vapour is decreased below its saturation temperature. In practice, this process usually takes place when the vapour is in contact with a cold surface. Thermodynamically, the thermal energy including the latent heat of vaporization is transferred to the cold surface and the condensate is formed. As shown in Figure 3.6, there are several features associated with the condensation. A thin layer of water condenses on the surface of the plate and flows downward under the influence of gravity. The condensate mass flow rate increases when the angle of the inclined plate θ from the vertical is decreased. The heat transfer takes place at the vapour-water interface, through a thin layer of water condensation to the cold surface, which is maintained at a temperature lower than the vapour temperature. The condensate mass flow rate increases with increasing the temperature difference between the vapour and the cold surface and with increasing the area of the cold surface [110].

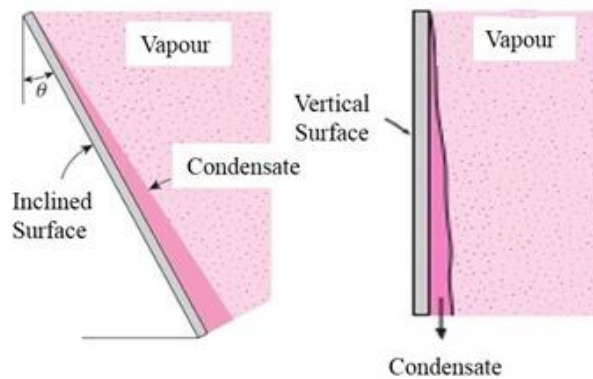


Figure 3.6: The inclined and vertical surfaces of a condenser.

In order to determine the heat transferred from the vapour to the condensation surface and subsequently the condensation rate, the following assumptions are made:

1. The thin water layer has constant properties and follows laminar flow (Reynolds number less than 1800).
2. The vapour is at a uniform temperature equal to the saturation temperature.
3. The influence of the vapour velocity and thermal boundary layers is negligible.

The heat conduction between the vapour and the thin water layer is anticipated to be much quick compared with the heat convection. Hence, the heat condensation $Q_{cond.}$ is calculated based on the convective heat transfer on the condensation surface [111]:

$$Q_{cond.} = h_l A_s (T_v - T_f) \quad 3.16$$

$$T_f = \frac{T_v + T_s}{2} \quad 3.17$$

Where h_l is the local convective heat transfer coefficient, A_s is the condensation surface area, T_v is the vapour temperature, T_s is the surface temperature of the condenser and T_f is the temperature of the thin water condensate. The condensation heat transfer in equation 3.16 depends on the following parameters:

1. Vapour heating and surface cooling processes
2. Geometry and material of the condenser surface
3. Physical properties of the vapour
4. The type of fluid flow.

Condensation is a rather complicated thermal process. There is a Nusselt's film theory to calculate the thin water condensate during the condensation process. The following correlation gives an explanation of the Nusselt theory on a vertical wall [108].

$$\dot{m}_{cond.} = \frac{\rho (\rho - \rho_v) g B \delta^3}{3 \mu} \quad 3.18$$

where ρ is the density, g is the gravity, B is a constant, δ is the water level and μ is the viscosity of the water condensate. To reduce the complexity of the film condensation process, the rate of water condensation $\dot{m}_{cond.}$ can be determined using the following correlation to reduce the complexity of the film condensation process [110]:

$$\dot{m}_{cond.} = \frac{Q_{cond.}}{L_{cond.}} \approx \frac{h_l A_s (T_v - T_f)}{L_{cond.}} \quad 3.19$$

where $L_{cond.}$ is the latent heat of condensation and obtained at a temperature T_f from the Steam Tables. Figures 3.7 and 3.8 show the calculated condensation heat flux and the rate of water condensation as a function of the temperature difference between the vapour and the thin water layer for different local heat transfer coefficients. It can be seen that both the condensation heat flux and the rate of water condensation increase with increasing temperature difference between the vapour and the thin water layer, as well as with increasing the local heat transfer coefficient. The results in the figures were calculated using the following assumptions:

1. The temperature difference between the vapour and the thin water layer is ranged between 5 °C to 20 °C.
2. The condensation surface is 0.041 m².
3. Heat transfer from the vapour to the thin water interface and to the cold surface can occur by natural and forced convection.
4. The pressure inside the system is the atmospheric pressure.

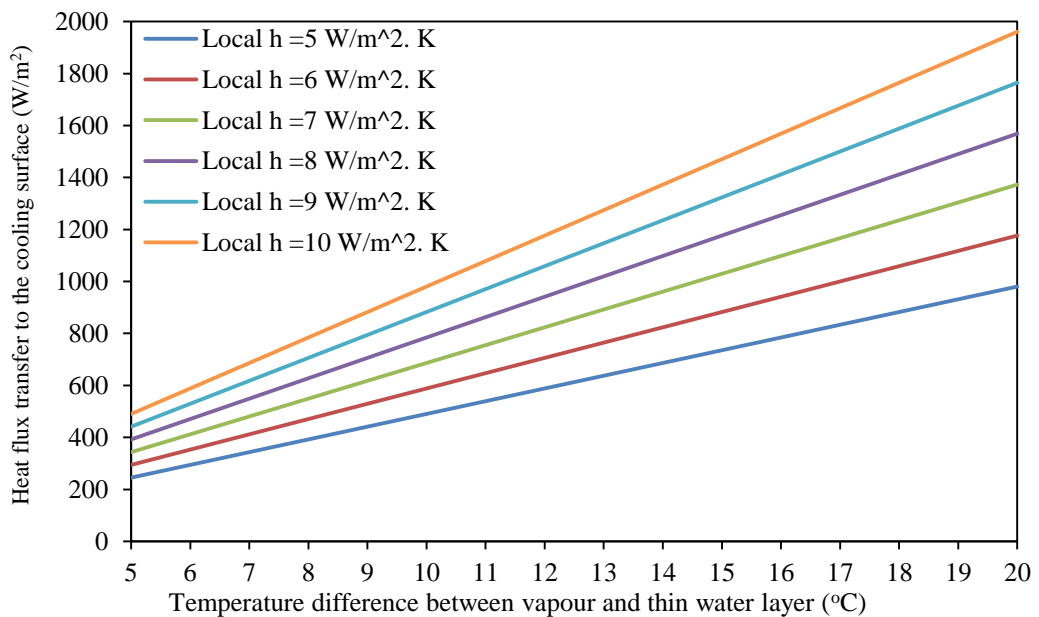


Figure 3.7: Variation of the heat flux transfer to the cooling surface as a function of the temperature difference and the local heat transfer coefficient.

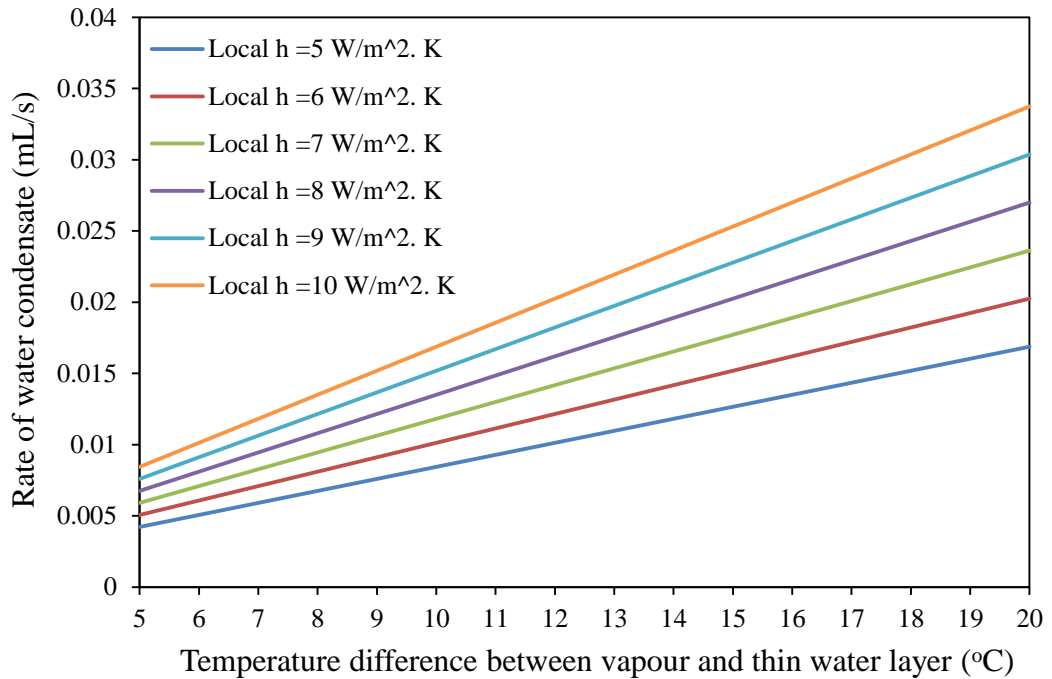


Figure 3.8: Variation of the rate of the water condensate on the cooling surface as a function of the temperature difference and the local heat transfer coefficient.

Condensation occurs when the temperature of the vapour is decreased below its saturation temperature. Practically, the process results from contact between the vapour and the cooled surfaces (fins). Figure 3.9 shows the temperature profile (from the vapour by free convection to the cold side of the thermoelectric module through the aluminium condenser by conduction and convection) which can be evaluated using the following calculations. Useful theoretical results are obtained by making the following assumptions to determine the removed heat due to the condensation process; (1) the water in the system has the thermal properties of pure water, (2) the vapour displays ideal gas behavior and it is at a uniform temperature equal to the saturation temperature of water at the water-vapour interface, (3) the water film and the vapour flows are laminar, (4) thermal conductivity of the condenser material is a constant value. Table 3.2 explains the mathematical approach to solve the heat transfer problem.

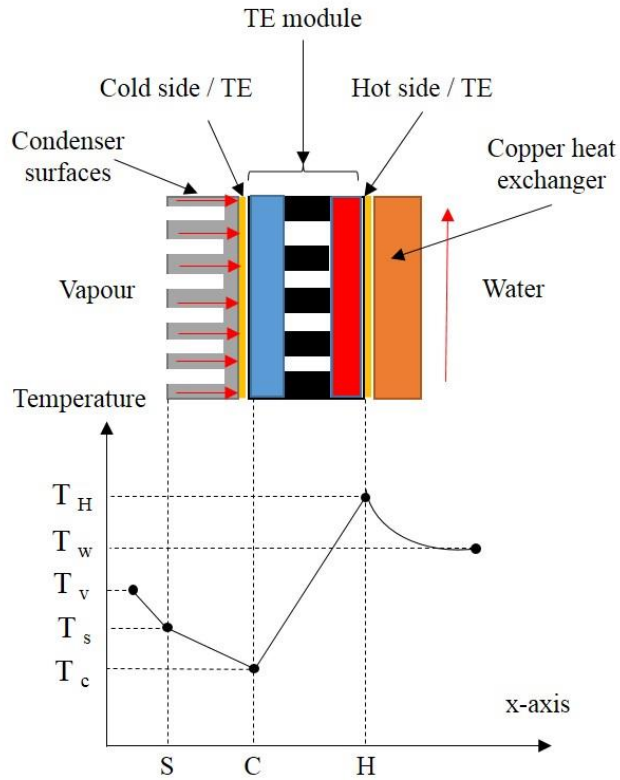


Figure 3.9: Schematic of the temperature profile in a thermoelectric assisted condenser.

Table 3.2: Solution steps of the heat transfer problem.

No.	Solution steps of the heat transfer problem
1	Conjugated heat transfer problem
2	Mathematical formulation (energy balance of the differential element)
3	General solution of the second order differential equation with constant coefficients
4	Apply the boundary conditions (evaluate the constant coefficients)
5	Solution of the problem (temperature and heat flux)

The first step is applying a heat balance condition to a differential element at one of the straight fins of the aluminum condenser, as shown in Figure 3.10.

$$q_x + dq_{conv.} = q_{x+dx} \quad 3.20$$

From Fourier's law

$$q_x = kA_c \frac{dT}{dx} \quad 3.21$$

The convection heat transfer rate expressed as

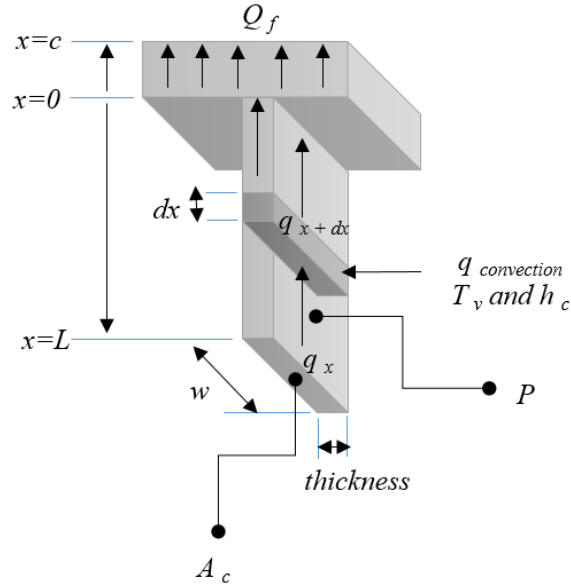


Figure 3.10: Heat balance of a straight fin of uniform cross section.

$$dq_{conv.} = h_c dA_s (T(x) - T_v) \quad 3.22$$

The conduction heat rate at $(x + dx)$ expressed as

$$q_{x+dx} = q_x + \frac{dq_x}{dx} dx = kA_c \frac{dT}{dx} + k \frac{d}{dx} (A_c \frac{dT}{dx}) \quad 3.23$$

where A_c is the cross-sectional area of the fin, dA_s is the surface area of the differential element, h_c is the convection heat transfer coefficient and k is the thermal conductivity of the fin material. Substituting equations. (3.21, 3.22 and 3.23) into (3.20)

$$\frac{d^2 T}{dx^2} - \frac{P_f h_c}{A_c k} (T(x) - T_v) = 0 \quad 3.24$$

where P_f is the fin perimeter (dA_s/dx) and $T(x)$ is a fin metal temperature, to simplify the form of equation (3.24), transform the dependent variable by defining an excess temperature $\theta(x)$

$$\theta(x) = T(x) - T_v \quad 3.25$$

$$\frac{d^2 \theta}{dx^2} - n^2 \theta = 0 \quad 3.26$$

$$n^2 = \frac{P_f h_c}{A_c k} \quad 3.27$$

where n is a constant. Equation (3.26) is a linear, homogeneous, second order differential equation with constant coefficients. The general solution is

$$\theta(x) = C_1 e^{nx} + C_2 e^{-nx} \quad 3.28$$

To evaluate the constants C_1 and C_2 , it is necessary to specify two boundary conditions

$$\text{At } x = c, \theta(x) = T_c - T_v \quad 3.29$$

where T_c is the cold side temperature of the thermoelectric module. At $x = L$, the tip of the fin, it is assumed that the rate of heat reached from the vapour by convection is equal to the rate of heat transferred by conduction

$$h_c A_c (T_L - T_v) = k A_c \frac{dT}{dx} \quad 3.30$$

where L is the fin length. Solving for C_1 and C_2 after some manipulation, the temperature distribution and heat transfer rate of the straight fin are

$$\frac{T(x) - T_v}{T_c - T_v} = \frac{\cosh n(L-x) + \left(\frac{h_c}{nk}\right) \sinh n(L-x)}{\cosh nL + \left(\frac{h_c}{nk}\right) \sinh nL} \quad 3.31$$

$$Q_f = \sqrt{h_c P_f k A_c} (T_c - T_v) \frac{\sinh nL + \left(\frac{h_c}{nk}\right) \cosh nL}{\cosh nL + \left(\frac{h_c}{nk}\right) \sinh nL} \quad 3.32$$

Equation (3.32) is the total heat transfer (W) from vapour state to the cold side thermoelectric area (assumed equal to Q_{cond} in Equation 3.16). It is governed by several factors, the cold side temperature of the thermoelectric module, vapour temperature,

convection heat transfer coefficient and the geometry of the condenser. It is a challenge to define precisely the convection heat transfer coefficient h_c . Hence, Q_f was calculated according to the experimental temperatures and geometry whilst h_c was fitted to the experimental results. The detailed derivation of the heat balance of the straight fin of uniform cross section can be found in the appendix section A.3.

3.3.3 Heating and cooling by thermoelectric module

The performance of a thermoelectric module operated in the cooling/heating mode is usually characterized by two parameters: the temperature difference between the hot side and the cold side of the thermoelectric module $\Delta T (T_h - T_c)$ and the pumping capacity at the cold side Q_c for given input voltage V and current I . In addition, the heat will be released at the hot side at the rate of Q_H . The thermoelectric cooling involves three energy conversion/transfer processes namely Joule's heating, the Peltier cooling and heat conduction [112].

The amount of heat pumped from the cold side to the hot side depends on the product of the Peltier coefficient and the current flowing through the module. This is offset by heat conduction from the hot side to the cold side, due to a temperature difference established between the hot and the cold side of the thermoelectric module. On top of this, there is Joule heat generated uniformly inside thermoelements, the half of which conducts to the hot side and the half to the cold side. Figure 3.11 shows the paths of the current and the heat through a thermoelectric leg. The electric current flows from the hot side (positive) to the cold side (negative). Heat flows from the hot side to the cold side of the leg. The released heat at the hot side and the absorbed heat at the cold side can be obtained by applying steady state energy balances for both sides of the thermoelectric module. In thermodynamics, a quasi-steady state process is a thermodynamic process (or a reversible process) that happens considerably slowly. The released energy at the hot

side and the absorbed energy at the cold side can be approximated as a quasi-steady state process by performing them very slowly. The Peltier, Seebeck and Thomson effects can be thermodynamically reversible with small temperature difference according to the second law of thermodynamics [113].

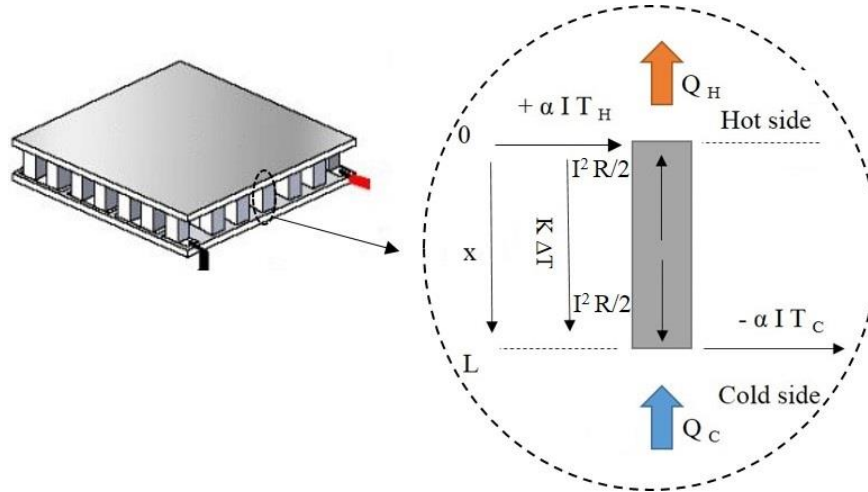


Figure 3.11: The paths of the current and the heat through a thermoelectric leg.

A photograph of a leg of the thermoelectric module, which utilises bismuth telluride materials (showing length and width of one side of a leg) is shown in Figure 3.12.

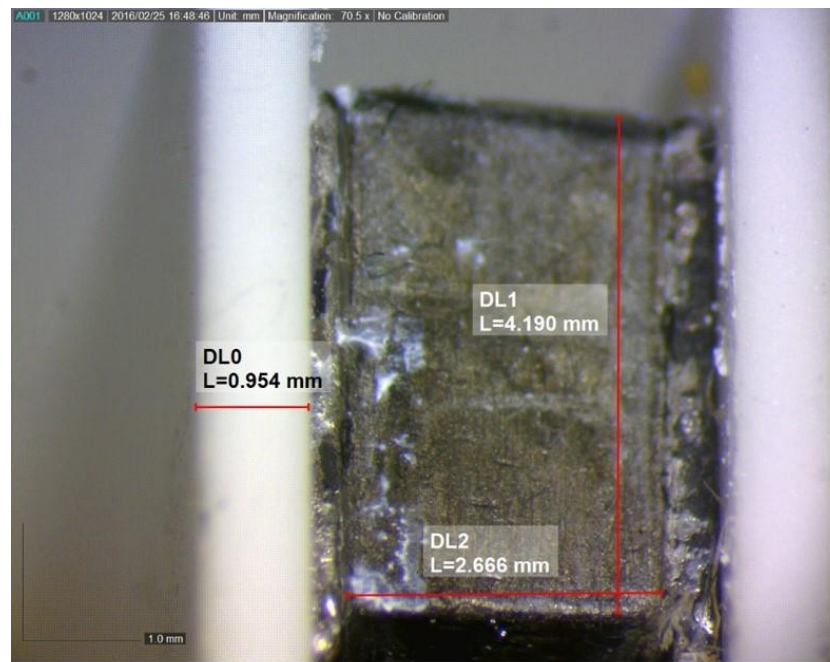


Figure 3.12: Length and width of one side of a leg of the thermoelectric module.

At the hot side, the energy balance is

$$-Q_H - K \Delta T + \alpha I T_H + \frac{1}{2} I^2 R = 0$$

$$Q_H = \alpha I T_H - K \Delta T + \frac{1}{2} I^2 R \quad 3.33$$

where α is the Seebeck coefficient, R is the electric resistance, and K is the thermal conductance of the TE module. They can be determined using the thermoelectric properties of the materials listed in Table 3.3.

Table 3.3: The properties and overall characteristics of the thermoelectric leg and module.

Properties of the thermoelectric leg			
Seebeck coefficient (α_{leg})	0.0002 V/K	No. of the legs	98
Thermal conductivity (k_{leg})	1.5 W/m. K	Length (L_{leg})	2.7 mm
Cross section area (A_{leg})	17.64 mm ²	Square A_{leg} (a = b)	4.2 mm
Overall characteristic of the thermoelectric module			
Seebeck coefficient (α)	$98 \alpha_{leg}$		0.0196 V/K
Thermal conductance (K)	$98 k_{leg} A_{leg} / L_{leg}$		0.96 W/ K
Electric resistance (R)			0.152 Ω

At the cold side, the energy balance is

$$Q_C + K \Delta T - \alpha I T_C + \frac{1}{2} I^2 R = 0$$

$$Q_C = \alpha I T_C - K \Delta T - \frac{1}{2} I^2 R \quad 3.34$$

In thermodynamics, the physical principle for all heat pumps is to create heat transfer from a cold to a hot part. In this system, electrical energy transforms to thermal energy (heat is extracted from the cold side of the thermoelectric and is pumped to the hot side). Hence, the heat released at the hot side of the thermoelectric module is the summation of the absorbed heat plus the power supplied to the module (dissipated as a heat in the bulk comes from the Seebeck voltage and the $I^2 R$ power is released at the hot

side). Figure 3.13 shows the heat profile (from the cold side of the thermoelectric module to the hot side).

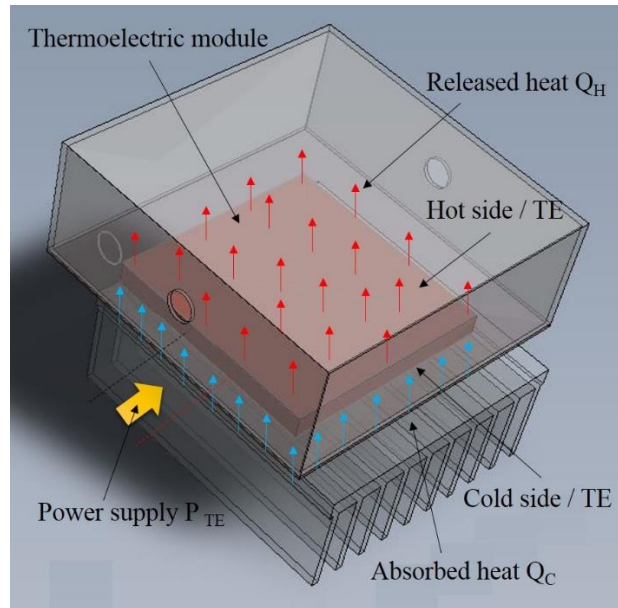


Figure 3.13: Schematic of the temperature profile in a thermoelectric module assisted condenser.

The difference between the heat dissipation at the hot side and the heat absorption at the cold side (subtract two equations 3.33 and 3.34) is given by

$$Q_H - Q_C = \alpha I (T_H - T_C) + I^2 R \quad 3.35$$

Figure 3.14 shows the difference between the dissipated and absorbed heat as a function of the temperature difference across the TE module for different input currents. The rate of heat transfer through the thermoelectric module increases when the current supplied and the temperature difference between the hot and cold sides increase. Based on the first law of thermodynamic, the dissipated heat at the hot side is the sum of the absorbed heat at the cold side and the input electric power P to the TE module, i.e.,

$$Q_H - Q_C = P$$

$$Q_H = Q_C + P \quad 3.36$$

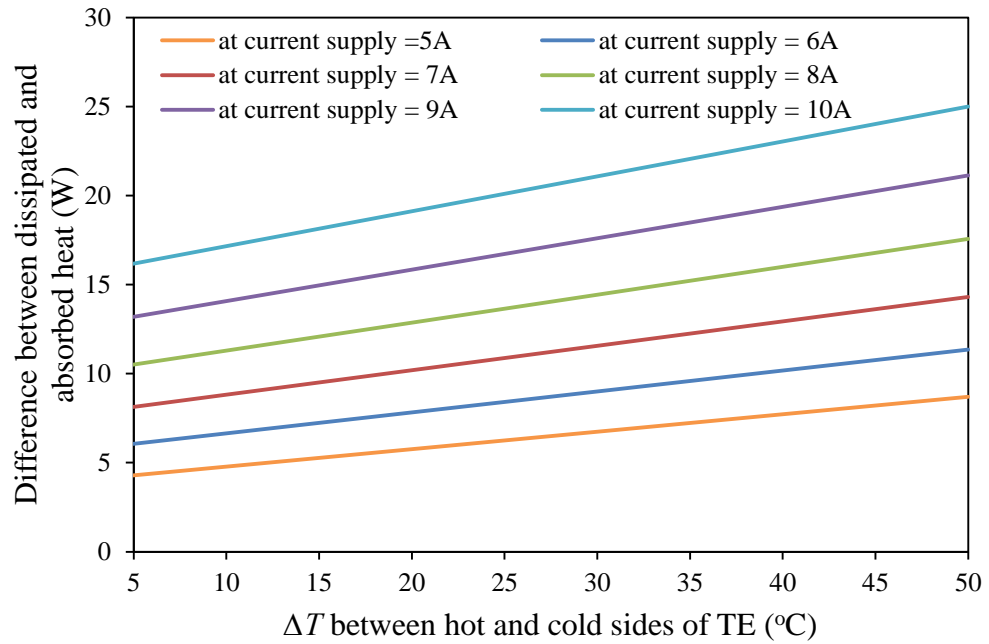


Figure 3.14: The difference between dissipated and absorbed heat as a function of the temperature difference across the thermoelectric module for different input currents.

The coefficient of performance (COP) is a measure of the cooling efficiency of any heat pump, which defined as the absorbed heat from the cold side divided by the supplied electric power [114].

$$COP = \frac{Q_c}{P} \quad 3.37$$

Based on the relationship displayed in Figure 3.14 for the absorbed heat of 1 W, it is anticipated that COP decreases with increasing the temperature difference between the hot and cold sides. The COP also decreases with increasing the input current to the thermoelectric module, as shown in Figure 3.15. The current supply was set to a desired value between 5 A and 10 A as recommended on the thermoelectric module data-sheet.

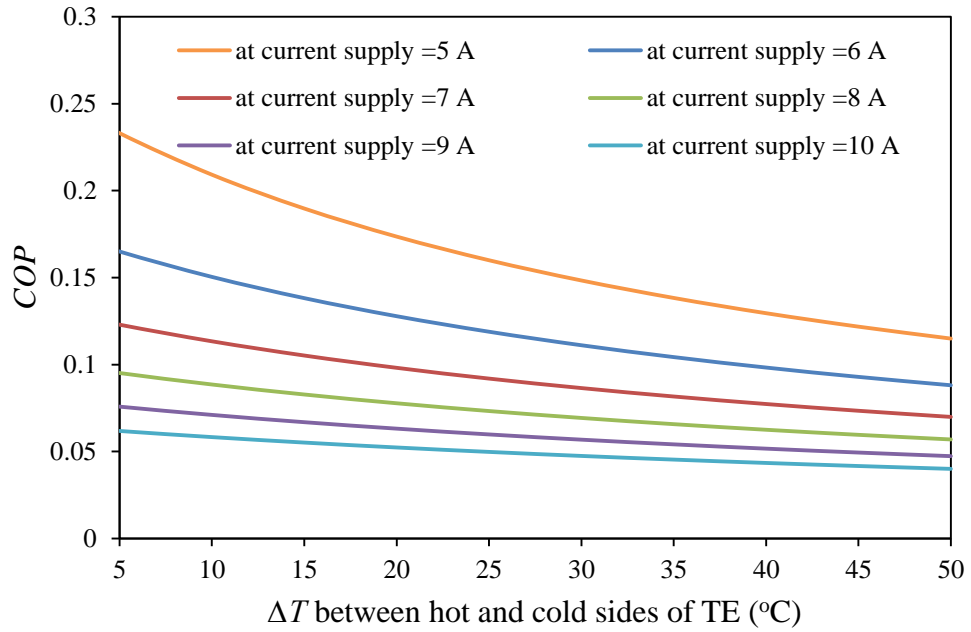


Figure 3.15: *COP* as a function of the temperature difference of the thermoelectric module for different input currents.

3.4 Design of the thermoelectric distillation system

A prototype thermoelectric distillation system was designed and constructed for this investigation. The system employs the concept of thermal distillation based on phase – change phenomena and the use of a thermoelectric module operating in the Peltier mode. The system consists of a water basin, where the evaporation process takes place and a thermoelectrically cooled surface, where the condensation process takes place. A key innovative aspect of this design is the use of waste heat dissipated from the hot side of the thermoelectric module for heating the sample water to enhance the evaporation, while the cold side is used to cool the condenser to improve the condensation. No energy is wasted in this design. A schematic diagram of this thermoelectric distillation system is shown in Figure 3.16. The proposed thermoelectric distillation process is a steady flow process in which distilled water would be produced while new feed water is added as

input sample water. Table 3.4 shows the maximum and minimum allowable values of the most important parameters for designing the thermoelectric distillation system.

Table 3.4: Maximum and minimum allowable values of the thermal parameters.

Parameter	Values	Parameters	Values	Parameters	Values
Current rating	5 – 10 A	Water capacity	0.1 - 0.7 L	Condensation heat	36 - 288 kJ
Condenser area	$\geq A_{TE} \text{ cm}^2$	Active area of TE	38.44 cm^2	Evaporation heat	10 - 235 kJ
Latent heat	750 - 693 kJ	Inclined angle	$5^\circ < \theta < 90^\circ$	Vapour pressure	$\leq P \text{ saturation}$
Water temp.	20 °C-60 °C	Mass fraction	$0.1 < x < 1$	h coefficient	5 -10 $\text{W/m}^2\text{K}$
Power supply	15 -30 W	Liquid type	Water	Gas type	Vapour

Table 3.4 presents the chosen design features, for example a single large thermoelectric module chosen for its suitability for the temperature range required and that it provided a working area of the needed dimensions. The inclined angle of the condenser also chosen to cover the copper fins of the heat exchanger when the water flows through a circulation process.

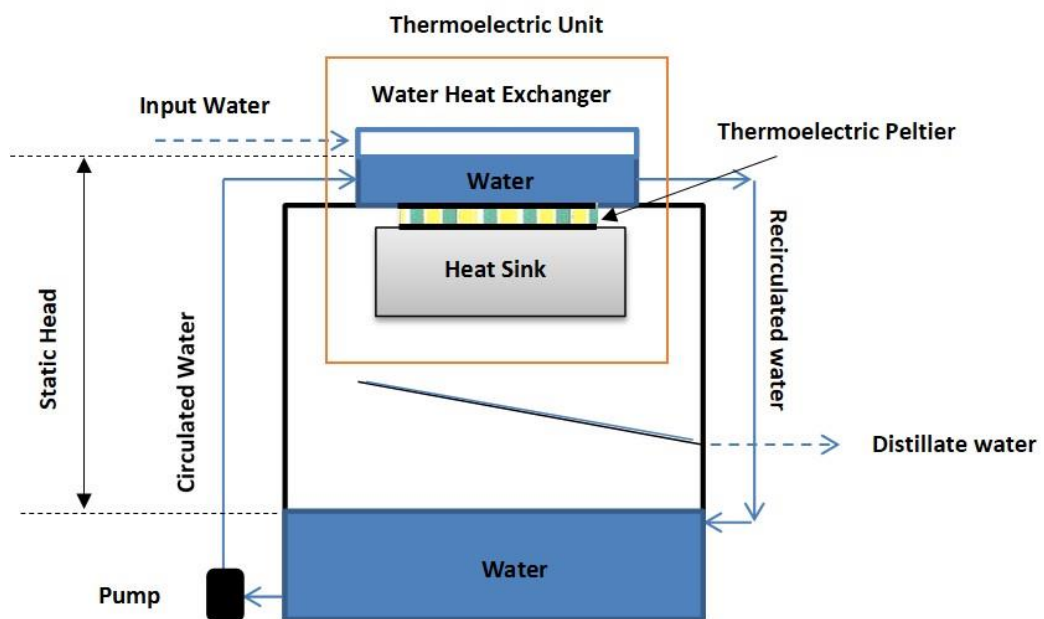


Figure 3.16: The main parts of the thermoelectric distillation design.

In order to implement this novel design into practice, the following challenges need to be addressed as follows:

3.4.1 Sample water recirculation

The first challenge was to design the system in a way that reduces the overall energy consumption. This was achieved by eliminating a conventional heater from the system (which was required to evaporate the sample water). The novel aspect of the design was to cool the hot side of the module using the sample water. This served two purposes; cooling of the hot side of the module and raising the temperature of the sample water, and consequently eliminating the need for a heater in the system. To achieve this, the sample water basin is connected to the heat exchanger on the hot side of the thermoelectric module in a closed loop. In this way, the sample water is able to circulate between the hot heat exchanger and the evaporation basin using a small pump. As a result, the heat at the hot side of the thermoelectric module is transferred into the sample water, which flows back to the evaporation basin with increased temperature and hence improved evaporation rate without the need for a conventional heater. Clearly, this will improve energy efficient of the system. The design parameters of the water circulation system include the type of the water pump, the water basin capacity and length of the pipes. To select a suitable water pump for the circulation process, the following points were considered:

- Maximum operating temperature $< 100^{\circ}\text{C}$.
- Range of the flow rate (0.1 L/min – 0.5 L/min).
- Small size.
- Static head ≥ 110 mm (see Figure 3.16).

In this design, the basin was filled with 300 mL of sample water, which occupied a surface area of 100 mm x 100 mm and a depth of 30 mm. In order to allow the condensed water to flow down to the collector channel without mixing with the sample water, there needed to be enough distance between the condenser surface and the sample water surface. For the same reason, there was a minimum clearance of 1.5 mm between the sample water surface and the collector channel. The vertical distance between the inlet and the outlet on the water basin is 9 mm and the diameter of both the inlet and outlet is 8 mm (see Figure 3.17 for details).

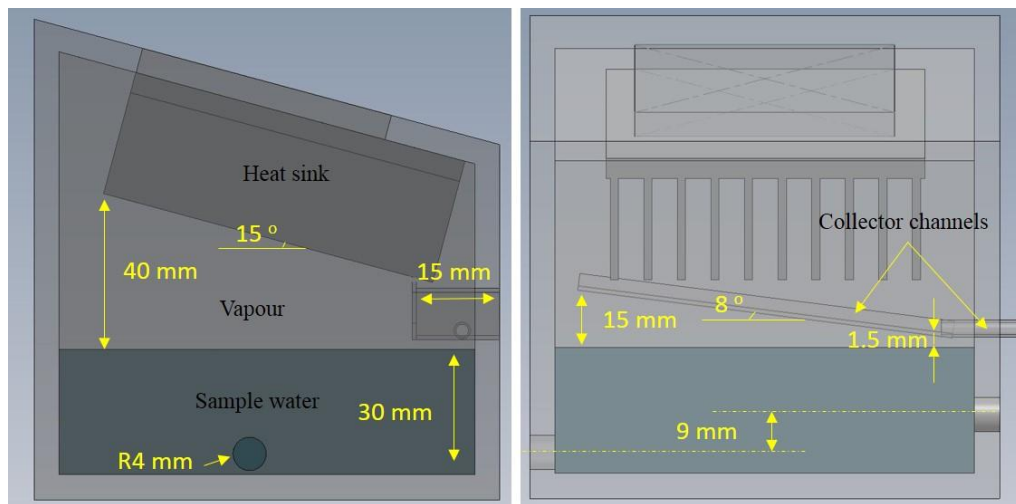


Figure 3.17: The main distances inside the system.

3.4.2 The thermoelectric module

As shown in Figure 3.18, a thermoelectric module consists of N-type and P-type semiconductor thermoelements (legs), constructed using bismuth telluride materials, connected electrically in series and thermally in parallel. The legs are sandwiched between two electrically insulating and thermally conducting ceramic plates [115, 116]. The dimension of the thermoelectric module used in this study is 62 mm x 62 mm x 5.8 mm with 98 thermoelements. The maximum supply current and voltage are 10 A and 3.6

V respectively. The model of thermoelectric module is GM250-49-45-30, which is purchased from European Thermodynamics Ltd (See Figure 3.19).

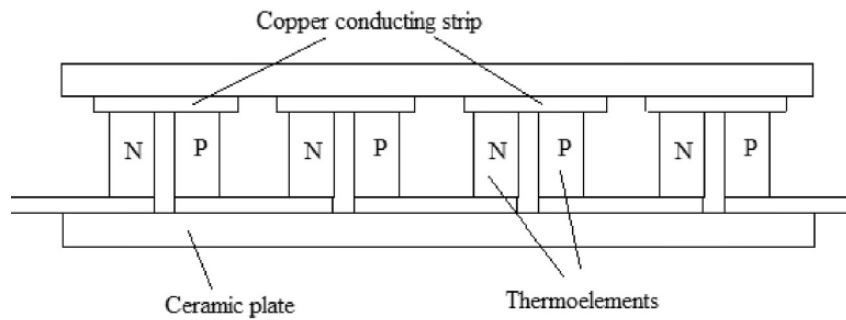


Figure 3.18: A sketch of a thermoelectric module composed of P-type and N-type semiconductors [11].

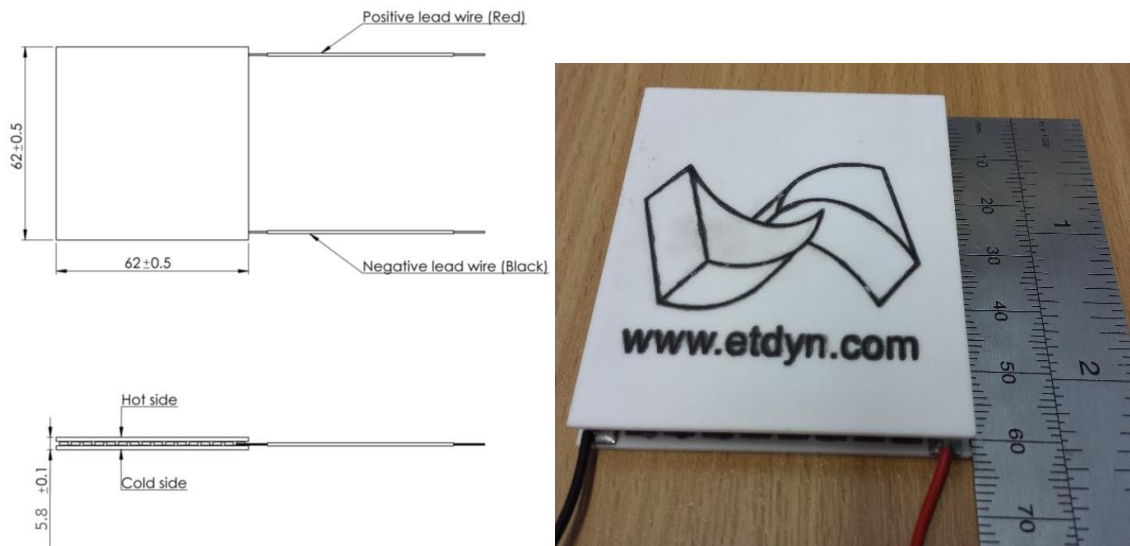


Figure 3.19: The thermoelectric module used in the design.

A thermoelectric cooling unit consists of a thermoelectric module with two heat exchangers at the cold side (condenser) and the hot side (heater) as shown in Figure 3.20. The heat exchangers allow the heat transfer from the fluids (water or vapour) to the solids and vice versa. The heat exchangers at the hot and cold sides play a key role in thermoelectric distillation processes. The aluminium condenser is connected to the cold side of the thermoelectric module to condense the vapour. The latent heat due to the condensation is released and consequently absorbed by the cold side of the module. The

water heat exchanger is mounted on the hot side of the module, where the heat is dissipated to the circulated feed water.

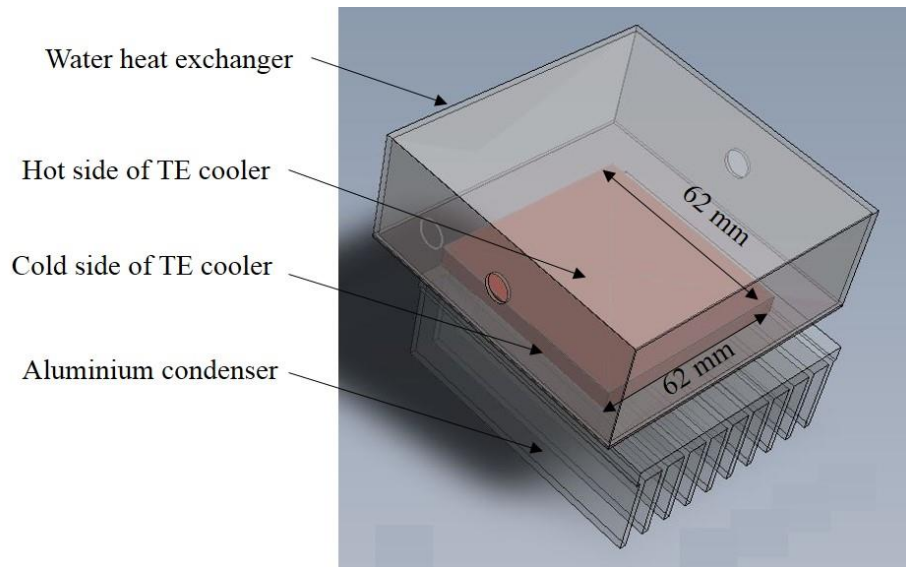


Figure 3.20: The thermoelectric cooling unit.

3.4.3 Evaporation/Condensation chamber

The design of the chamber is an important part of the thermoelectric distillation system. To reduce the heat losses to the surroundings from the vapour and the hot water, it is essential to choose a suitable materials and thickness of the walls. Heat losses from the vapour and hot water will reduce the rates of condensation and evaporation, respectively and accordingly reduce the water production. A clear Plexiglas is selected to be the material of the frame. The locations of holes for water inlet and outlet were designed on two sides of the chamber, the diameter of the hole is 8 mm and the distance between the centres of the holes is 9 mm, see Figure 3.17. The locations of the holes with the position of the inclined collector keep the sample water at a different desired level between 10 mm to 30 mm. The angle of the cover needs to be decided in order to facilitate the condensation water to flow under the force of gravity. Figure 3.21 shows a design drawing and a photograph of the constructed chamber.

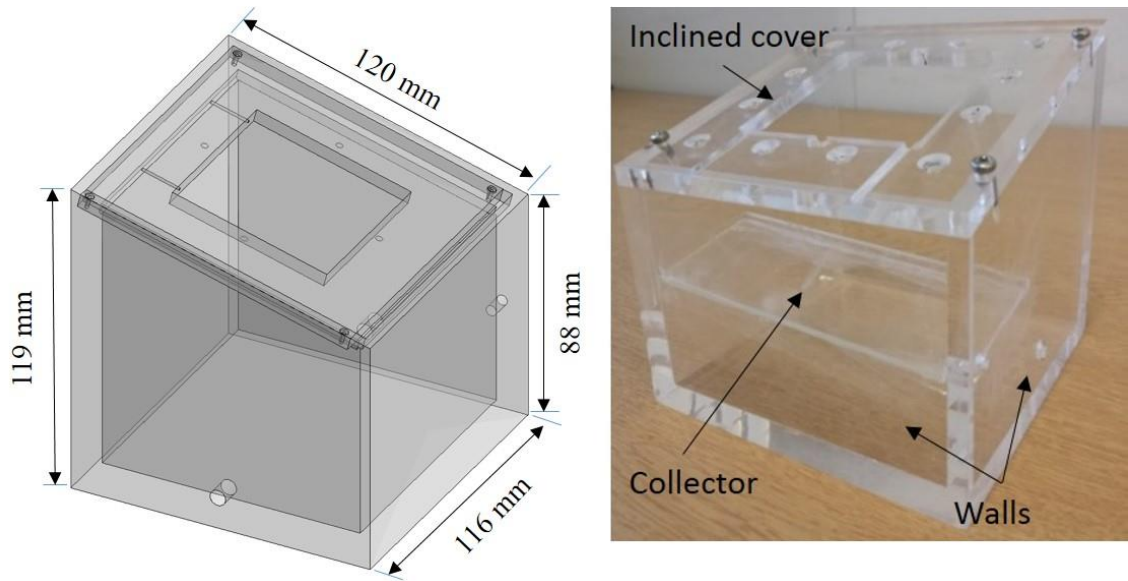


Figure 3.21: Chamber's frame including the inclined cover.

All walls are made of 8 mm clear Plexiglas sheets. The area of the bottom inside of the chamber is 100 mm x 100 mm. The inclined cover uses the same material with the thickness of 5.6 mm, which is positioned at an angle of 15° in respect to the horizontal axis. The thickness of the cover is smaller than the thickness of the walls to ensure good thermal contact between the thermoelectric module and the two heat exchangers. The maximum operation temperature of the Plexiglas is 120°C and the water absorption ratio for 48 hours is 0.35 %. The inclined Plexiglas cover has holes to hold the thermoelectric cooling unit (Figure 3.21) in position using screws.

3.4.4 Hot side water heat exchanger for sample water heating

The hot side heat exchanger (shown in Figure 3.20) is employed for heating the sample water using the waste heat from the thermoelectric module and at the same time to cool the hot side of the thermoelectric module. Figure 3.22 shows a design drawing and a photograph of the hot side water heat exchanger shown in Figure 3.20. The heat exchanger consists of two parts; the bottom part is a box made of a thick PVC plastic and

the top part is a cover made of copper with fins. The outside dimensions of the heat exchanger are 89 mm x 89 mm x 35 mm with 7 fins. The sample water flows through the fins and the heat is dissipated from the copper plate into the sample water by forced convection.

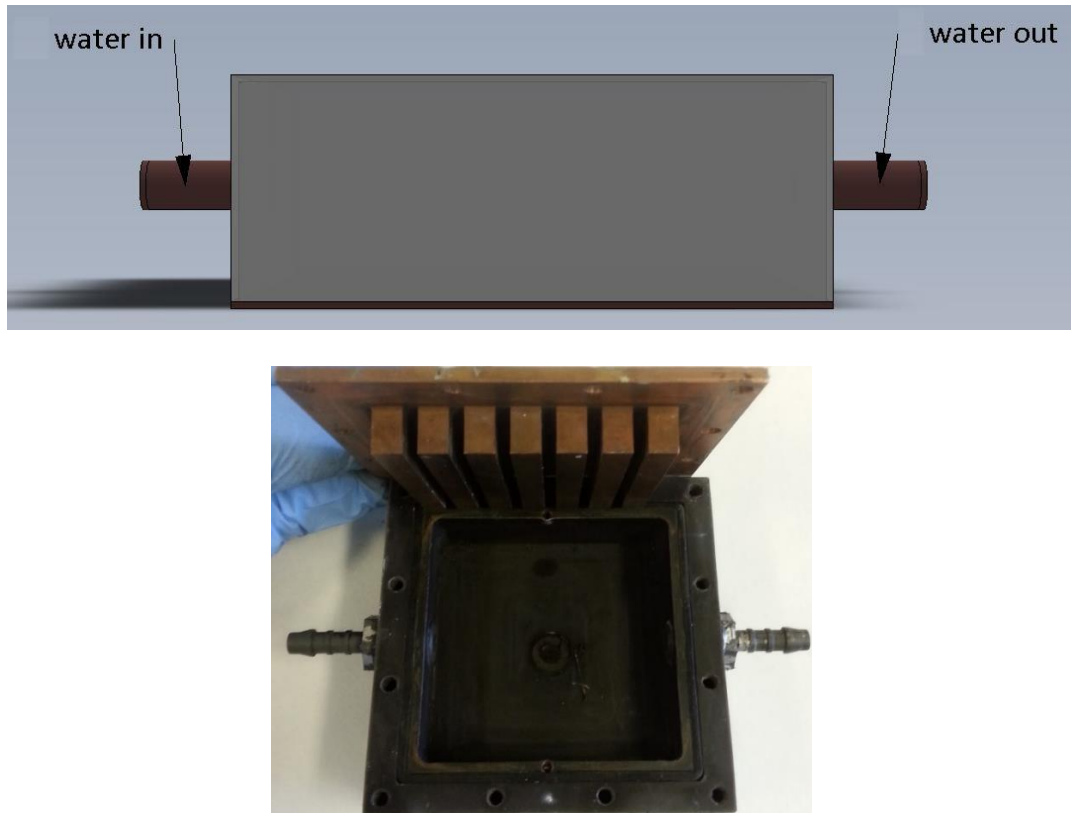


Figure 3.22: Schematic and photograph of the hot side water heat exchanger.

3.4.5 Cold side heat sink for water condensation

Condensation occurs when the water vapour loses the thermal energy to a surface it is in contact with. The rate of condensation is mainly dependent on the temperature and surface area. In the study, the condenser is a fin-type heat exchanger attached to the cold side of the thermoelectric module, which controls the temperature of the condensation process. The use of fins can significantly increase the surface area of the condenser within the limited space of the evaporation/condensation chamber. Aluminium 6063 is the

chosen material for the cold side heat exchanger because of its high thermal conductivity (200 W/m. K at 25 °C) and availability at a reasonable price. In addition, its density is low and has a good resistance to corrosion due to formation of an oxide layer on its surface. The dimension of the condenser is 82 mm x 76 mm x 25 mm with 10 fins and the dimension of each fin is 82 mm x 25 mm x 1 mm. Figure 3.23 shows a design drawing and photograph of the aluminium condenser.

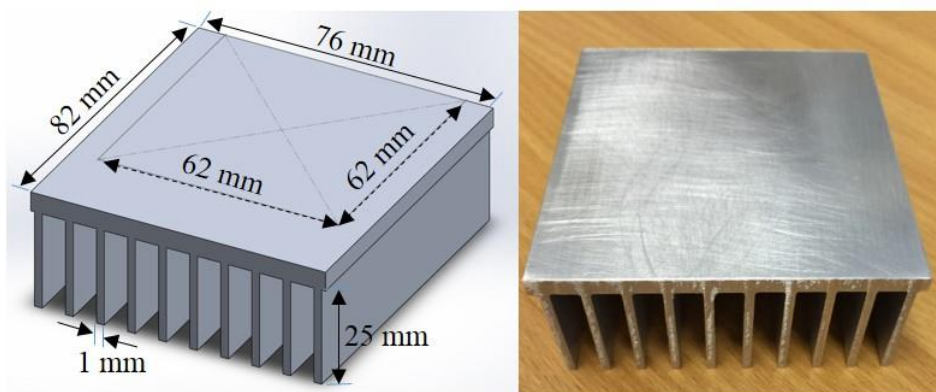


Figure 3.23: The design drawing and photograph of the aluminium condenser.

In order to encourage the water to flow easily, the surface of the condenser should be hydrophobic. This property facilitates the formation of drops when the water is condensed on the surface and allows the water drops to slide into the water channel below for collection. Figure 3.24 shows a photograph of water drops on the surface of aluminium condenser, demonstrating the hydrophobic properties required.



Figure 3.24: A photograph of water drops on the surface of aluminium condenser.

The position of the aluminium condenser is below the cold side of the thermoelectric module and is joined together by 2 screws of 1.5 mm in diameter. Assembly of the thermoelectric module with the heat exchangers and the Plexiglas cover is shown in Figure 3.25. The contact surfaces between the hot and cold sides of the thermoelectric cooler and the heat exchangers are filled with thermal paste to ensure a good thermal contact.

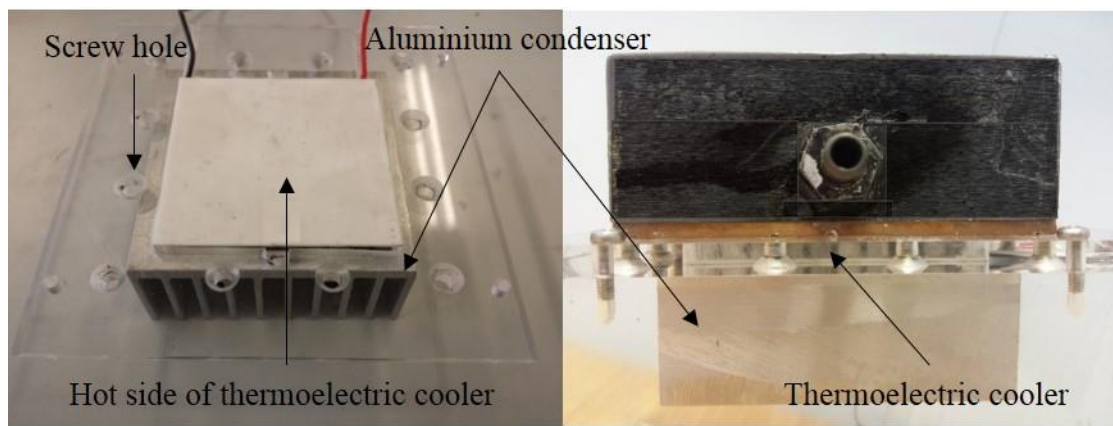


Figure 3.25: Assembly the thermoelectric module with the heat exchangers and the Plexiglas cover.

3.5 Assembly of thermoelectric distillation system

The components described in previous sections were constructed and assembled to build a thermoelectric distillation system for this study. Figure 3.26 shows the main components and assembly order (prepared using SOLIDWORKS). Figure 3.27 shows the assembled system, indicating the positions and connections of all the components. The drawing on the right-hand side is a cross-sectional view, providing a clear view of the internal components. Figure 3.28 shows a photograph of the actual system constructed based on the design described in this chapter.

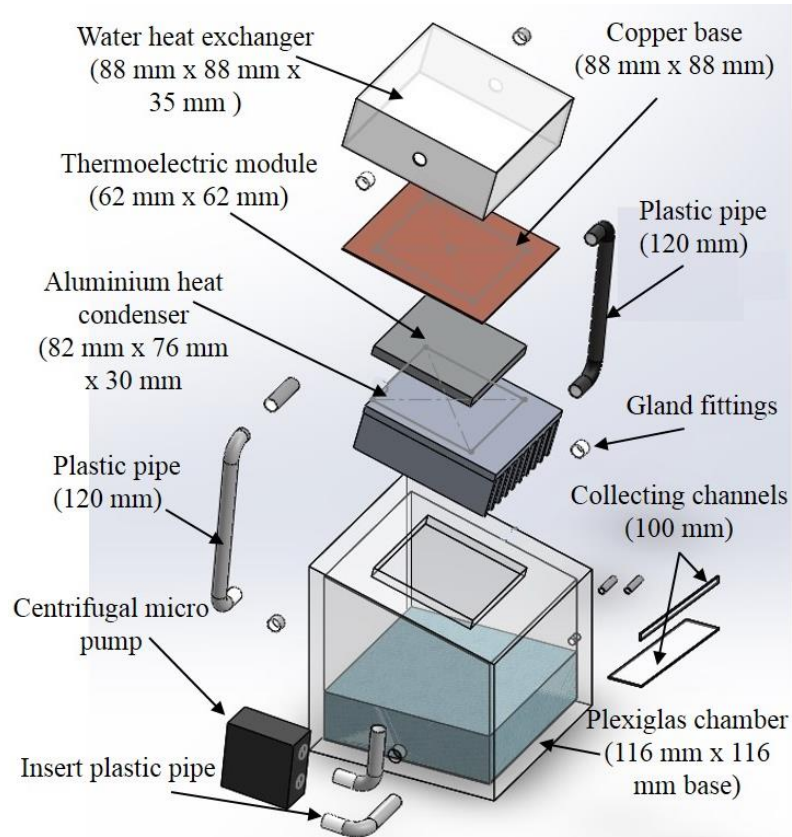


Figure 3.26: The main components and assembly order of the developed thermoelectric distillation system.

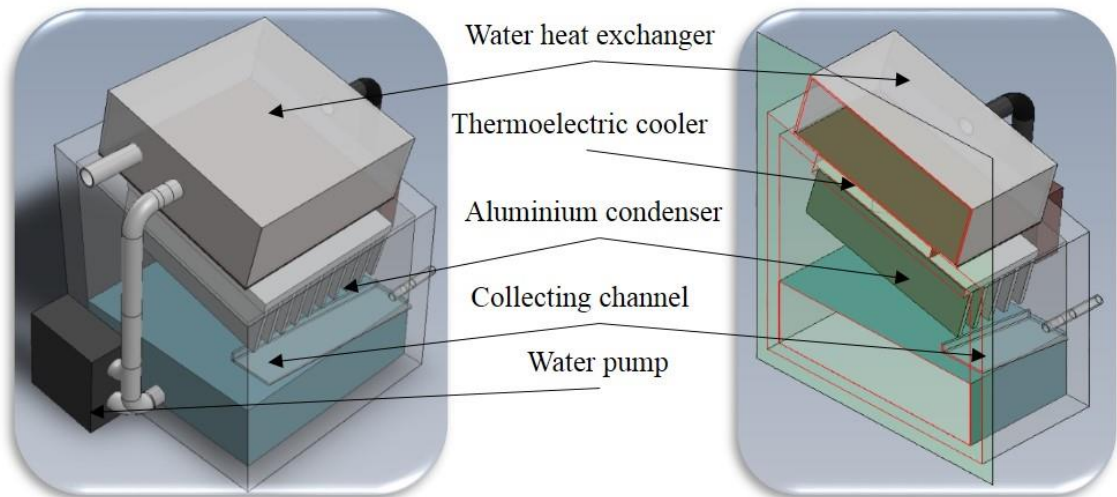


Figure 3.27: Design drawing of the assembled system (left) and cross-section views of the system (right).

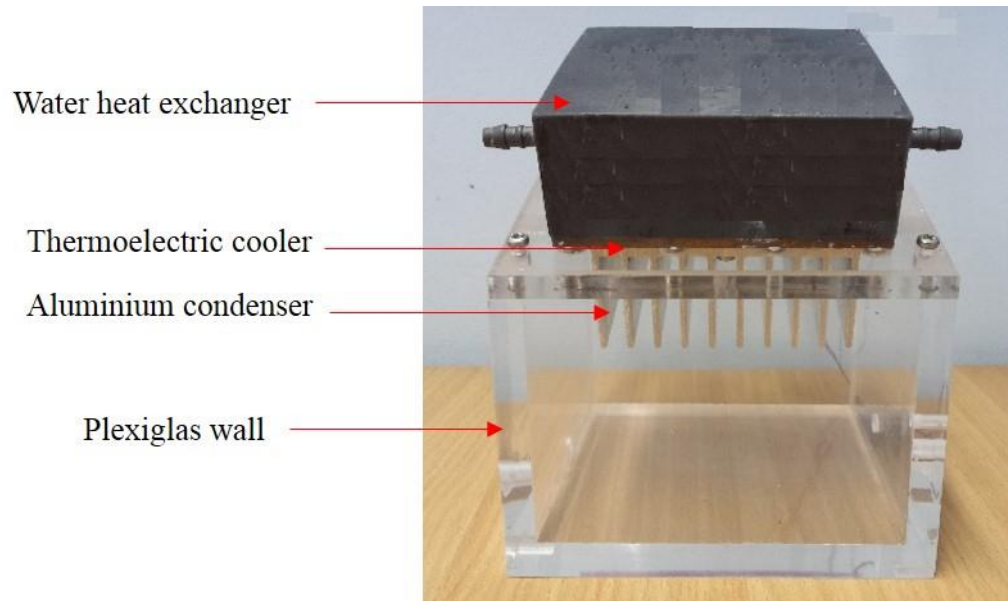


Figure 3.28: A photograph of the actual system developed based on the above design.

3.6 Summary of outcomes

A thermoelectric distillation system was developed with a unique aspect: the system uses a thermoelectric module to improve both the evaporation and condensation processes in a still distillation system. Theoretical foundations associated with the evaporation and condensation processes were outlined to provide insights and guidelines for the design of the proposed thermoelectric distillation system. They can also be used to determine the mass of vapour produced by evaporation and the thermal energy required for evaporation for a given sample water temperature. The rate of water condensation can also be calculated for different local heat transfer coefficients and temperature difference between the vapour and condenser surface.

Energy balance equations of thermoelectric modules were employed to estimate the temperature difference and heat pumping capacity that a thermoelectric module can provide for the distillation system. A prototype of the proposed thermoelectric distillation system were designed and constructed. The chapter provided a detailed description on the design and construction of the main components and assembly of the prototype system.

Chapter 4

Experimental Investigations of Utilizing Hot and Cold Sides of a Thermoelectric Module for Water Distillation System

4.1 Introduction

In this chapter, the thermoelectric distillation system presented in the previous chapter was used to investigate the performance of this unique system. The experimental setup was planned and implemented to facilitate acquisition of several key parameters including temperature, humidity, water productivity and energy consumption. The main objective of this chapter is to evaluate experimentally the performance of the proposed thermoelectric distillation system, in an attempt to demonstrate unique advantages of this system in terms of water productivity and energy efficiency.

4.2 System description

The key part of the main experimental setup employed for this investigation is the thermoelectric distillation system developed in Chapter 3, as shown in Figure 4.1. One of the main design features of this system is the recirculation of sample water. A water heat exchanger is mounted on the hot side of the thermoelectric module that transfers the heat to the circulating water. In operation, the sample water is pumped to circulate from the hot side heat exchanger to the bottom basin to increase the temperature of the sample water.

On the cold side of thermoelectric module, an aluminium heat sink with fins is attached to serve as the condenser, the temperature of which is reduced by thermoelectric cooling and consequently the condensation rate can be improved. The key parameters to be investigated include the temperatures at various positions in the system, the humidity in the chamber, the water production rate and energy consumption. The techniques and instruments used for these measurements are presented in the following section.

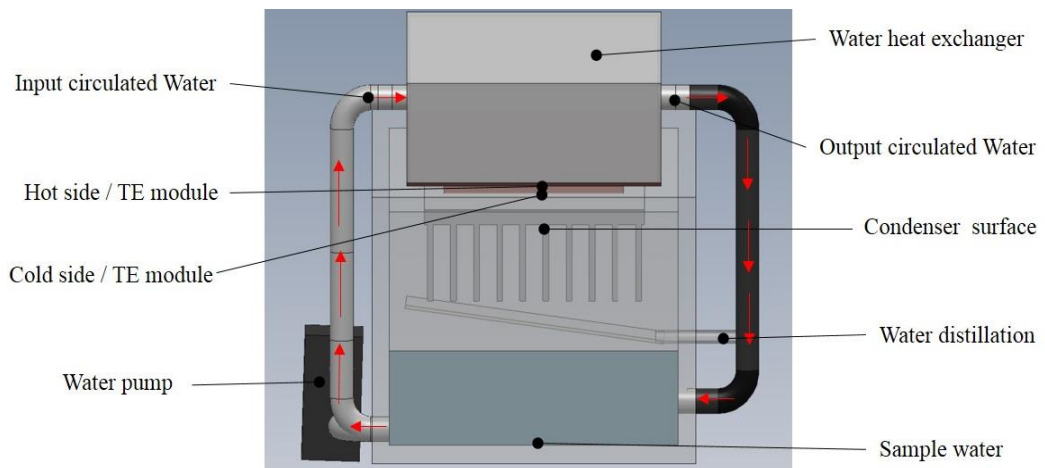


Figure 4.1: Schematic diagram of the thermoelectric distillation system.

4.3 Instruments and sensors

For the experimental investigation, the thermoelectric distillation system was connected to a number of sensors, power supplies and data acquisition instruments as shown in Figure 4.2. Two power supplies were used for powering a thermoelectric module and a water pump, respectively. A water flow meter was used to monitor the flow rate of the sample water that circulated between the evaporation chamber and hot side heat exchanger. The thermocouples and a data logger were employed to measure/record the temperature at various positions of the thermoelectric distillation system.

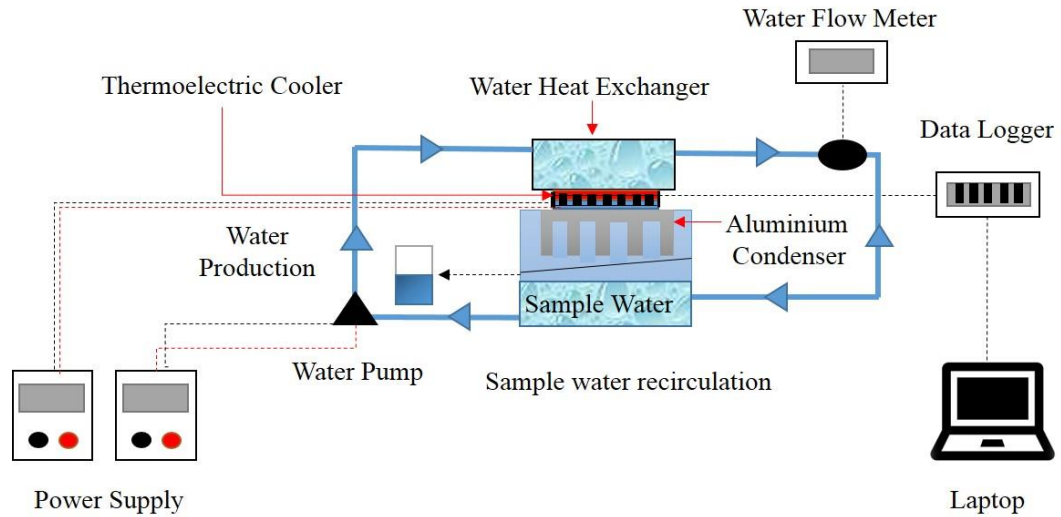


Figure 4.2: Schematic diagram of the instruments and sensors used in the experimental set up.

The water pump employed is a small water diaphragm pump (SKU082613). The specifications of the pump are listed in Table 4.1 and a photograph is shown in Figure 4.3. The flow meter employed in the study is a panel-mounted flow meter (Digi Flow 6710M-34TM). The specifications of the flow meter are shown in Table 4.2. The input power for thermoelectric module was provided by a high precision power supply (EP-925) and the diaphragm pump was powered by a *TTi* (TSX 1820) power supply.

Table 4.1: The specifications of the diaphragm pump used in the thermoelectric distillation system.

Characteristic	diaphragm pump
Installation dimension	100 mm x 73 mm x 40 mm
Outer / Inner diameter	8 and 6 mm
Operating voltage	12 V
Current	0.4 – 0.8 A
Max Pump Head	10 m
Flow	400 L/h
Pressure	1.2 MPa

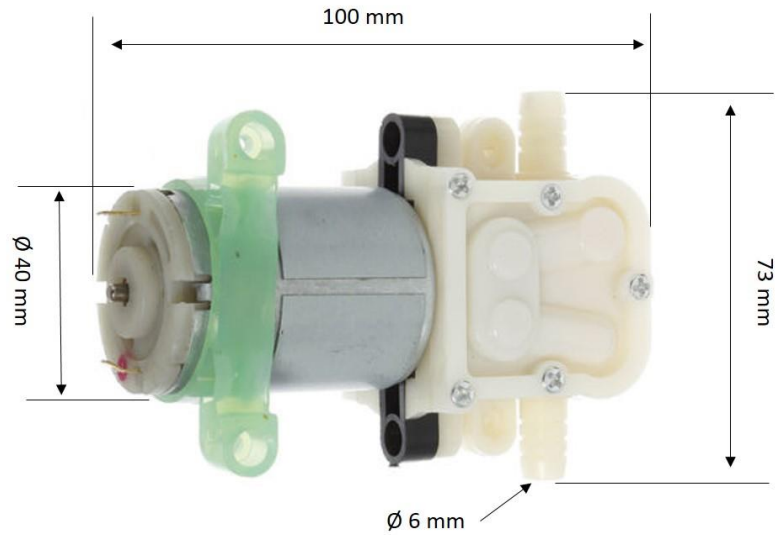


Figure 4.3: A photograph of the diaphragm pump used in the thermoelectric distillation system.

Table 4.2: The specifications of the Digi Flow 6710M-34TM employed for this study.

Characteristic	Water Flow Meter
Outer diameter	12.7 mm
Flow range	0.05 – 1 L/min
Working temperature	0 – 80 °C
Working pressure	0.1 – 1 MPa
Operating current	4 mA
Operating voltage	3 V

Four K-type thermocouples were attached directly to the measuring points as shown in Figure 4.4 to measure the temperatures of the sample water T_w , vapour T_v , condenser surface T_s and the ambient T_{amb} , while two thermocouples were attached and secured through a small groove in the copper and aluminium surfaces to measure the temperatures of the hot side of thermoelectric module T_H and cold side of thermoelectric module T_c . The specifications of the K-type thermocouples used are shown in Table 4.3 and a photograph is shown in Figure 4.5a.

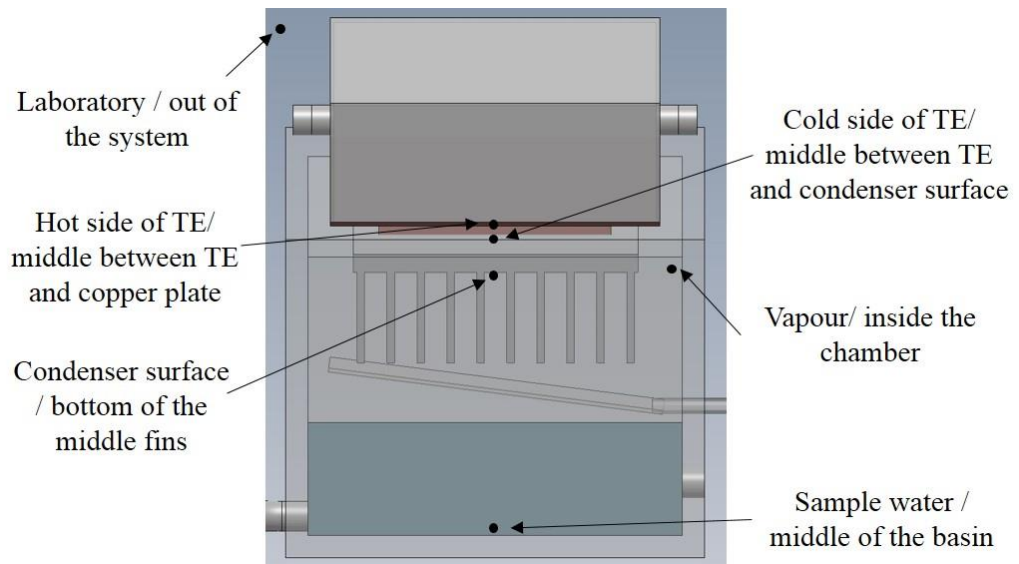


Figure 4.4: Positions of the thermocouples in the system.

Table 4.3: The specifications of K- type thermocouple used in the experiments.

Characteristic	Type K
Maximum and minimum temperature sensed	From $-60\text{ }^{\circ}\text{C}$ to $350\text{ }^{\circ}\text{C}$
Termination type, Cable length	Miniature plug, 1m

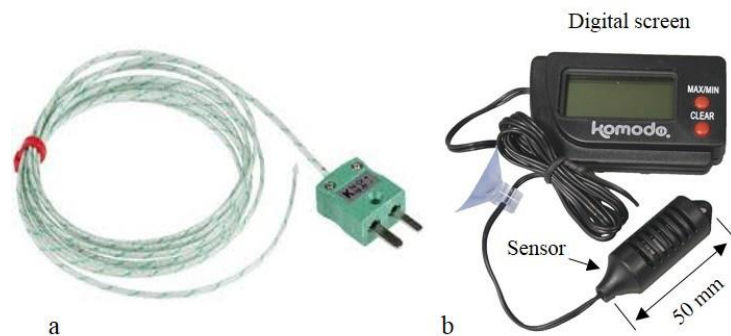


Figure 4.5: Photograph of a) K-type thermocouple and b) digital humidity sensor.

The thermocouples were connected to a computer through a six-channel data logger (pico technology limited, T-08 supplied by RS Components, UK 205-7572) for automatic data acquisition. The data logger has a wide temperature range (from $-270\text{ }^{\circ}\text{C}$ to $1800\text{ }^{\circ}\text{C}$) with software to support convenient configuration with the computer for data acquisition. Figure 4.6 shows a photograph of the pico data logger.



Figure 4.6: TC-08 Serial thermocouple data logger by pico technology Ltd.

Two humidity meter sensors (Komodo 82404 Hygrometer digital) were used to measure the humidity ratio inside and outside the evaporation chamber of the thermoelectric distillation system. The humidity range of the sensor is from 20% to 99%. The dimensions of the humidity sensor are 50 mm x 16 mm x 12 mm (see Figure 4.5b). An electronic digital scale (0.01 gram – 200 gram) is used to measure the mass of the distillate water. The dimension of the scale is 115 mm x 62 mm x 15 mm. The operation temperature range of the scale is 10 °C – 30 °C. In addition, two multi-meters (*TTi* – 1906 and LINI-TUT58C) were used to measure the voltage and current to the diaphragm water pump.

4.4 Experimental setup

Figure 4.7 shows a photograph of the actual experimental setup. The evaporation chamber was filled with 300 mL of sample water through the input valve. The diaphragm pump circulates the sample water through the top heat exchanger which is mounted at the hot side of the thermoelectric module. The water circulation was controlled by the power supplied to the diaphragm pump. A temperature difference was created between the hot and cold side of the thermoelectric module. As a result, the circulating sample water is

heated by the hot side of the thermoelectric module, while the aluminium condenser is cooled by the cold side. After 10 minutes of operation, the temperature of the sample water in the basin increased and vapour production became significant. The vapour molecules evaporate at the water-vapour interface (100 mm x 100 mm) and rise up to the aluminium condenser. With an increase in vapour production, the humidity in the evaporation chamber was increased. The condensation occurs on the fins of the aluminium condenser and the water drops follows the inclined surfaces and flow into a collecting channel under the influence of gravity. The distillate water is collected in a container and its mass was determined using an electronic digital scale. The accuracies, ranges and standard uncertainty of the measuring instruments are presented in Table 4.4.

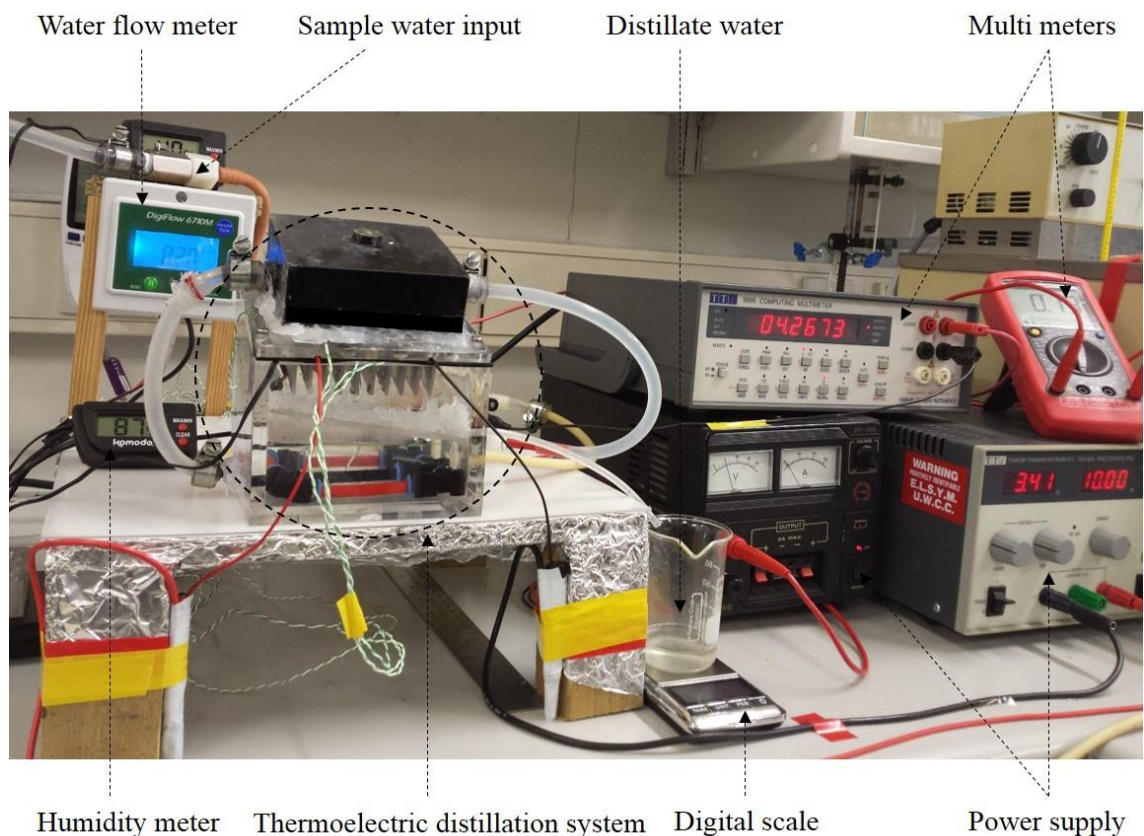


Figure 4.7: A photograph of the experimental setup of the thermoelectric distillation system.

Table 4.4: Accuracies, ranges and standard uncertainty of the measuring instruments.

Instrument	Accuracy	Range	Standard uncertainty
Thermocouple (type K)	0.1 °C	-75-250 °C	0.06 °C
Digital scale	0.01 Gram	0-200 Gram	0.006 Gram
Weir 423 power supply	0.01 V	0-15 V	0.006 V
	0.002 A	0-2 A	0.001 A
TTi (TS 1820) power supply	0.001 V	0-18 V	0.0006 V
	0.002 A	0-20 A	0.001 A
Humidity meter	0.1 %	20-99 %	0.05 %
Water flow meter (6710M)	0.01 L/min	0.05-1 L/min	0.01 L/min

4.5 Experimental procedure

To evaluate the performance of the thermoelectric distillation system, the experimental setup was investigated in laboratory conditions with the initial temperature of the sample water at 22 °C, an ambient temperature of 24 °C and a humidity of 29 %. The experiments were carried out for 240 minutes and the basin was filled with 300 mL of tap water with constant water flow rate of 0.2 L/min. To maintain a constant water level in the system during the experiments, a one-way valve was installed between the water heat exchanger and the replacement water. During experiments, the temperatures at various locations in the system were measured and recorded. In addition, the humidity inside the chamber, the amount of collected distilled water and total power input to the system were measured.

4.6 Results and discussion

4.6.1 Thermal behaviour of the system

Figure 4.8 shows the temperature profiles of the sample water, vapour, condenser surface, ambient, the hot and the cold sides of the thermoelectric module over a 4-hour period of operation. It can be seen in the Figure 4.8 that it took about 180 minutes for this system to reach the steady state. The steady state process is a thermal behaviour in which the temperature and humidity of the water and vapour in the evaporation/condensation chamber does not change with time.

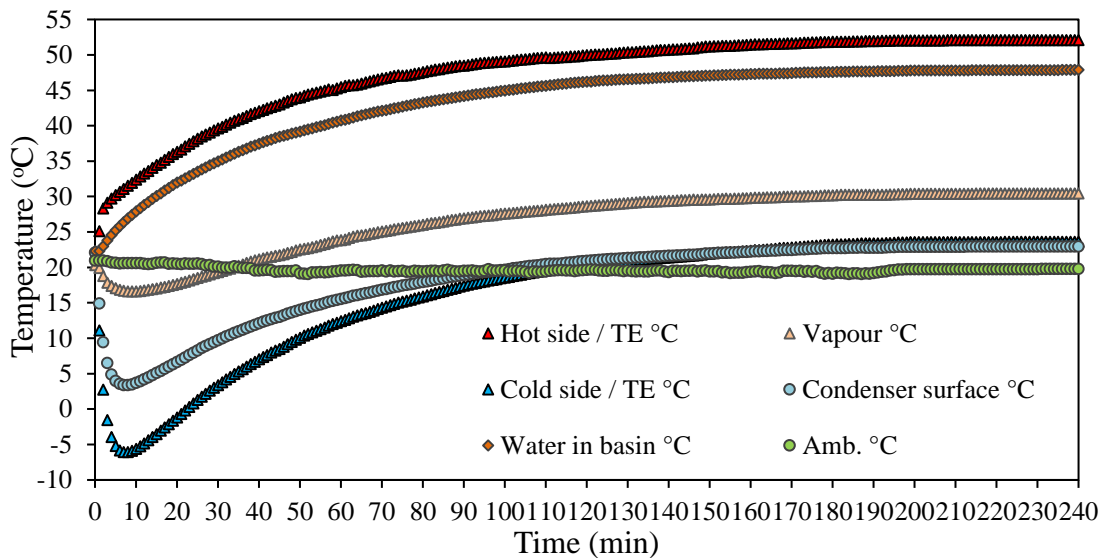


Figure 4.8: The temperature variation of the system components.

As mentioned previously (in Chapter 3), the main feature of the system is the use of the hot side of the thermoelectric module to raise the temperature of the sample water for the evaporation process and thus eliminating the need of a separate heater for vapour production. It can be seen that the hot side of the thermoelectric module is increased from an initial temperature of 21.8 °C to a final temperature of 52.1 °C at steady state. The heat rejected from the hot side is transferred effectively to the sample water, the temperature

of which was increased from 22.3 °C to 47.8 °C, and led to an increase in the evaporation rate. The vapour temperature increased moderately from 20.3 °C initially to 30.4 °C at steady state. The second feature of the system is to use the cold side of the thermoelectric module to cool the aluminium condenser for water condensation, or in other words, convert the vapour into liquid water. During the transient state, the minimum temperatures of the cold side of the thermoelectric module and at the condenser surface were -6.1 °C and 3.4 °C, respectively. The condensation process in this system relies significantly on the heat convection between the condenser surface and the vapour. To achieve a high condensation rate, the temperature difference between the vapour and the condenser surface should be high. It can be seen from Figure 4.9 that the temperature difference between the condenser surface and the vapour $\Delta T / (T_v - T_s)$ follows a similar trend to that between the hot and cold sides of the thermoelectric cooler $\Delta T / TE$.

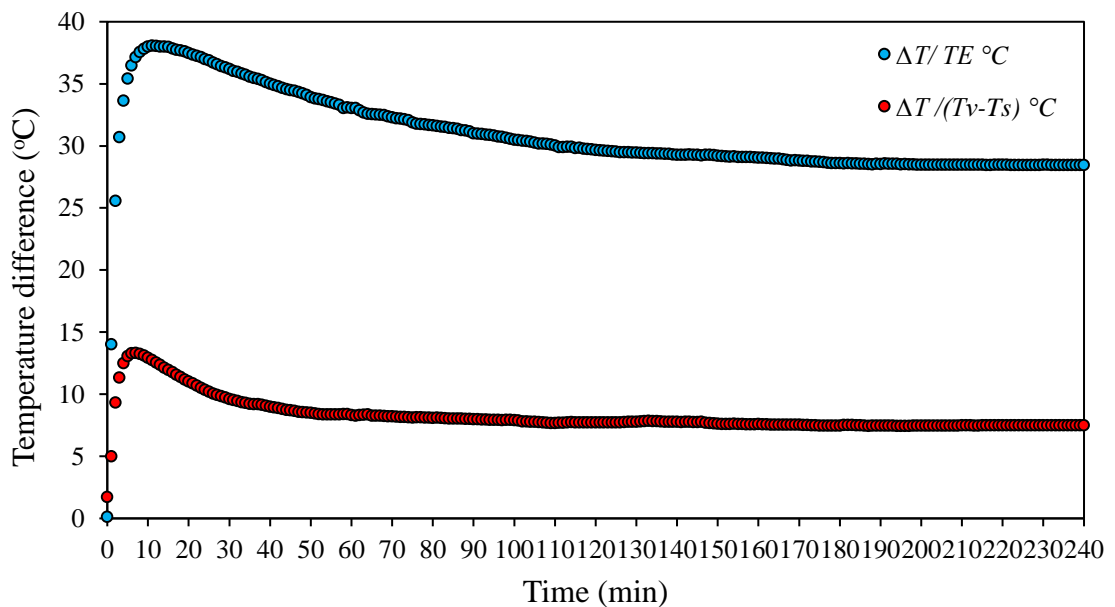


Figure 4.9: The temperature differences across the thermoelectric module (blue) and between the vapour and condenser (red).

The relative humidity is the amount of water vapour in air, which is expressed in a percentage as mentioned in Chapter 3. The reading of the humidity in the evaporation chamber is higher than a large space works (Lab) because an equilibrium with small amount of water in the chamber happens faster (*RH* is started from 55% at the beginning of the experiments). The relative humidity is also changed with time as shown in Figure 4.10. In the first 10 minutes of operation, the humidity of the chamber is slightly decreased from 55% to reach 51% due to an initial significant cooling effect (e.g., condenser surface temperature was 3.4 °C and air temperature was 16.6 °C). Then, with the increase in the vapour production due to the heating of the sample water, a large amount of vapour molecules evaporated from the interface and the humidity increased to approximately 81% at steady state.

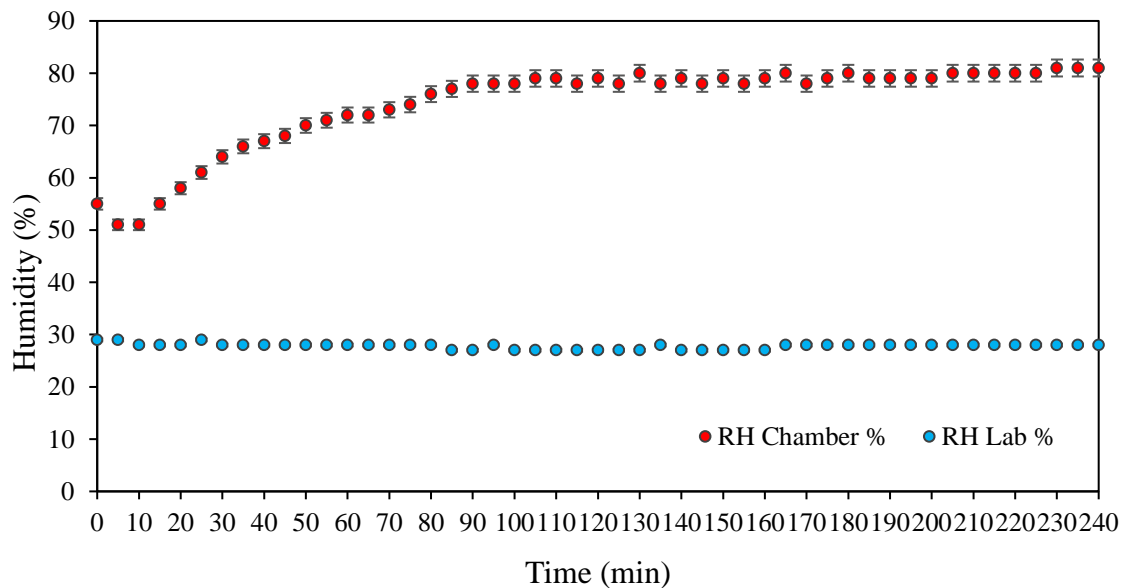


Figure 4.10: The relative humidity in the chamber compared with that of ambient in the laboratory.

In summary, after the system reaches the steady state after running for 6 hours, the temperature difference across the thermoelectric module is $T_H - T_c \approx 28.5$ °C; the

temperature difference between the vapour and the surface of the condenser is $T_v - T_s \approx 7.5$ °C; the temperatures of the sample water and the vapour are $T_w \approx 47.8$ °C and $T_v \approx 30.4$ °C, respectively, and the relative humidity in the chamber is 81% at the corresponding input power to the system is 32.4 W.

4.6.2 Thermal behaviour of the thermoelectric module

At a DC electric current supply of 10 A, the heat absorbed at the cold side of the thermoelectric module and the heat released at the hot side can be calculated from the experimental data using equations 3.33 and 3.34 in Chapter 3. Using the thermoelectric module properties listed in Table 3.3 in Chapter 3 and the data presented in Figure 4.8, the temperatures of the hot and the cold sides of the thermoelectric module, the released and the absorbed heat can be calculated. In a transient state, part of the Peltier heat is needed to pump the internal heat from the cold side to hot side to reduce the temperature at cold side. Only a part of the Peltier heat in equation 3.34 is contributed to the absorption of heat from vapour. Similarly, part of heat transport to the hot side is absorbed internally to increase the hot side temperature. Consequently, the absorbed and released heat were started from 15 minutes of operation in Figure 4.11 because the temperatures of the cold and hot side were changed very quickly during this period.

After that time, the absorbed and released heat gradually increases to reach steady state values of 33.8 W and 54.6 W, respectively. At the maximum temperature difference between the hot and cold sides of thermoelectric module (38.1 °C), the absorbed and released heat from the thermoelectric module are 22.5 W and 45.1 W, respectively. This behaviour can be explained by examining the equations 3.33 and 3.34. The Peltier heat (1st term in these equations) changes slightly for the temperature variation obtained in this study because it is proportional to absolute temperature. On the other hand, the heat

conduction (2nd term of these equations) changes more significantly because it is proportional to the temperature difference. The heat conduction is low when the temperature difference of the TE module is small. For a given electrical current, the thermoelectric module pumps more heat when the temperature difference is small.

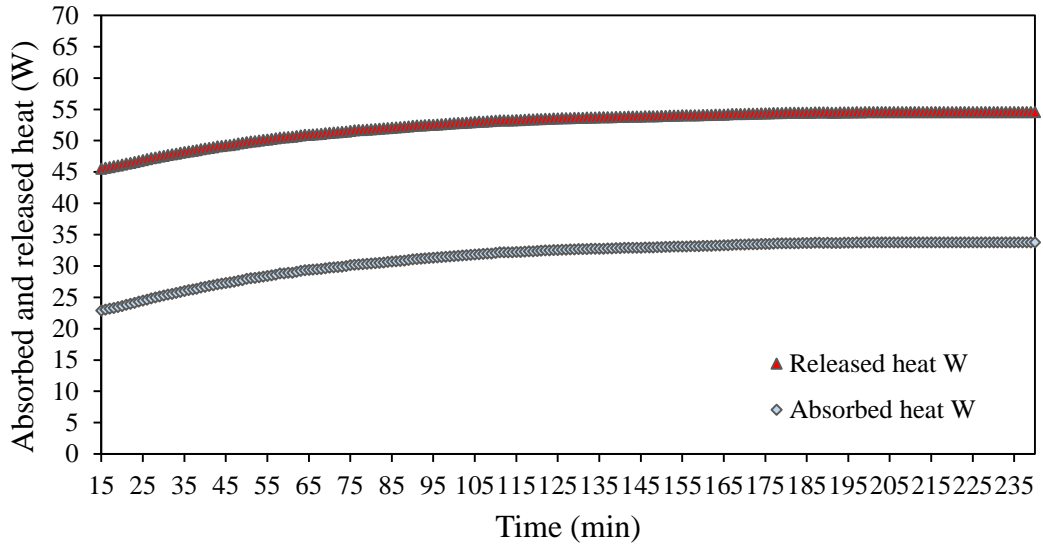


Figure 4.11: The absorbed and released heat variation of the thermoelectric module.

The coefficient of performance *COP* of the thermoelectric module which can be calculated using equation 3.37 derived in Chapter Three. Using the results presented in Figure 4.11 and the input power recorded for the thermoelectric module and the total power input to the system can be used for the *COP* calculation. Figure 4.12 shows the *COP* of the system and the module in the quasi-steady state condition. There is small difference between the two coefficients. The red dots indicate the *COP* of the thermoelectric module calculated using the input power of $P_{TE} = Q_H - Q_C$ while the blue dots indicate the *COP* of the thermoelectric distillation system calculated using the input power that included the power to the water pump, i.e., $P_{system} = P_{TE} + P_{pump}$. The *COP* of the thermoelectric distillation system and thermoelectric module at steady state are 1.04 and 1.06 respectively. The *COP* of the system is 0.69 at the time equal to 15

minutes which is corresponding to the temperature difference of 38 °C between the hot and cold sides of the TE module. Figure 4.13 shows both the *COP* and the temperature difference on the same plot, indicating the change in both but in opposite trends.

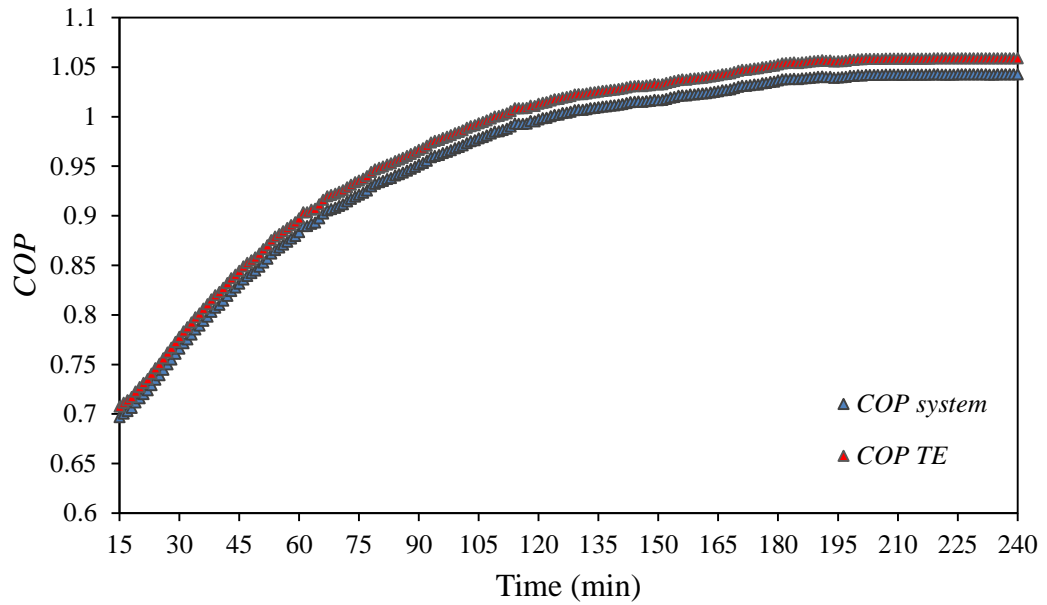


Figure 4.12: The *COP* of the TE module and TE distillation system.

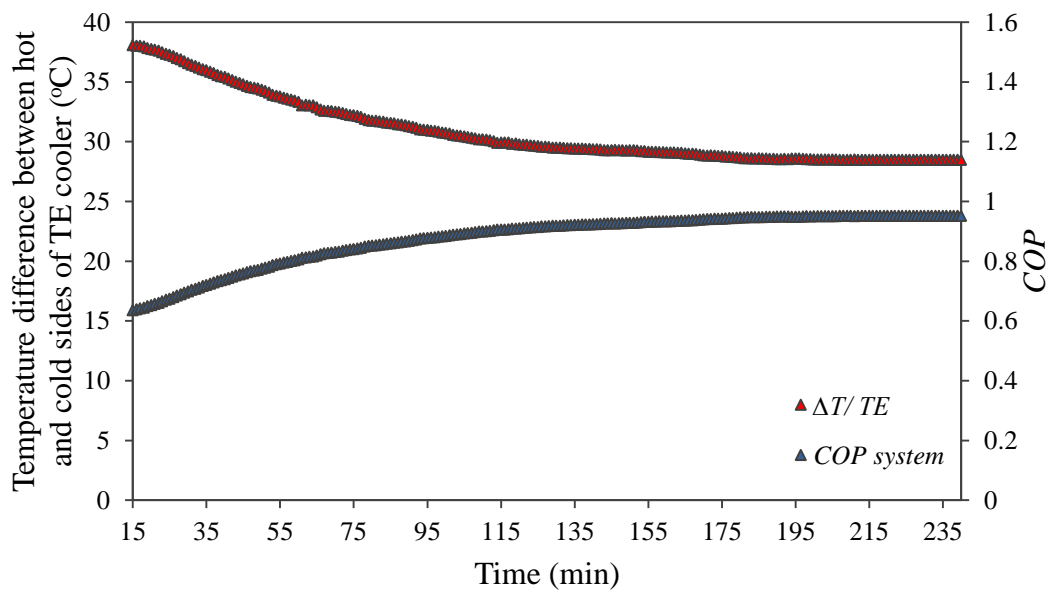


Figure 4.13: The relationship between the ΔT and the *COP* of thermoelectric module.

This trend because of the COP_{system} increased when the temperature difference between the hot and the cold side of the thermoelectric module decreased which means the module pumped more heat from the cold to the hot side of the module.

4.6.3 Water productivity and energy consumption

The hourly water production and the total electrical power input to the thermoelectric distillation system are shown in Figure 4.14. The results presented in the figure were average values of three experiments under the same conditions.

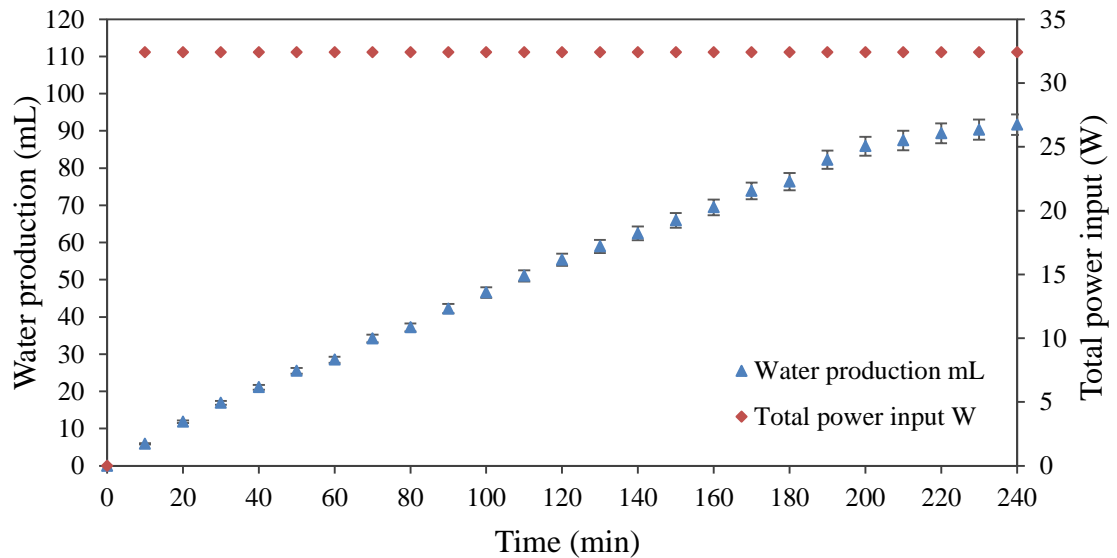


Figure 4.14: The distillate water collected and total power input during more than three hours.

The average total amount of fresh water produced was 91.7 mL from a condenser area of 0.042 m^2 (equivalent to 2.2 L/m^2) after 4 hours of operation, with a constant input power (thermoelectric and pump) of 32.4 W. The total energy consumption was 0.1296 kWh over 4 hours. Using the data presented in Figure 4.14, the amount of the water produced per hour can be estimated. Figure 4.15 shows the hourly rate water production of the developed prototype system. The maximum hourly rate (28.5 mL) was obtained

within the first hour (0h – 1h) of operation and then the water production rate decreased with time due to the reduction in the temperature difference between the vapour and the condenser surface. The hourly rate during the second (1h – 2h), the third (2h – 3h) and the fourth (3h – 4h) hour were 26.8 mL, 21.0 mL and 15.3 mL, respectively. The reason of this decrease is because the temperature difference between the vapour and the condenser is decreased and not enough cooling at the cold side of the thermoelectric module to absorb the latent heat of the condensation in the fourth hour of system operation. The water production rate of the thermoelectric distillation system also depends on several other factors, which will be discussed in later chapters.

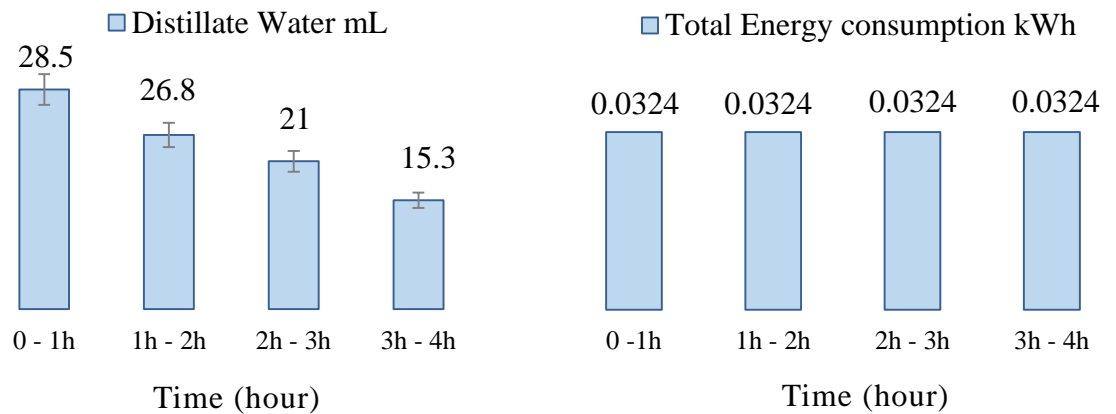


Figure 4.15: The hourly water distillate and total power consumption during four hours operation.

4.6.4 Comparison with other technologies

The total power consumption is mainly due to the power to the thermoelectric module (31.9 W) with a small fraction to the water pump (0.5 W). The results show that the energy required to produce 28.5 mL of freshwater is 0.0324 kWh over one hour of operation. This is equivalent to a specific energy consumption of 0.00114 kWh/mL. A literature survey reveals that all existing water distillation systems have a specific energy consumption ranging from 0.00122 to 0.05945 kWh/mL, with some systems utilising

solar heating (see Table 2.5 in Chapter Two). Clearly, this result demonstrates that the developed system of this work represents the most efficient thermoelectric distillation system known to date.

4.6.5 Power generation after switching off

It has been observed that after the system was switched off, there was still a temperature difference between the hot and cold side of thermoelectric module due to the temperature difference between the sample water and the vapour. Since thermoelectric module can also use as a power generator, the power output after switching off was investigated. A multi meter was connected to the terminals of the thermoelectric module to measure the open circuit voltage. The output voltage was small because the temperature difference between the hot and cold sides of the thermoelectric module ($\Delta T / TE$) was very small. Figure 4.16 shows the measured values of ($\Delta T / TE$) as a function of time, which were in a range of 28.1 °C to 10.9 °C. During one hour, the temperature of the water decreased from a steady state temperature of 47.8 °C to 33.2 °C, the temperature of the vapour also decreased slightly from 30.9 °C to 24.3 °C.

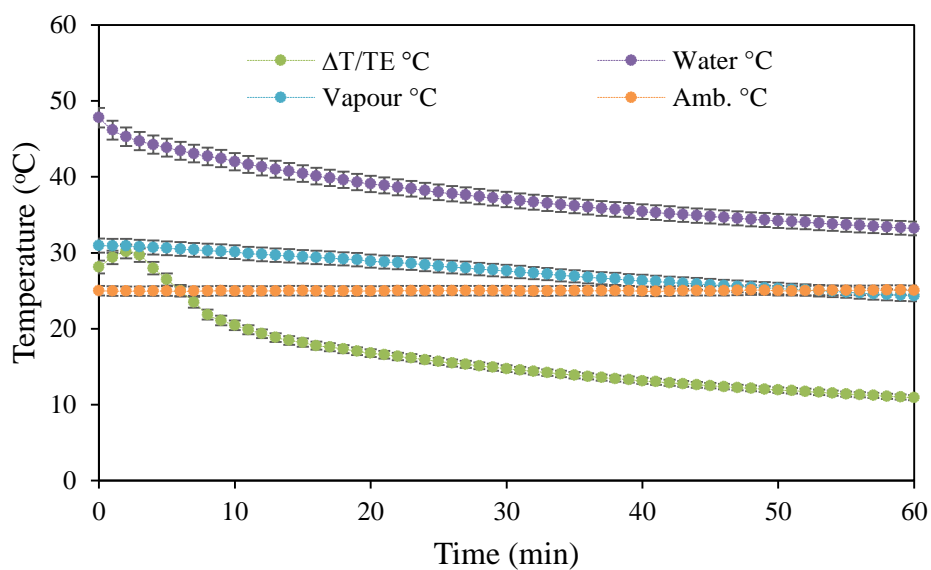


Figure 4.16: The temperatures profiles of the system after switching off.

Figure 4.17 shows the open-circuit output voltage and the power output. The open-circuit voltage were measured directly and the power output was calculated using the measured open-circuit voltage and the load resistance of the thermoelectric module (0.152Ω). The maximum output voltage (36.6 mV) occurred during the first 10 minutes. The output voltage then decreased due to decrease of the $(\Delta T / TE)$ to reach 5.1 mV after 60 minutes. Similarly, the maximum output power was 8.8 mW and decreased with time to 0.2 mW . The results demonstrate that a small power (a few mW) can be generated by the thermoelectric distillation system after switching off. Although the power level generated is very low, it may be used for low power wireless sensors and transmitters. It may also be used as a sensor to monitor the temperature change in the system.

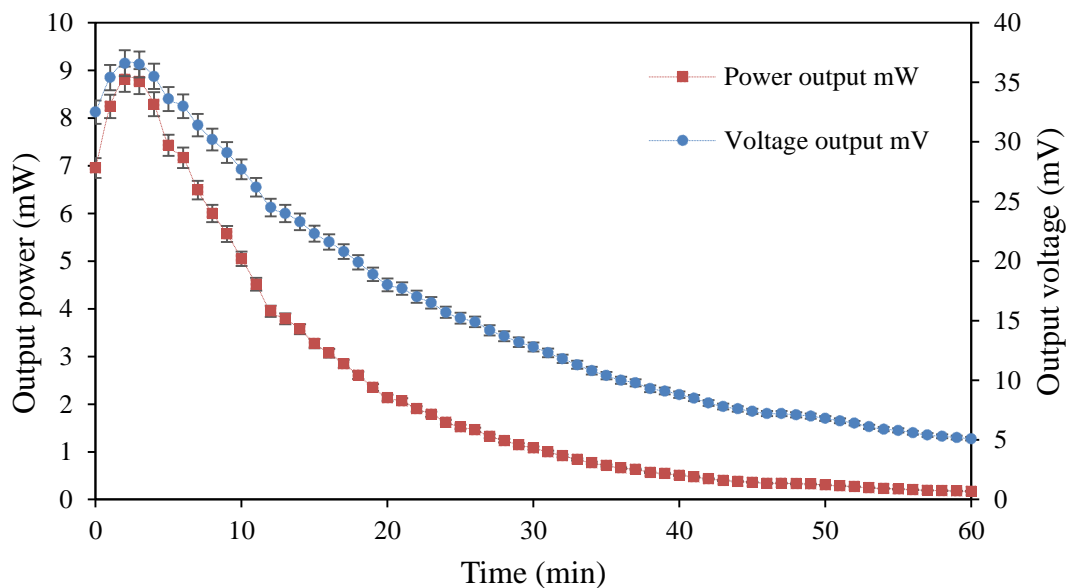


Figure 4.17: The output power and open circuit voltage of the system after switch off.

4.7 Conclusions

In this chapter, the thermoelectric distillation system developed in Chapter 3 was investigated experimentally. The system produces 28.5 mL (equivalent to 678 mL/m^2)

over a period of 1 hour. The corresponding electrical energy required for the water production is 0.0324 kWh, which gives a specific energy consumption of 0.00114 kWh/mL. This can be compared with the values ranging from 0.00122 to 0.05945 kWh/mL for a number of previously reported systems. It is noted that the reported values at the low end were actually obtained from systems where evaporation is assisted by solar heating while the results obtained from this study is without solar heating. It is clear that the system developed in this study has significantly lower energy consumption than any of the existing thermoelectric distillation systems. The improvement is due to the use of the hot side of the thermoelectric module to heat the water for increasing evaporation and the use of the cold side to cool the condenser to improve condensation. As a result, both the water productivity and the power consumption are improved, as demonstrated in this experimental study. The results provide direct experimental validation of the proposed concept - the water productivity and energy consumption can be significantly improved by using the waste heat from the hot side of the thermoelectric module to enhance the evaporation through recirculation of the sample water.

Chapter 5

Validation and Analysis of the Evaporation and Condensation Processes in the Thermoelectric Distillation System

5.1 Introduction

The water-vapour transition plays a key role in the thermal distillation process and the heat transfer associated with evaporation and condensation has to be managed. To determine energy required or removed during the distillation process, it is necessary to develop predictive models for the evaporation and condensation processes. The thermoelectric distillation system involves the evaporation and the condensation processes for vapour and water production, respectively. The objective of this chapter is to validate the theoretical models, which were described in chapter 3, to determine the rate of evaporation and condensation in the system. The evaporation rate depends on several parameters including water and vapour temperatures, pressure, specific volume, latent heat of evaporation and water-vapour surface area. The condensation rate depends on the temperature and pressure of the vapour, temperature of the condenser surface, area of the condenser surface, latent heat of condensation and the local convective coefficient. Both rates are related to the heat flow of the thermoelectric module. The thermal performance of a thermoelectric distillation system depends on the dynamic equilibrium between the evaporation and condensation processes. The developed models are validated using the experimental results obtained under controlled conditions.

5.2 Process description in the thermoelectric distillation system

Figure 5.1 is a graphical representation of the thermoelectric distillation system showing heat transfer, evaporation and condensation processes. Evaporation and condensation are principally convective heat transfer processes involving phase change.

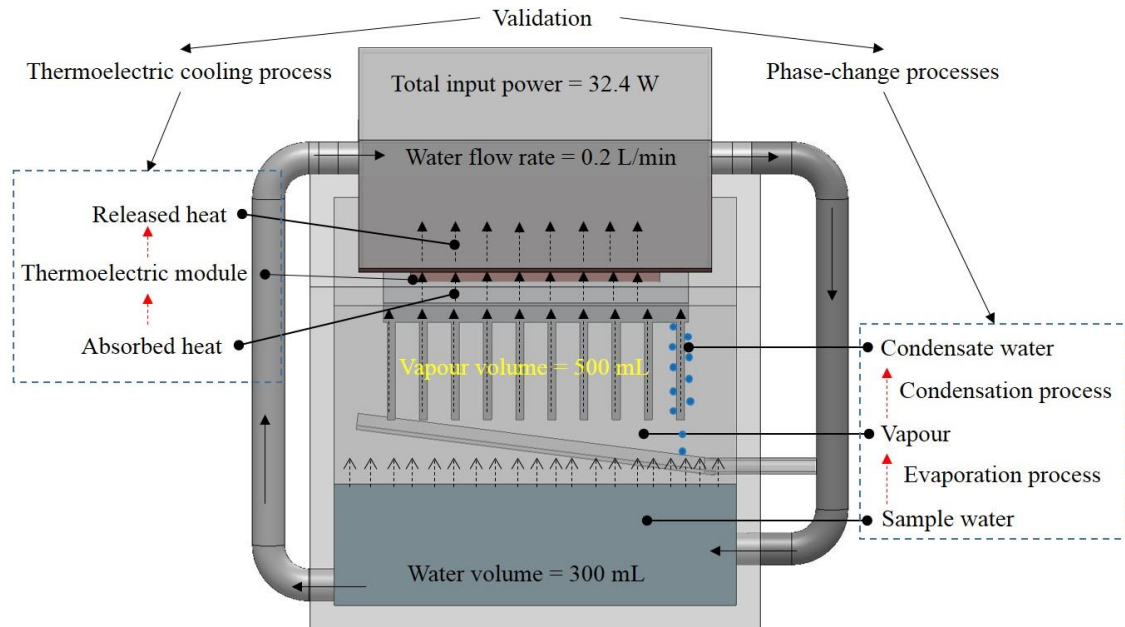


Figure 5.1: Schematic diagram of the heat transfer mechanism in the system.

Vaporization occurs at the water–vapour interface inside the system. Once the temperature of the sample water increases, vapour spontaneously rises up to the aluminium heat sink, where it condenses to water at the cooled fins and flows down under the influence of the gravity to the collector. Condensation occurs when the temperature of the vapour is decreased below its saturation temperature. The condensation process commonly results from contact between the vapour and the condenser surface (fins). Two common forms of latent heat are involved inside the system; latent heat of evaporation and latent heat of condensation. These terms describe the direction of energy flow when changing from one phase to the other. When the latent heat of the vapour is released, heat is transferred to the condenser surface, and the condensate is formed.

The core of the thermoelectric distillation system is the thermoelectric module, which uses the Peltier effect to enhance the temperature difference between the evaporation water surface and the condensation metal surface for water production. An aluminium heat sink with fins is connected to the cold side of the thermoelectric module to condense the vapour particles (condensation process). Sample water is pumped to the top of the system where it passes over the copper heat exchanger that is connected to the hot side of the thermoelectric module. During this process, the temperature of the feed water is raised and then returns to the bottom basin to improve the evaporation process. The theoretical outlines are provided based on the water-vapour theory to model the vapour and the water production processes of the thermoelectric distillation system. The models are validated by the results from experiments.

5.3 Theoretical models validation with the experimental results

5.3.1 Evaporation process at the water-vapour interface

The theoretical model of the evaporation process to estimate the evaporation rate was reported in section 3.3.1. The model is validated using the experimental results of the measured humidity in the system. Humidity and evaporation rates are two phenomenon that are closely related to each other as one condition governs the other. The experiments give a reasonable idea of how the humidity affects the evaporation rate. It can be clearly interpreted that if the humidity of the system is high, the density of the vapour will be higher, because it is related to the vapour temperature increasing. The initial volumes of the sample water and the vapour are $3 \times 10^{-4} \text{ m}^3$ and $5 \times 10^{-4} \text{ m}^3$ respectively. The surface area of the water-vapour interface is 0.01 m^2 . The system is sealed using General Purposes Silicon between the edges of the chamber cover and the walls. The General Purposes Silicon product is EN15651-3: Type S Class S1. The properties of the product are

transparent, water proof, permanently flexible, interior or exterior use, quick draying and mould resistance. The distilled water was captured in a sealed container. The total mass of the water in the system is equal to the mass of the produced water (after the distillation process) and the mass of the water remain in the system (not evaporated and not collected). Useful results are obtained by making three assumptions; 1) the vapour pressure increases by a small amount in the system and so an atmospheric pressure in the system can be assumed, 2) the mass of the gas inside the chamber is mixture of vapour and air masses and 3) there is a saturation region at the water / vapour interface which is in thermal equilibrium.

In the experiments, the system was filled with 300 mL of water and the mass of the distillate water was measured every 10 minutes. Hence, the mass of water remaining in the basin after the distillation process is:

$$m_{remain} + m_{distillate} = m_{initial} \quad 5.1$$

Where m_{remain} is the mass of water remaining in the chamber which is not evaporated and not collected, $m_{initial}$ is the mass of the initial water at the start of the experiments and $m_{distillate}$ is the mass of the fresh water produced during system operation. All these terms are recorded in grams and are measured experimentally. The performance of the distillation system can be assessed by the distillation ratio, which is defined as the mass of the water distillate, divided by the initial mass of the water in the basin:

$$Distillation\ ratio = m_{distillate} / m_{initial} \quad 5.2$$

The relative humidity RH of the system is the ratio of the actual density ρ_{actual} in (kg/m^3) to the saturation density $\rho_{saturation}$ of the vapour in (kg/m^3) at a given vapour temperature. The saturation density of the vapour can be obtained from the Steam Tables at atmospheric pressure [117]. Therefore, the mass of the produced vapour can be estimated from the measurements of RH and the vapour temperature:

$$RH = \rho_{\text{actual vapour}} / \rho_{\text{saturation vapour}} \quad 5.3$$

$$V_{\text{actual vapour}} = V_{\text{total}} - V_{\text{water remaining in the chamber}} \quad 5.4$$

$$m_{\text{actual vapour}} = \rho_{\text{actual vapour}} V_{\text{actual vapour}} \quad 5.5$$

where $V_{\text{actual vapour}}$ is the volume of actual vapour in (m^3), V_{total} is the total volume of the water/vapour chamber, $V_{\text{water remaining in the chamber}}$ is the volume of the water remaining in the chamber in (m^3) and $m_{\text{actual vapour}}$ is the actual mass of the vapour produced in grams. From the theoretical results in Chapter 3, heating water causes the molecules to speed up and spread slightly further apart and this results in a decrease in the density and an increase in the specific volume of the hot water. There is also an increase in the vapour density (adding mass to a known volume due to the evaporation process) and this leads to a decrease in the specific volume of the vapour. The result is a decrease in the specific volume difference between the water and the vapour, as well as an increase in the vapour mass fraction.

With the same experimental setup of the thermoelectric distillation system in Chapter 4, an additional instrument (pressure gauge) was connected to the vapour chamber within the system (see Figure 5.2). To evaluate the thermal properties of the vapour (temperatures, humidity, pressure and dew point), the setup was tested under standard laboratory conditions (initial feed water temperature of 21 °C, air temperature of 20°C and air humidity of 29%). The experiments were carried out for 60 minutes and the basin was filled with 300 mL of tap water. The distillate water due to the condensation process was collected and measured with thermoelectric module and water pump in operation. Table 5.1 shows the water production in one hour with and without operation of the thermoelectric module (heating at the hot side and cooling at the cold side) and with and without water pump circulation. It can be seen clearly the advantage of operating both the thermoelectric and the pump to increase water productivity.

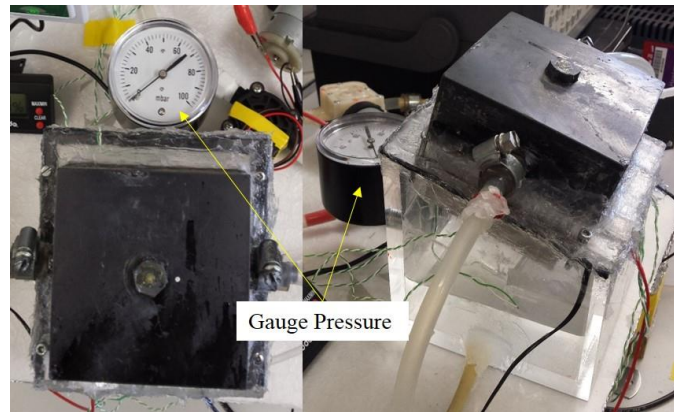


Figure 5.2: Two views of the pressure gauge connected to the thermoelectric distillation system.

Table 5.1: Water production with and without thermoelectric module operation and water pump circulation.

Thermoelectric operation	Water pump circulation	Water production (mL)
✓	✓	28.5
✓	✗	0
✗	✓	0
✗	✗	0

During the one-hour system operation, the water temperature is increased due to the heat transferred from the hot side of the thermoelectric module to the circulating water. This leads to an increase in the temperature of basin water and consequently distillate production (see Figure 5.3). It was observed that the increase in water temperature (from 21.9 °C to 25.2 °C) is particularly great within the first 10 minutes of thermoelectric operation compared with 50 minutes steadily increasing of water temperature. The average amount of distillate water after one hour of system operation was 28.5 mL (at water temperature of 43 °C) with a 9.5% distillation ratio. The experiments were fixed with a constant input power (thermoelectric and pump) of 32.4 W and with a constant electric current to the thermoelectric module of 10 A.

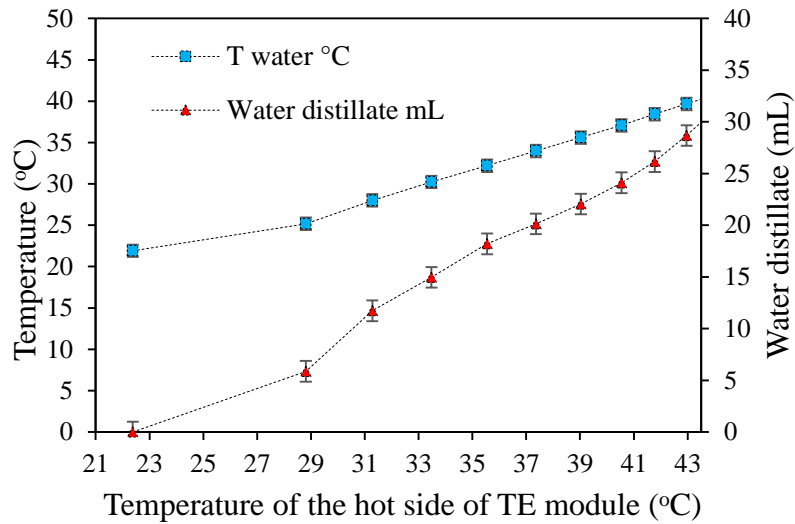


Figure 5.3: The water temperature and water production rate as a function of the hot side of the thermoelectric temperature.

Figure 5.4 shows the relative humidity RH and the vapour temperature as a function of the water temperature. Although there was an initial decrease in the RH of the system from 55% to 51%, it subsequently increased to 74% after one hour of operation. In addition to the humidity, the temperature of the vapour followed a similar behaviour with decrease from 21.9 °C to 16.6 °C then a subsequent increased to 25.6 °C. The results show a clear correlation between the relative humidity and vapour temperature.

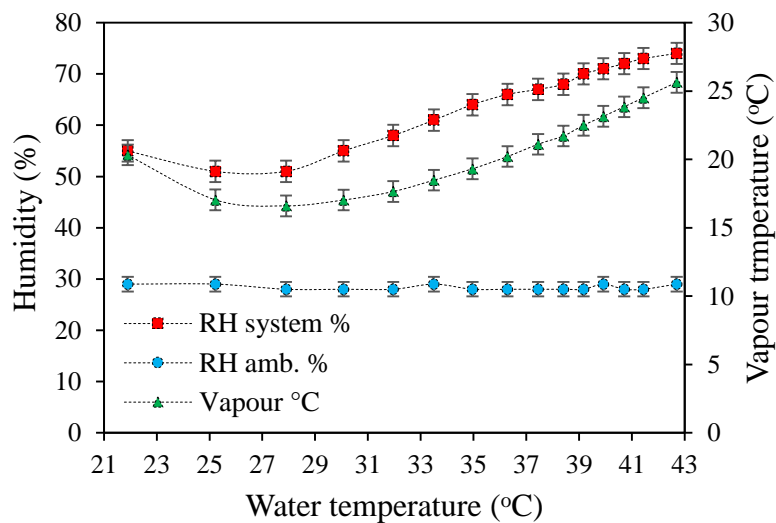


Figure 5.4: The experimental data of vapour temperature and humidity.

A pressure gauge is often used to measure the pressure difference between a system and the surrounding atmosphere. In other words, the gauge pressure is the pressure inside the system relative to atmospheric pressure. Therefore, it reads a positive value for pressures above atmospheric pressure, and negative values for pressures below it. Repeatable experiments have been conducted to measure the properties of the vapour inside the chamber such as the dew point and pressure, to confirm that the vapour pressure is equivalent to the atmospheric pressure as assumed (see Figure 5.5). Dew point is a temperature of a vapour at which water begin to condense. It can be calculated using the dew point calculator (see Appendix A.2) based on the temperature and the humidity of the vapour presented in Figure 5.4. During a one-hour period, the dew point temperature varies over a small range from 6 °C to 19 °C with zero gauge pressure as shown in Figure 5.5.

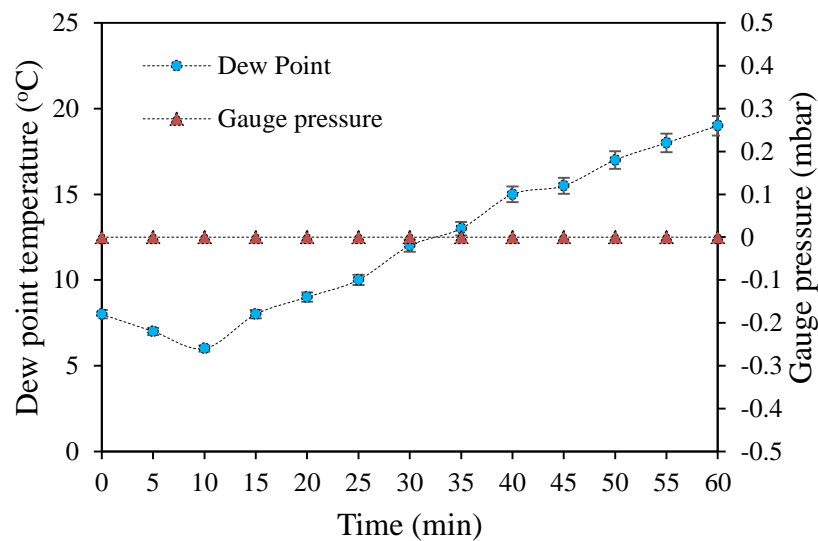


Figure 5.5: The dew point and gauge pressure of the vapour produced.

Figure 5.6 shows the vapour mass determined using the experimentally obtained relative humidity values based on Equation 5.5. The theoretical calculations based on equation 3.11 using Steam Table are also presented in the figure by solid line. The validation is

shown for two-hour system operation and with the water temperature ranging from 20 °C to 60 °C. A reasonable agreement is evident.

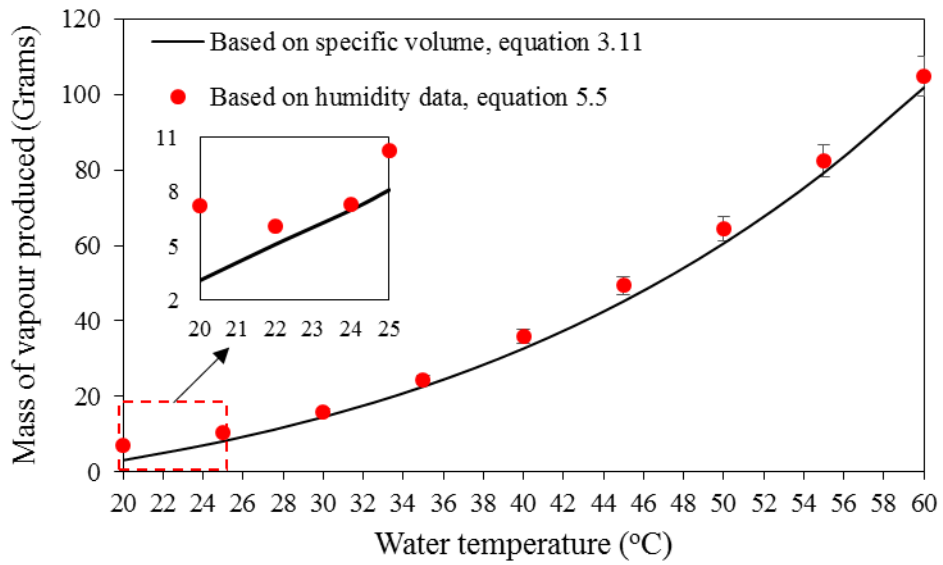


Figure 5.6: The validation of the vapour mass produced with two-hour system operation.

Figure 5.7 shows a plot of water remaining in the system (experimentally determined using equation 5.1) as a function of different water temperatures (represented by red dots). The theoretical value was calculated from $m_{total} (1-x)$ and is shown by the solid line on the graph.

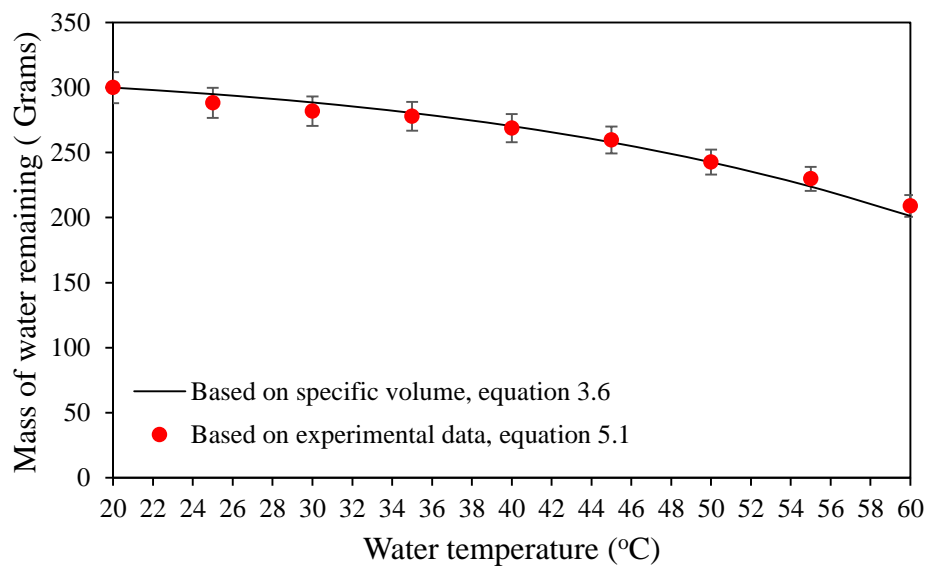


Figure 5.7: The validation of the water mass remain with two-hour system operation.

The ratio of the water distillate from the system (28.5 mL) to the total water filled into the evaporation chamber (300 mL) is the experimental distillation ratio while, the theoretical distillation ratio can be calculated using the results of the Figure 3.4. The validation corresponds to a theoretical distillation ratio of 12% when the system reached a water temperature of 42.7 °C and is in reasonable agreement with the 9.5% value experimentally obtained. There is a small difference between the experimental and theoretical values and this is due to thermal losses during the condensation process. The overall energy losses of the system will be discussed in section 5.5.

5.3.2 Condensation process at the vertical fins

Condensation occurs when the temperature of the vapour is decreased below its saturation temperature. Practically, the process results from contact between the vapour and the cooled surfaces (fins). Figure 5.8 shows the measured variation in temperature of the system components; sample water, vapour, condenser surface, ambient and the hot / cold side of the thermoelectric module and ambient during the one-hour operation of thermoelectric and water pump. For high condensation, the convection heat transfer between the vapour and the cooling surface should be high, in order to increase the water production. The experiments were conducted with the thermoelectric module operating at 10 A. There is a significant variation in temperature for the cold side of the thermoelectric and condenser, with both recording minima during the first 10 minutes. The minimum cold side temperature was -10.4 °C, with a value of 1.7 °C for the minimum condenser surface temperature. The thermoelectric hot side temperature and water basin temperature both increase gradually in a similar manner. The experimental data was used to calculate the amount of heat transferred and the water condensation rate (equations 3.32 and 3.19).

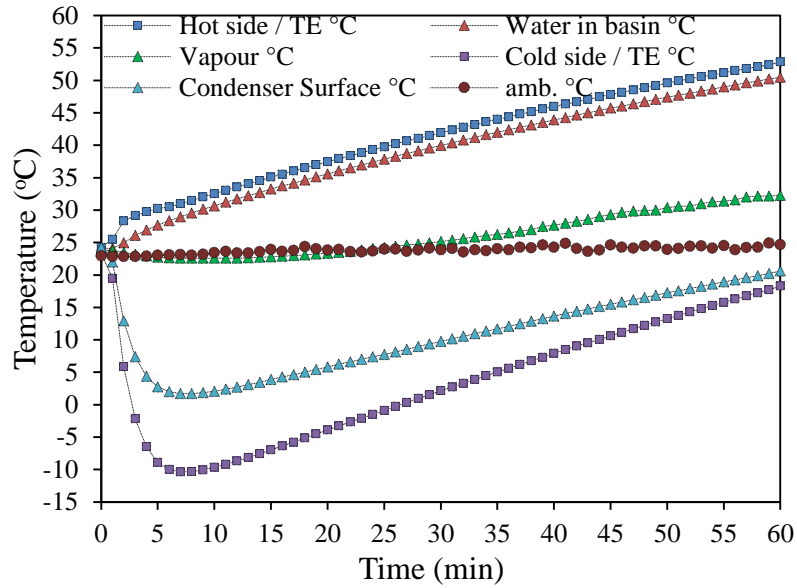


Figure 5.8: The temperature variation of the system components.

The average amount of water produced was 28.5 mL over a period of one-hour system operation. The total electrical power (thermoelectric module and water pump operation) required for the water production was 32.4 W. The total energy consumption of the system for one hour was 0.0324 kWh. Figure 5.9 shows the amount of water condensate collected over one hour for experimentally measured and theoretically predicted values.

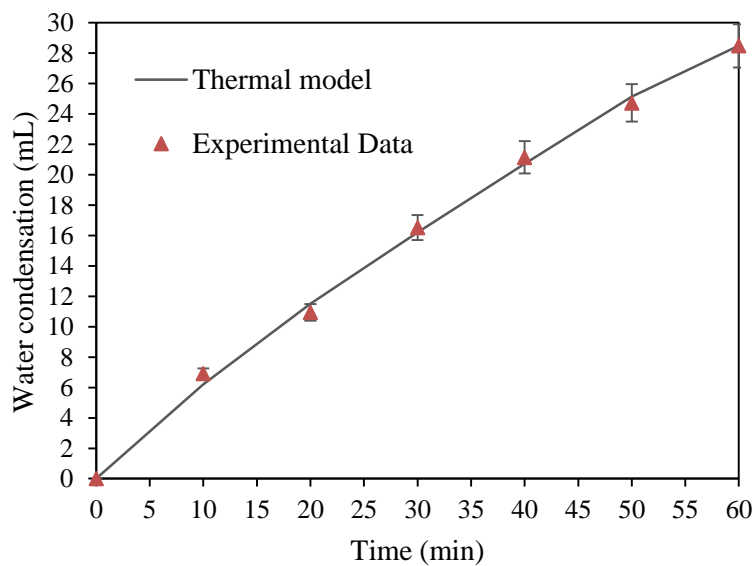


Figure 5.9: The validation of the water condensation rate with the fitted h_c of = 8 W/m².K.

The theoretical model (R-squared value =0.9929) reliably predicts the amount of water condensate produced by the thermoelectric distillation system for a fitted heat transfer coefficient $h_c = 8 \text{ W/m}^2\cdot\text{K}$. The convective heat transfer coefficient is a very significant parameter during the thermoelectric distillation system, and depends on many parameters such as the condenser material and its geometry and the thermal conditions of the fluids in the system.

5.4 Water and vapour flows in the system

Water and vapour flows are invisible sources of many problems in today's thermal distillation systems such as cavitation. This section provides a fundamental understanding of how water and vapour transport occurs, the fluids' properties, the types of flow and effects on the system. The circulation of water flow is from the basin to the water heat exchanger, while the direction of vapour flow is from the interface of the water up to the condenser surface of the fins. Table 5.2 shows the properties of the water and vapour at steady state for the flow simulation.

Table 5.2: The properties of the water and vapour in the system.

Property	Water / heat exchanger	Vapour / Chamber
volume	128 cm ³	479.5 cm ³
Temperature	$T_w = 47 \text{ }^\circ\text{C}$	$T_v = 28 \text{ }^\circ\text{C}$
P and T lab.	101.32 kPa and 20 °C	101.32 kPa and 20 °C
Flow length	0.09 m	0.06 m

Figures 5.10 and 5.11 show the flow simulation results of the water and the vapour in the thermoelectric distillation system. Table 5.3 shows the mesh information, for more details about the materials properties and the boundary conditions see Appendix A.3.

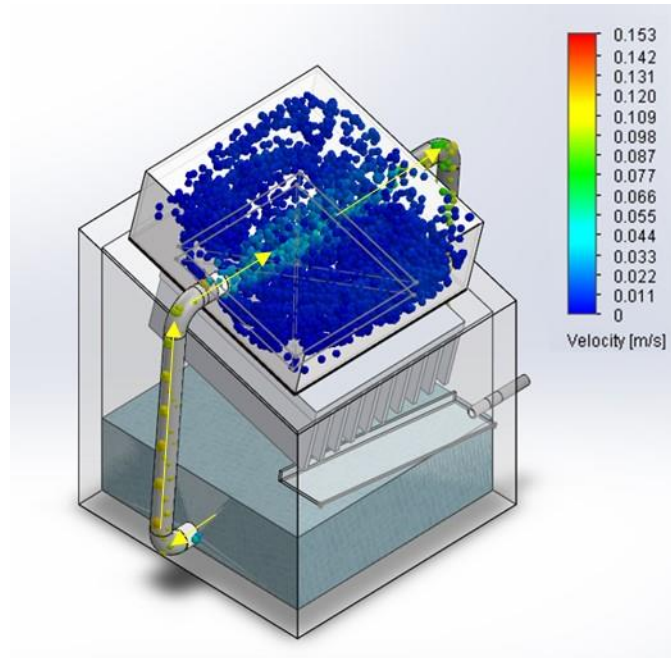


Figure 5.10: Water flow in the hot side heat exchanger at steady state.

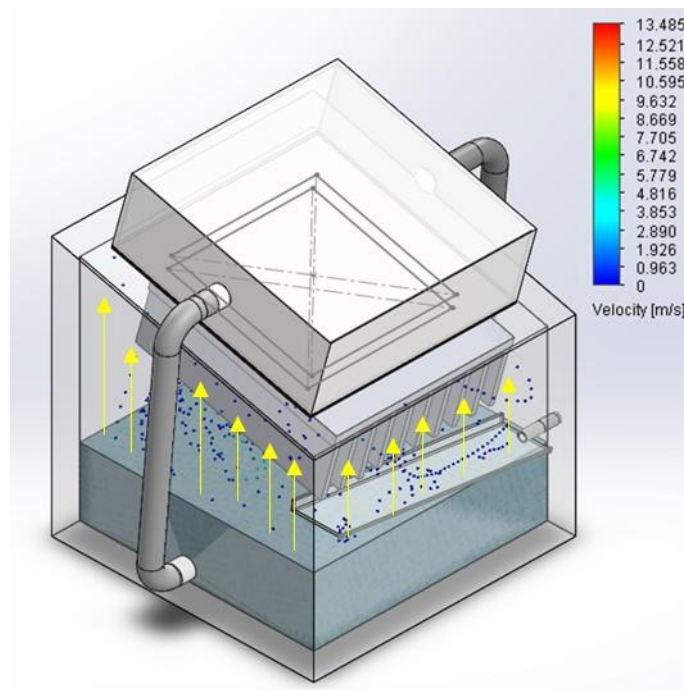


Figure 5.11: Vapour flow inside the chamber at steady state.

Table 5.3: Mesh information of the thermoelectric system.

Mesh type	Mesher Used	Total nodes	Total elements	Max. aspect ratio
Solid mesh	Curvature based mesh	16399	8743	94.34

SolidWorks flow simulation is a branch of computational fluid dynamics that uses numerical analysis to solve and analyse problems that involve fluid flows. Flow simulation is used to perform the calculations required to simulate the interaction of water and vapour with surfaces, defined by fluid domain, geometry and flow conditions. The output flow simulation results are listed in Table 5.4.

Table 5.4: The output results of the water and vapour in the system.

Property	Water / heat exchanger	Vapour / Chamber
Kinematic viscosity	$0.553 \times 10^{-6} \text{ m}^2/\text{s}$	$329.2 \times 10^{-6} \text{ m}^2/\text{s}$
Maximum velocity	0.033 m/s	1.92 m/s
Reynolds number	5370	350
Flow type	Turbulent	Laminar

Using these results, we can obtain some idea of the physical properties of the water and vapour in the system. The Reynolds number of the vapour flow is much lower than that for the water flow, this indicates that the vapour flows along smooth paths in the chamber with constant velocity. Therefore, the risk of cavitation (damage to a solid surface due to turbulent vapour flow) of the Plexiglas surfaces inside the chamber is insignificant. Whilst, the risk of water-circulating cavitation in the heat exchanger could be significant when the water flow is circulated for long time.

5.5 Overall energy losses at steady state

When energy is transformed from one form to another, or moved from one place to another, or from one system to another there are some energy losses. This means that when energy is converted to a different form, some of the input energy is turned into a highly unsettled form of energy, such as heat. Functionally, turning all of the input energy

into useful output energy is almost impossible. Also, whenever electrical energy is transported through power lines, the energy into the power lines is always more than the energy that comes out at the other end. From the results in the Figure 4.11 in chapter 4, the steady state thermoelectric cooling power was 29.1 W. The overall losses of the system are considered to be the following:

1. The thermal losses from the thermoelectric distillation system, as shown in Figure 5.12.

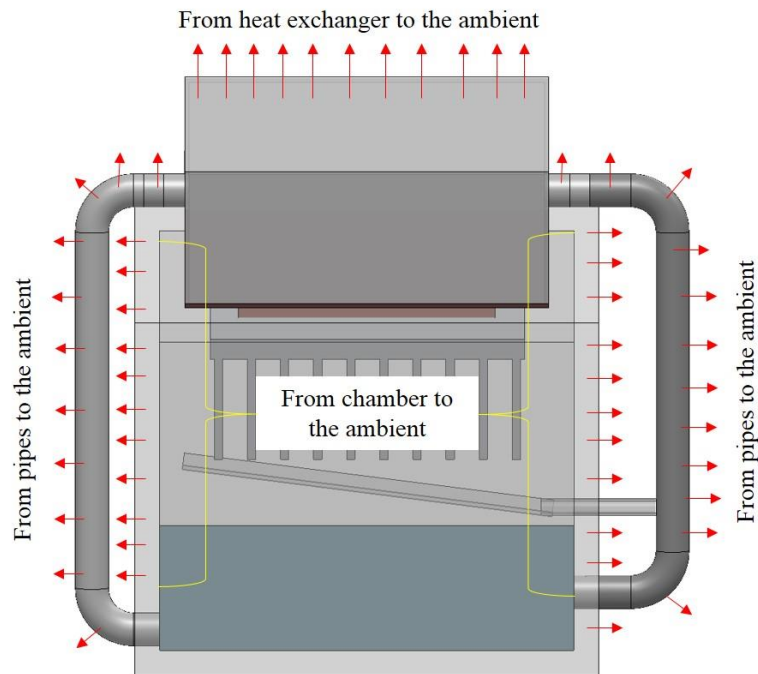


Figure 5.12: Thermal losses from the thermoelectric distillation system to the ambient.

The losses include the heat dissipated to the ambient from the Plexiglas chamber, top heat exchanger box and pipes. The general heat loss formula is

$$L_T = h_a A_s \Delta T \quad 5.6$$

where L_T is the total thermal losses, h_a is the heat transfer coefficient of the ambient, A_s is the surface area and ΔT is the temperature difference between the system components

and the ambient. The calculations of the thermal losses can be shown in Table 5.5 at the steady state. The h_a depends on the air velocity in lab u_a which can be expressed as [70]

$$h_a = 5.7 + 3.8 u_a \quad 5.7$$

The air velocity was measured in the lab using Anemometer *TL017* and it was 0 m/s at any position around the system when there were no air movements in the lab.

Table 5.5: Thermal losses calculations.

Part	$A_s (m^2)$	$\Delta T (K)$	$L_T (W)$
Chamber	0.037	6.7	1.41
Top heat exchanger	0.019	5.1	0.55
Pipes	0.005	12.2	0.35

From the Table 5.5, the total thermal losses (L_T) of the thermoelectric distillation system to the surroundings at the steady state condition was 2.31 W.

2. The electrical losses of wires from the power supply to the thermoelectric module can be measured at the steady state condition. The wires are not perfect conductors, and as such resistance to flow is encountered. This resistance causes power to be lost along the length of wire, in accordance with this Equation

$$Power\ losses = I^2 R \quad 5.8$$

where I is the electric current flowing through a wire, and R is the total electrical resistance of the wire. At 10 A DC current supply and 0.001 Ω and 0.002 Ω resistance of black and red wires, the DC resistance was calculated in accordance with (black copper

wire: 60 cm length and 4 mm diameter and red cooper wire: 75 cm length and 3 mm diameter), the total electrical power losses for both wires was 0.3 W.

3. There are some other losses in the system which are a quite complicated to calculate such as the heat flow losses in the water pump at high water temperature, the evaporation / condensation losses at the walls of the chamber and internal heat losses in the thermoelectric module due to the heat transfer from the thermoelements legs to the surroundings. The total losses of the thermoelectric distillation system (as a percentage) are shown in Figure 5.13.

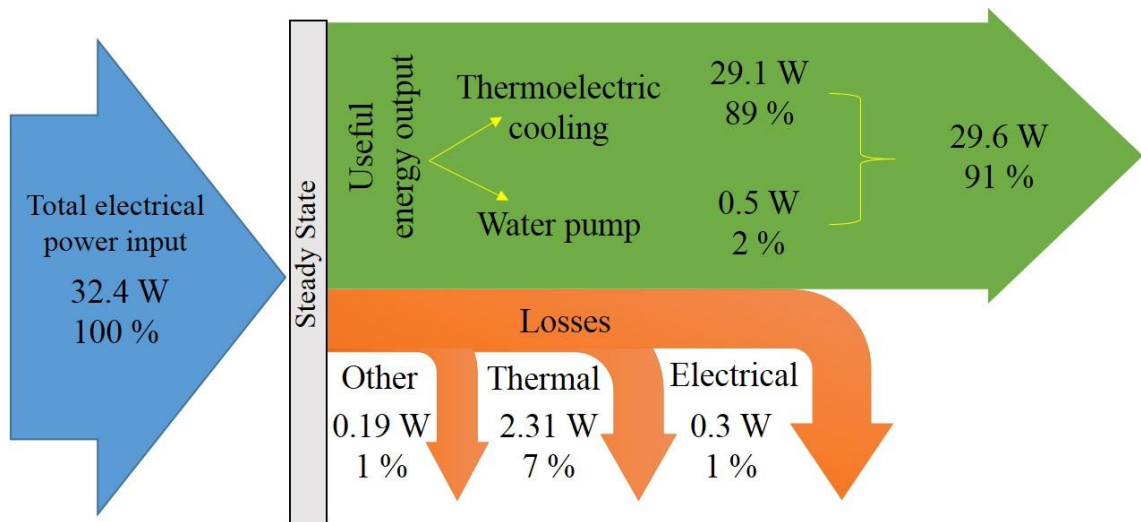


Figure 5.13: Diagram of the total losses of the system.

5.6 Conclusions

The developed models of the water and vapour production are validated using the experimental results obtained under controlled conditions in the thermoelectric distillation system. The experimental results confirm the increase of the relative humidity in the system has a direct effect on the increase of the water productivity because of the increase in the evaporation rate. Liquid water to vapour phase change calculations were

used to assess the performance of the system and to find a theoretical distillation ratio of 12% with a water temperature of 42.7 °C. After operating the system for one hour, the distillation ratio was experimentally determined to be 9.5 % and is in reasonable agreement with the model. Moreover, a thermal model has been developed for the water condensation process which uses a thermoelectric module. The following specific conclusions can be made on the basis of this chapter:

- For the thermoelectric distillation system, the thermal models can be used for the determination of the key parameters that control the evaporation and the condensation processes and the system thermal performance.
- The model shows that the rate of water condensation is dependent upon the convective heat transfer coefficient of the cold-side heat exchanger.
- The fitted value of the convective heat transfer coefficient by the thermal model for the thermoelectric distillation system is 8 W/m².K.
- The total percentage loss of the thermoelectric distillation system when operating under steady state condition is 9 %.

Chapter 6

Key Factors Affecting the Water Production in the Thermoelectric Distillation System

6.1 Introduction

There are a number of theoretical and experimental studies that investigate various parameters affecting the performance of thermal distillation systems [118-125]. The use of a thermoelectric technology to conduct seawater distillation is regarded as a bit complicated technology. The difficulty occurs in simultaneously raising the evaporation temperature and decreasing the condensation temperature, since heating, evaporation and condensation all take place in one system. Hence, previous research written about the thermal distillation systems are not comprehensive enough to properly investigate the effect of a thermoelectric module on the water productivity. The aim of this chapter is to modify the setup of the thermoelectric distillation system to investigate experimentally the key factors that affecting the water productivity. The modified system allows to control the key factors by maintaining all the factors constant and change one of them in order to study the influence of this factor on the water productivity.

6.2 Factors affecting water productivity

The performance of a distillation system can be affected by several factors such as water and vapour temperatures, dew point, water-vapour surface area, water volume (or water depth at a constant water-vapour surface area), vapour density and fluid pressure. Once a thermoelectric module is employed to assist the distillation process, there are additional factors that can affect the performance of the system.

The additional factors include; input power, Peltier current, cooling capacity, cold side and hot side temperatures of the thermoelectric module and the size of the module. These factors are dependent of each other. In a thermal distillation system employing thermoelectric module, these factors can significantly influence the rates of evaporation and condensation. The higher the temperature of the water, the higher the rate of evaporation. The lower the temperature of the cooling surfaces, the higher the rate of condensation. Both heating and cooling are provided by the thermoelectric module (operating in the Peltier mode). However, it is almost impossible to design and build a system that can investigate all the above mentioned factors on the total water production using constant geometric factors.

There are factors that can be carefully adjusted in a cost effective way to improve the performance of the thermoelectric distillation system. Therefore, the purpose of this chapter is to present and explain the key factors that influence the water production rate, thereby improving its performance. The experimental investigations require changing one factor at the operation period and keep others factors constant. These factors include; sample water temperature, vapour volume, Peltier current, input power and hot side temperature of the thermoelectric module. The constant geometric factors through the experiments are shown in Table 6.1.

Table 6.1: Constant geometric factors through the experiments.

Geometric factors	Values
Area of one thermoelement of thermoelectric (mm ²)	17.6
Number of thermoelements in the module	98
Condenser surface area (m ²)	0.041
Condenser angle	15 °
Water-vapour surface area (m ²)	0.01

6.3 System description

A schematic diagram of the thermoelectric distillation system employed for this study is shown in Figure 6.1. The system was configured in such way that the temperatures of evaporation and cooling can be controlled independently to enable the investigation of these key factors accordingly. The system consists of a heated water circulation (a connection between the sample water basin and a constant temperature water bath) and a cooling water supply (connecting between the mains water supply and the water heat exchanger). An aluminium heat sink with fins is connected to the cold side of the thermoelectric module to condense the vapour particles and a copper heat exchanger is used to reject heat from the hot side of thermoelectric module. A small pump is used to return the unevaporated water to the water bath. The system uses two power supplies; one for powering the thermoelectric module and the other for the water pump. A data logger was connected to a laptop PC to record the temperatures of the system components.

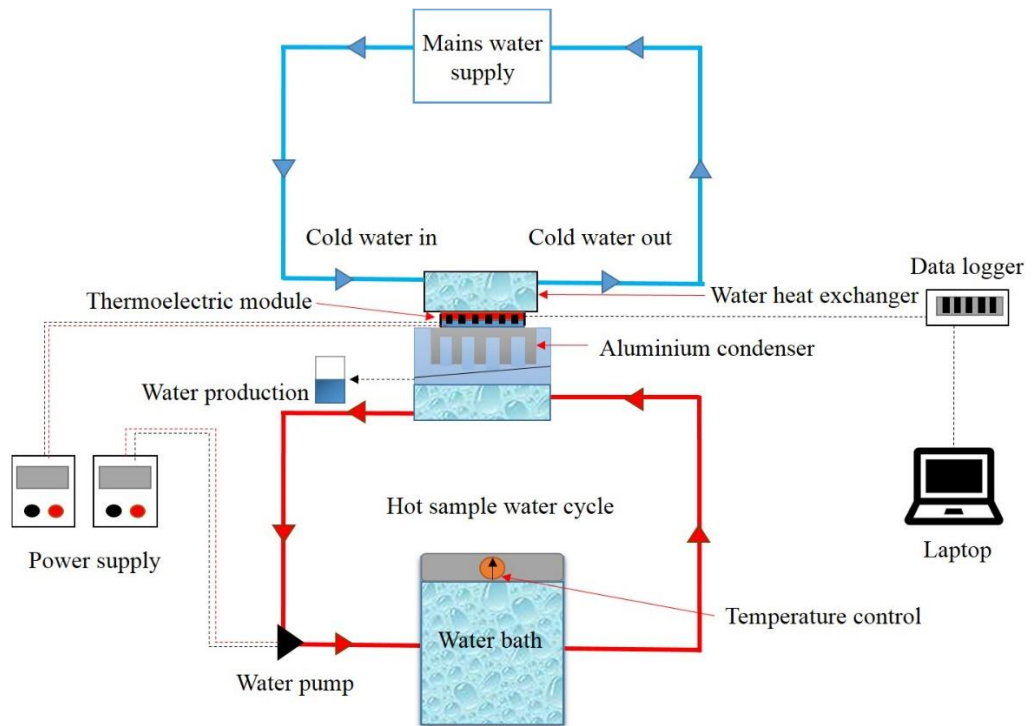


Figure 6.1: Schematic diagram of a thermoelectric distillation system with independently controlled water circulations.

6.4 Modified experimental setup

The experiments were designed to observe and investigate the effect of the key factors on the water productivity of the thermoelectric distillation system. Figure 6.2 demonstrates an experimental setup, including a high temperature water bath, two power supplies, a digital scale and a digital flow meter with one-side valve connected to the hot water bath. The setup is intended to suit one thermoelectric module (effective area of 38.4 cm^2) sandwiched between two heat exchangers. The volume of the condenser is 150 cm^3 and the effective area of the condenser fins is 410 cm^2 . The volume of the evaporation-condensation chamber is 850 cm^3 and the water-vapour surface area is 0.01 m^2 . A small ruler scale (3 cm) was fixed on the corner of the chamber walls to check and read the water level in the system. The water bath and sink provide hot and cold water to the system at a specific temperature. To investigate these key factors, experiments were conducted in controlled lab conditions. The experiments were carried out for 180 minutes and the basin was filled with tap water. During the experiments, the temperature of the laboratory, water in the basin, vapour, condenser surface and hot / cold sides of the thermoelectric module was measured and recorded. The water production and the input power were measured manually.

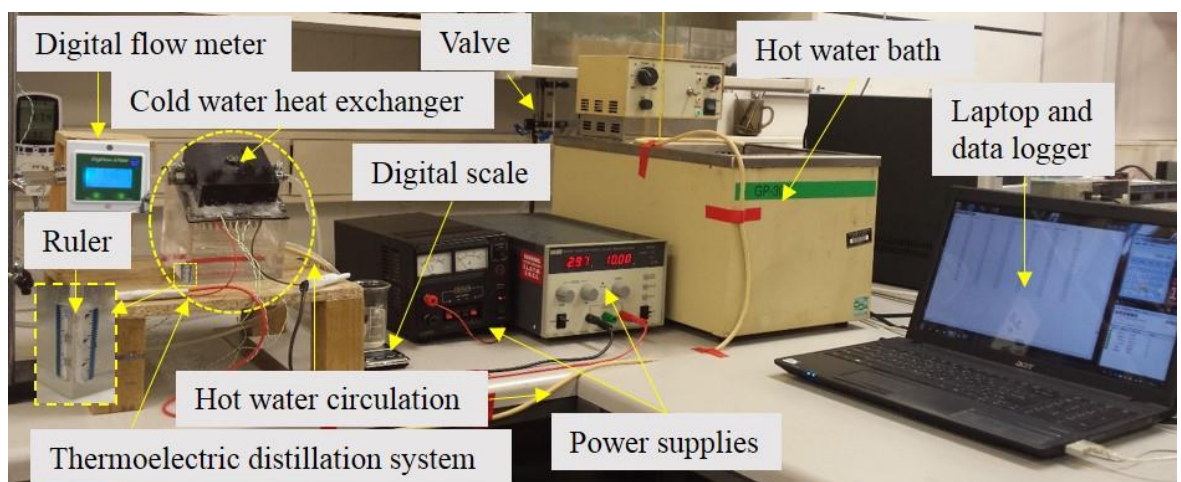


Figure 6.2: A photograph of the modified experimental setup of the system.

6.5 Measurement procedure

The following experimental procedures were designed and executed to ensure the accuracy of the measurements

1. All experiments were repeated three times to test the repeatability of the measurements.

2. Water inside the water bath was heated to a specific temperature before connecting to the thermoelectric distillation system. This enables the sample water in the basin to reach the desirable temperature as quick as possible. Care was taken at the highest water temperatures by covering the water bath.

3. The flow rate of the sample water from the water bath to the basin was adjusted by one-side valve and a digital flow meter (0.05 L/min – 1 L/min), to keep the sample water at a desirable level.

4. The Peltier current was set to a desired value between 5 A and 10 A as recommended on the module data-sheet. The Peltier current plays a key role in controlling the cold side temperature of the module.

5. The cooling water was connected to the mains water supply directly. The temperature of the cooling water is 12 °C at noon. To examine the experiments more precisely, specifications of the additional components used in the experiments, including models and manufacturers are listed in Table 6.2. Accuracies, ranges and standard uncertainty of the additional instruments are listed in Table 6.3.

6. Laboratory door and windows were closed to ensure no air movements inside the lab during the experiments. Laboratory conditions were temperature of the lab ≈ 24 °C, RH $\approx 28\%$ and air velocity ≈ 0 m/s.

There is a difference between the experimental setup in Chapter Four / (section 4.4) and the current setup. However, the experimental setup of the thermoelectric distillation system is changed and modified by including additional instruments and sensors to investigate the key factors that affecting the water production rate.

Table 6.2: Properties of the additional components used in the experiments.

Component	Properties	Model / Suppliers
Condenser	Surface Area = 82 x 76 mm ²	6082 T6 Aluminium
	Angle = 15 °	ABL Aluminium Components
Diaphragm	Maximum Head = 10 m, Outer / Inner	SKU082613
Pump	diameter = 8/6 mm, Voltage= 12 V, Current = 0.4 – 0.8 A and Flow Rate= 400 L/h	Oil and Fuel Pumps
Heated Water	Fluid Temperature = -30 – 150 °C, Tank Size	GP-300
Bath	= 24 L, Voltage= 115 V and Current= 11.5 A	NESLAB
Anemometer	Weight = 70 g, 3 Voltage, Humidity ≤ 90%,	PST-TL017
	Temp. = -10 °C – 45 °C, Current = 3 mA	PROSTER

Table 6.3: Accuracies, ranges and standard uncertainty of the additional instruments.

Instrument	Accuracy	Range	Standard uncertainty
Humidity meter (Komodo)	0.1 %	20-99 %	0.05 %
Digital flow meter (6710M)	0.01 L/min	0.05-1 L/min	0.01 L/min
Anemometer	0.1 m/s	0 – 30 m/s	0.06/s

6.6 Results and discussions

The water production was measured every 10 minutes and the results of the key factors that affect the total water production and water production rate are summarised in the following section.

6.6 .1 Effect of sample water temperature

The experiments were performed at constant Peltier current of 7 Amps and a sample water level of 30 mm. The temperatures recorded at the cold and hot side of the thermoelectric module is $-15.5\text{ }^{\circ}\text{C}$ and $12\text{ }^{\circ}\text{C}$, respectively. Figure 6.3 shows the water production rate for the sample water temperature at $30\text{ }^{\circ}\text{C}$, $40\text{ }^{\circ}\text{C}$, $50\text{ }^{\circ}\text{C}$ and $60\text{ }^{\circ}\text{C}$, respectively. It can be seen that the water production increases with increasing the sample water temperature. The higher the sample water temperature, the greater the vapour temperature in the chamber as shown in Figure 6.4. In turn, this led to a higher water evaporation rate. The effect of sample water temperature on the water production rate is significant. It can be seen from Figure 6.3 that the total water production increased from 49.3 mL to 72.4 mL as the temperature of the sample water increased from $30\text{ }^{\circ}\text{C}$ to $60\text{ }^{\circ}\text{C}$. The represent a 47 % increase in the total water production after a three - hour operation. First row of Table 6.4 shows the temperature of the condenser increased with increasing of the water temperature. It is difficult to control the temperature of the condenser directly without controlling the cold side temperature in the experiments.

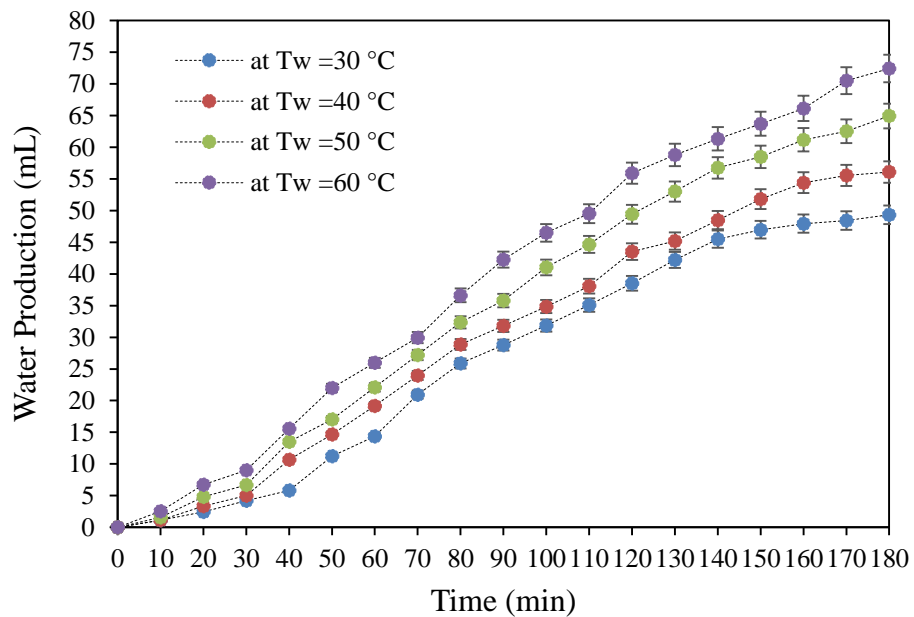


Figure 6.3: Total water production at different sample water temperatures.

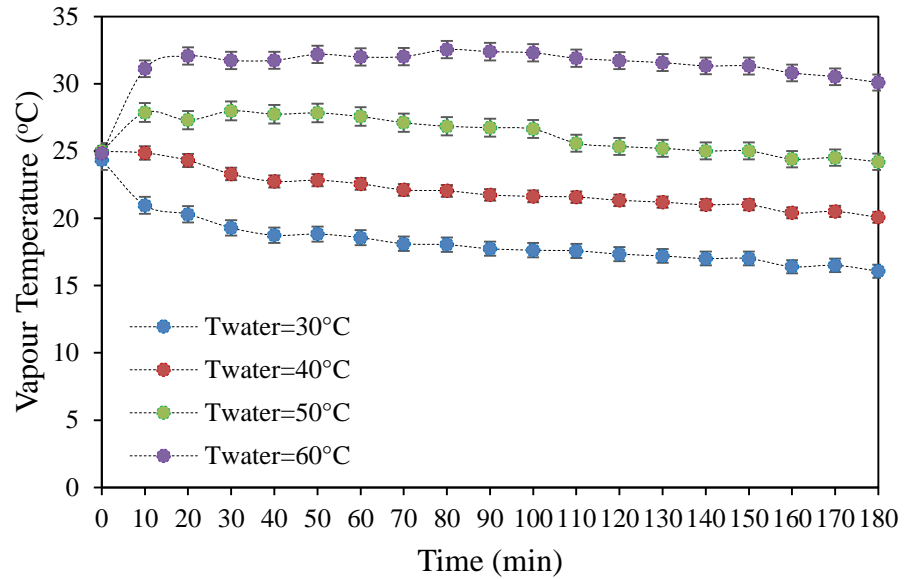


Figure 6.4: Vapour temperature at different sample water temperatures.

The amount of water vapour in the evaporation/condensation chamber can be measured from the humidity data. Table 6.4 shows the measurements of the average humidity in the chamber compared with that of the ambient in the laboratory for the four sample water temperatures (30 °C, 40 °C, 50 °C and 60 °C respectively). It can be seen from Table 6.4 that the average humidity in the chamber increased by 50% when the temperature of the sample water increases from 30 °C to 60 °C.

Table 6.4: Average condenser temperature and humidity for different sample water temperatures.

Sample water temperature	At 30 °C	At 40 °C	At 50 °C	At 60 °C
Average condenser temperature	-0.8 °C	-2.7 °C	0.9 °C	5.8 °C
Average humidity	60 %	72 %	81 %	90 %
Lab humidity	28 %	28 %	28 %	28 %

6.6.2 Effect of cooling water flow rate

The experiments were performed at constant Peltier current of 7 Amps and a sample water level of 30 mm. The water temperature and the temperature difference recorded

between the cold and hot side of the thermoelectric module are 30 °C and 27.5 °C, respectively. Figure 6.5 shows the water production rate for different cooling water flow rate at 0.1 L/min, 0.2 L/min and 0.3 L/min through the hot side water exchanger. Increasing cooling water flow rate leads to a slight decrease in the hot side temperature of the thermoelectric module from 13.3 °C at 0.1 L/min to 11 °C at 0.3 L/min. The Figure 6.5 indicates that there is no significant increase in the water production rate due to the small increment of the cooling water flow rate. The water production obtained after three hours about 51.2 mL and 49.3 mL for maximum and minimum flow rates, respectively. The percentage increase in the water production rate was 3.7% by increasing the cooling flow rate from 0.1 L/min to 0.3 L/min.

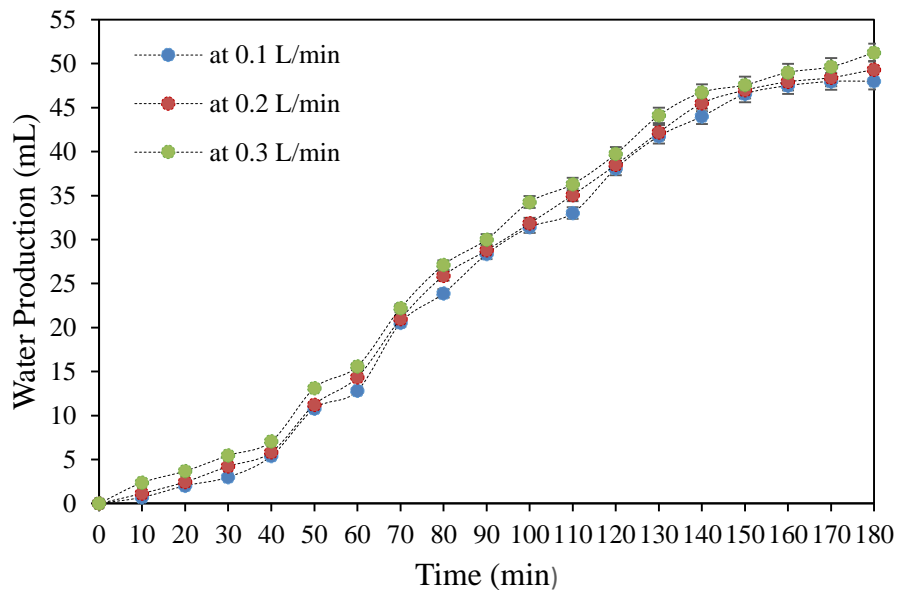


Figure 6.5: Total water production at different cooling water flow rates.

6.6.3 Effect of vapour volume

This experiment was performed by maintaining a constant sample water temperature at 30 °C, and maintaining the hot side and the cold side temperatures of the thermoelectric module at 12 °C and -15.5 °C, respectively (Peltier current was set to 7 A). The vapour volume for the sample water level at water levels of 30 mm, 20 mm and 10 mm is equal

to 400 cm³, 500 cm³ and 600 cm³, respectively. Figure 6.6 shows the total water production for the sample water level at 10 mm, 20 mm and 30 mm, respectively. It can be seen that total water production increases with increasing the sample water level, which may be attributed to an increase in the vapour density.

Clearly, the vapour volume in the chamber is small for the sample water level at 30 mm and a large vapour density is expected in this case. Since there are more water molecules reaching the condenser due to high vapour density, the water production rate will be higher. The result of the experiment shows that the total water production is increased by 61% when the sample water level is increased from 10 mm to 30 mm. It is to be noted that this experiment shows an increase of water production rate, due to the reduction of the vapour volume by increasing the sample water level. However, it is also possibly due to reduction in vapour volume (available space for vapour). Unfortunately, this cannot be demonstrated using the experiment setup reported in this work.

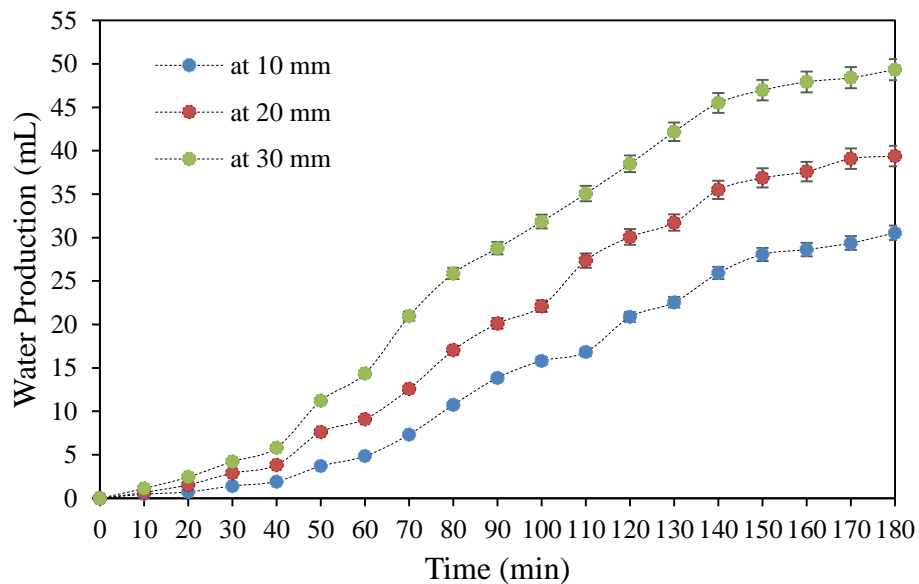


Figure 6.6: Total water production at different sample water levels.

Table 6.5 shows the humidity in the chamber and the average and dew point temperatures of the vapour at three sample water levels. It clearly indicates that the increase in the

vapour volume (decreasing in the sample water level) leads to a decrease in the humidity, the dew point and the vapour temperature.

Table 6.5: Thermodynamic properties of the vapour at different sample water levels.

Vapour property	At 30 mm	At 20 mm	At 10 mm
Average temperature	18.3 °C	15.7 °C	13.1 °C
Dew point	11 °C	7.2 °C	3.2 °C
Humidity	62%	57%	51%

6.6.4 Effect of Peltier current

The electric current supplied to a thermoelectric module when operating in the Peltier mode (cooling mode) is referred to as the Peltier current in the thesis for simplicity. The Peltier current determines the temperature difference between the hot and cold side of thermoelectric module and hence the condenser temperature of the thermoelectric distillation system. The experiment was carried out by maintaining the sample water temperature at 30 °C (the rest of the water temperatures were taken into consider in sections 6.6.1 and 6.6.5), the sample water level at 30 mm and the hot side temperature of the thermoelectric module at 12 °C. Figures 6.7 shows the water production rate as a function of time with the Peltier current changed every 30 minutes from 10 A to 5 A. Figure 6.8 shows the water production rate as a function of the time with the Peltier current varying every 30 minutes from 5 A to 10 A. The Peltier current was changed every 30 minutes and the water production was measured every 10 minutes. It can be seen that the maximum water production rates (1.4 mL/min and 1.1 mL/min) were achieved for a Peltier current of between 6 A and 7 A. If the Peltier current is smaller than such values, the water production rate increases with increasing the Peltier current, due to the condenser temperature decreasing.

However, if the Peltier current is larger than this value, the water production decreases with increasing Peltier current. This is due to the formation of ice at the condenser fins as shown in Figure 6.9. The lower the condenser temperature, the more ice forms on the surface of the condenser and consequently, the less water is produced. Figure 6.10 displays the temperatures of the cold side of thermoelectric module and the condenser fins as a function of the Peltier current. At sample water temperature 30 °C, it can be seen that the temperature of the condenser ranges from 1.1 °C to -1.2 °C for the Peltier current between 6 and 7 A. Clearly, this is a current range that generates the lowest condenser temperature without causing significant ice formation on the surface of the condenser. The result from this experiment shows that selection of an appropriate Peltier current (supplied to the thermoelectric module) is an important consideration in the design of an effective thermoelectric distillation system.

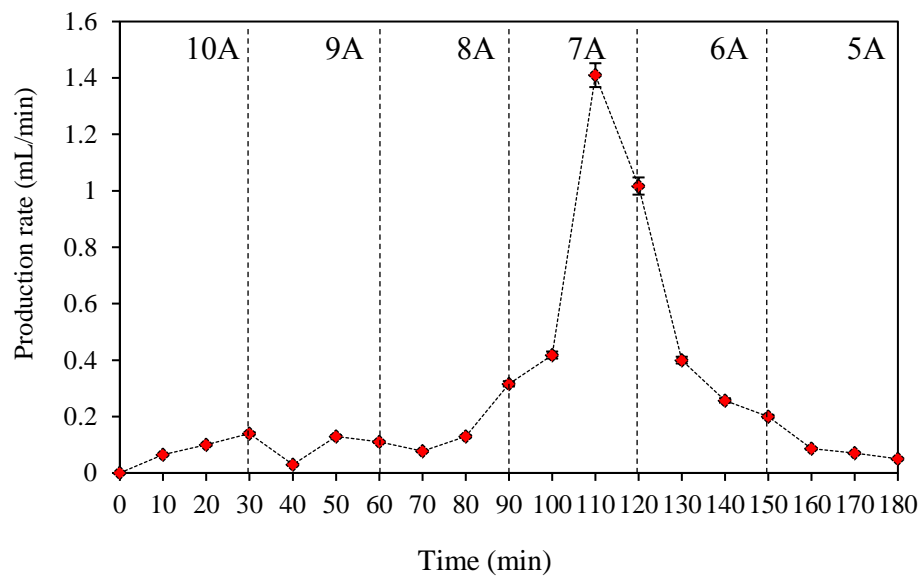


Figure 6.7: Water production rate vs. operation time for different Peltier currents from 10 A to 5 A. The Peltier current changes every 30 minutes but remains constant for given period of 30 minutes indicated by dashed-lines.

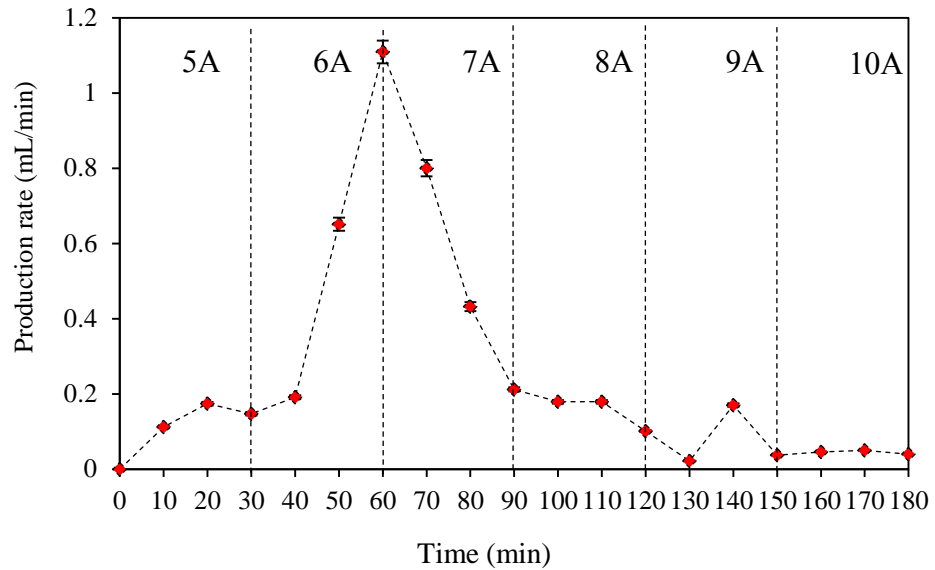


Figure 6.8: Water production rate vs. operation time for different Peltier currents from 5 A to 10 A. The Peltier current changes every 30 minutes but remains constant for given period of 30 minutes indicated by dashed-line.

As a result, ice is formed and gradually more ice began to build up and eventually causes the condenser freezes up (high cooling). The minimum temperature of the condenser was -6.7°C at 10 Amp Peltier current and 30° sample water temperature. When the sample water temperature increases (causes high evaporation), the formed ice on the condenser will reduce obviously.



Figure 6.9: A photograph of ice formation on the condenser during an operation, in which the temperature of the sample water is 30°C and the Peltier current is 10 A.

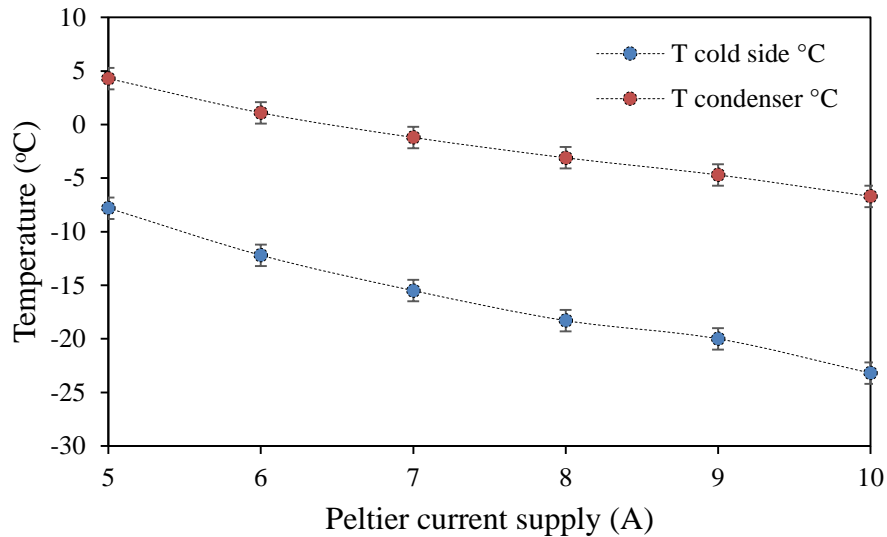


Figure 6.10: Temperatures of the condenser and the cold side of the module as a function of the Peltier current.

6.6.5 Optimisation of input power to the thermoelectric module

For a sample water level at 30 mm, Figure 6.11 shows the total water production as a function of thermoelectric input power for different sample water temperatures after operation for 3 hours. The thermoelectric input power is given by the product of the thermoelectric voltage and the Peltier current supply, as shown in Table 6.6. It can be seen from the Figure 6.10 that a maximum water production rate is achieved corresponding to an optimised thermoelectric input power for a given sample water temperature. The peak of the water production rate shifts with an increase in the sample water temperature. It clearly indicates that the increase in the sample water temperature causes faster evaporation and, the increase in the thermoelectric power supply (increased Peltier current) causes faster condensation. In addition to this reason, the lower the condenser temperature (less than $-1.2\text{ }^{\circ}\text{C}$), the more ice forms on the surface of the condenser (fins) and consequently, the less water is produced. After three hours, maximum water production was (49.3 mL at $30\text{ }^{\circ}\text{C}$ and 14.7 W), (62.7 mL at $40\text{ }^{\circ}\text{C}$ and

19.2 W), (77.2 mL at 50 °C and 24.3 W) and (90.7 mL at 60 °C and 31.9 W). Based on these results, an increase in the thermoelectric input power from 7.5 W to 31.9 W (325%) for a 60 °C sample water temperature, resulted in an increase in water production by approximately 53%.

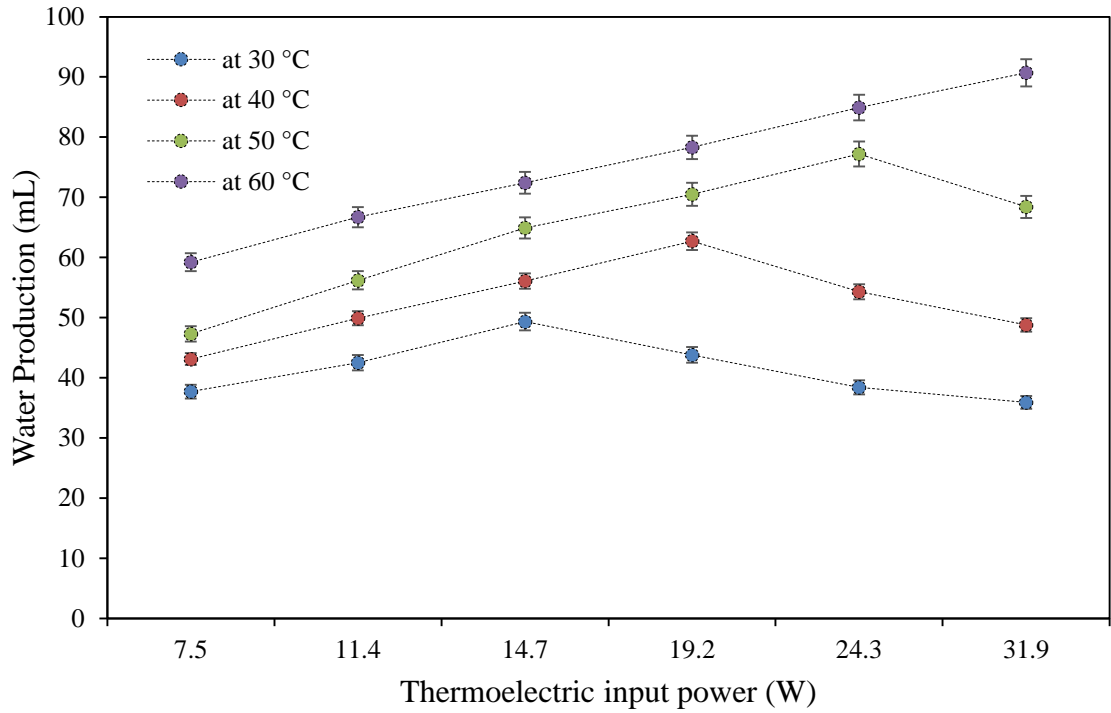


Figure 6.11: Total water production at different thermoelectric input powers and sample water temperatures.

Table 6.6: Corresponding currents and voltages of the thermoelectric input power.

Peltier current (A)	5	6	7	8	9	10
Voltage (V)	1.5	1.9	2.1	2.4	2.7	3.19
Input power (W)	7.5	11.4	14.7	19.2	24.3	31.9

The results show that the maximum water production rate for a given temperature of the sample water is obtained corresponding to an optimised input power of thermoelectric module. The higher the temperature of the sample water, the larger the optimised input

power is required. This result indicate that a thermoelectric distillation system can be tuned to increase the water production rate by increasing the temperature of the sample water and the corresponding optimised input power or to achieve an efficient water production with a moderate rate. As a summarised of these investigations, the best performance of the thermoelectric distillation system is achieved when the condenser is working on the edge of ice formation.

6.7 Conclusions

The effect of the key factors on water production have been investigated, which include; sample water temperature, vapour volume at sample water level, Peltier current and thermoelectric input power. The following conclusions were reached, based on the above discussions:

- The experimental data shows that an increase in sample water temperature from 30 °C to 60 °C gives a 47 % increase in total water production.
- Peltier current supply is demonstrated as a control factor in the design of an effective thermoelectric distillation system.
- The best performance of the thermoelectric distillation system is achieved when the condenser is working on the edge of ice formation.
- The results show that the total water production increases by 61% when reducing vapour volume from 600 cm³ to 400 cm³ by increasing sample water level from 10 mm to 30 mm.
- There is no significant increase in the water production rate due to the small increment of the cooling water flow rate (0.1 L/min-0.3 l/min).
- The maximum water production is achieved by increasing sample water temperature and the corresponding optimised input power.

Chapter 7

Water Production Analysis and Solar Panel Evaluation System

7.1 Introduction

Water is certainly the most important chemical on Earth, as it makes life possible. Plants, animals, and humans require water for survival. With the growing need for fresh water sources, especially in developing countries with its water crisis, together with the global energy crisis, there is rising demand for economically viable fresh water production. This chapter describes the testing of the developed thermoelectric distillation system of this study using seawater samples from randomly selected places in Cardiff Bay, UK. The water produced from the distillation of the seawater is compared with the key parameters of drinking water, which include the pH level, total dissolved solids and electrical conductivity.

Also in this chapter, a brief evaluation of using a solar panel as the power supply for the developed distillation system is presented. It is noted that the amount of electricity generation obtained from a solar panel will vary with the location of the installation. A very useful tool, provided free by the European Commission Joint Research Centre, can be used to estimate the solar irradiation and electricity generation from a solar panel in a specific region. This tool is used to assess the suitability of using the solar panel to power the developed thermoelectric distillation system.

7.2 Water quality testing

To test the drinking quality of the produced water, a pH & Water Analysis Meter (Hanna Instruments HI-98129) was used as shown in Figure 7.1.



Figure 7.1: Hanna Instruments HI-98129 for water quality analysis.

The meter tests pH level, total dissolved solids and electrical conductivity. The objective of the test is to investigate whether the water is suitable to drink in terms of the above three quantities. The pH test measures the acidic or basic character of water, with values in the range of 6.9 - 7.5, generally accepted as suitable [78]. The total dissolved solids (TDS) are the total amount of movable charged ions, including minerals, salts or metals dissolved in a given volume of water, expressed in units of mg per unit volume of water (mg/L). TDS is also referred to the salinity in water as parts per million (ppm). TDS is directly related to the purity of water and the quality of water purification systems; ideal values are 80-180 ppm [79]. TDS meter readings are based on the electrical conductivity (EC) of the water. Its unit is micro Siemens per centimetre ($\mu\text{S}/\text{cm}$). Pure water isn't a good conductor of electricity because the electrical current is carried by the ions in solution, the electrical conductivity increases as the concentration of ions increases. The

electrical conductivity of water varies from very low values ($0 \mu\text{S}/\text{cm}$) to very high values ($50000 \mu\text{S}/\text{cm}$) which are unsuitable for drinking, fresh water is usually between $30 \mu\text{S}/\text{cm}$ to $1500 \mu\text{S}/\text{cm}$ [80]. The capability of the Hanna Instruments HI-98129 is shown in Table 7.1.

Table 7.1: Specifications of the Hanna Instruments HI-98129 pH water analysis meter.

Specification	Range / Resolution
Minimum and maximum pH	0 pH to +14pH
pH resolution	0.01 pH
Minimum and maximum TDS	0 ppm to 2000 ppm
TDS resolution	1 ppm
Minimum and maximum EC	$0 \mu\text{S}/\text{cm}$ to $3999 \mu\text{S}/\text{cm}$
EC resolution	$1 \mu\text{S}/\text{cm}$
Minimum and maximum operating temperature	0°C to $+50^\circ\text{C}$
Weight	100 g

Feed water properties have a considerable effect on the produced water quality. To test the quality of the water produced by the developed thermoelectric distillation system, four samples of seawater (one litre for each sample) were collected from various locations at Cardiff Bay, UK as shown in Figure 7.2. During the experiments, 300 mL of the collected seawater was fed into the system at ambient temperature.

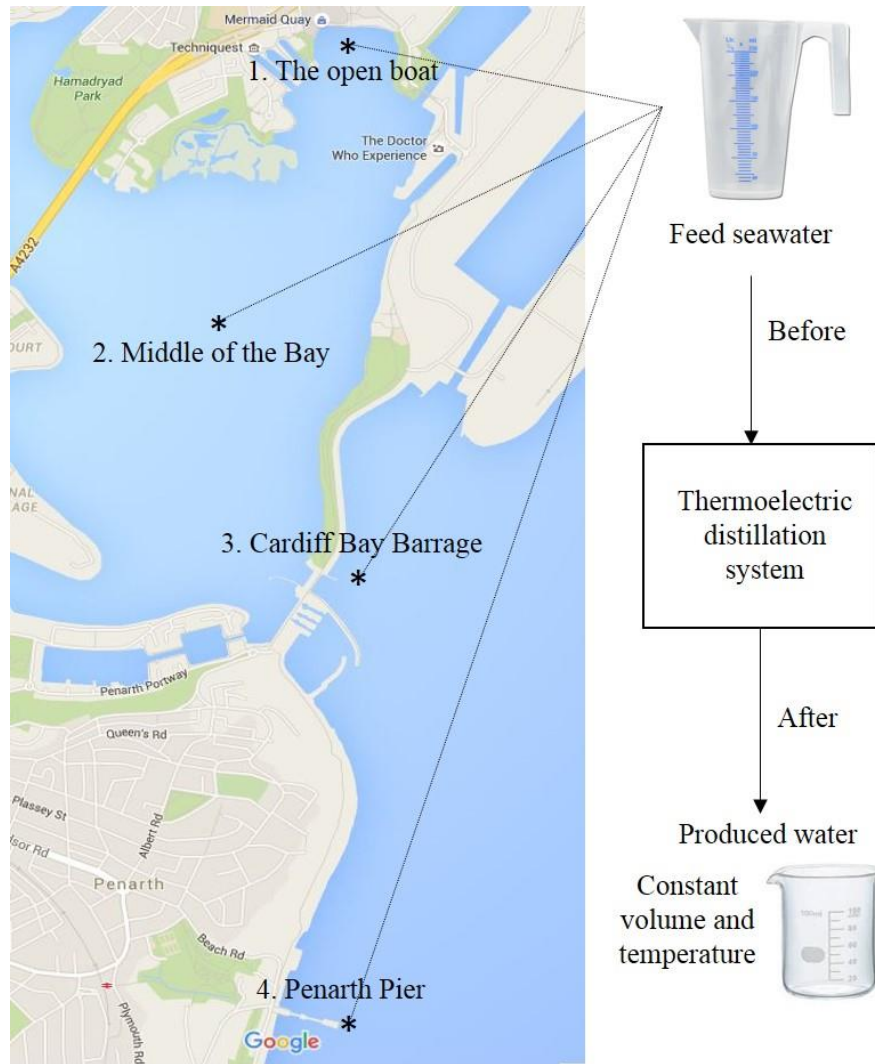


Figure 7.2: The four locations of the seawater collected at Cardiff Bay.

Pure distilled water has a pH of 7.0 (neutral). The pH scale ranges from 0 to 14 with pH levels less than 7.0 considered acids and pH levels over 7.0 considered bases. Distilled water at a perfect 7.0 pH is generally hard to achieve. The pH scale measures the concentration of the hydrogen and hydroxide ions present in a water sample. Acids have more hydrogen ions, while bases have more hydroxide ions. Since distilled water is neutral, this means it contains an equivalent concentration of hydrogen and hydroxide ions. Table 7.2 summarizes the pH test results before and after the distillation process. It can be seen that the pH levels for all samples were reduced within the drinkable range from the pH levels slightly outside of the drinkable range before the distillation. The

acceptable values of pH of drinking water are between 6.9 and 7.5, according to the Guidelines for drinking-water quality from the World Health Organisation (WHO) [126].

Table 7.2: pH levels before and after the distillation process.

Location	Water Type	pH
1. The open boat	Sample Water (Before)	7.78
	Distillate Water (After)	7.39
2. Middle of the Bay	Sample Water (Before)	7.76
	Distillate Water (After)	7.34
3. Cardiff Bay Barrage	Sample Water (Before)	7.79
	Distillate Water (After)	7.36
4. Penarth Pier	Sample Water (Before)	7.77
	Distillate Water (After)	7.35

Tables 7.3 and 7.4 summarize the TDS and EC test results before and after the thermoelectric distillation. It can be seen that before going through the thermoelectric distillation system all the water samples had high values of TDS and EC. After the distillation, the values of the TDS and EC of the produced water were decreased noticeably. Permissible ranges of TDS and EC in drinking water (by WHO) are less than 300 ppm and less than 800 $\mu\text{S}/\text{cm}$, respectively. Clearly, from the Tables 7.2, 7.3 and 7.4, the pH, TDS and EC values of the distilled water were within the acceptable range of drinking water conditions. These results demonstrate the capability of the developed thermoelectric distillation system for fresh water production.

Table 7.3: TDS tests before and after the distillation process.

Location	Water Type	TDS (ppm)
1. The open boat	Sample Water (Before)	482
	Distillate Water (After)	153
2. Middle of the Bay	Sample Water (Before)	194
	Distillate Water (After)	149
3. Cardiff Bay Barrage	Sample Water (Before)	677
	Distillate Water (After)	151
4. Penarth Pier	Sample Water (Before)	858
	Distillate Water (After)	154

Table 7.4: EC tests before and after the distillation process.

Location	Water Type	EC (μ S/cm)
1. The open boat	Sample Water (Before)	975
	Distillate Water (After)	302
2. Middle of the Bay	Sample Water (Before)	340
	Distillate Water (After)	300
3. Cardiff Bay Barrage	Sample Water (Before)	1341
	Distillate Water (After)	309
4. Penarth Pier	Sample Water (Before)	1398
	Distillate Water (After)	297

7.3 Solar energy evaluation

The final stage of the research is to evaluate a capable and competent solar panel to power the developed thermoelectric distillation system in a selected area. There is a need to use sustainable energy sources, with solar energy being one of the most promising options. Improvements in solar distillation technology make it ideal for desalinating water in remote areas (especially in areas with no electricity). Nevertheless, there is still a need to increase the productivity of the distillation technology at an affordable cost, especially in developing parts of the world. Moreover, many countries (Iraq for example) receive relatively high levels of solar radiation [127]. The aim of this section is to present a mathematical evaluation of a suitable solar panel for powering the developed thermoelectric distillation system.

To evaluate the solar irradiance of a fixed system and to estimate the power delivered to the thermoelectric distillation system from a solar panel, the University of Kufa (32° North, 44° East and Elevation 33 m) is selected as a specific region. The University of Kufa is an Iraqi university located in Najaf, in central Iraq. The Photovoltaic Geographical Information System (PVGIS) is used to estimate the global irradiation per square meter and the solar electricity generation in kWh received by a photovoltaic PV panel. The radiation reaching the earth's surface can be represented in a number of different ways. Global Irradiation is the total amount of shortwave radiation received from above by a surface to the ground. PVGIS provides web access to solar radiation and temperature data and to PV performance assessment tools for any location in Europe and Africa, as well as a large part of Asia. The PV solar panel is fixed at 30° inclination and 0° orientation (no tracking system). PVGIS provides three types of losses of the PV solar panel: 1) Losses due to a local ambient temperature of the specific area (14.7%); 2)

Constant losses due to angular reflectance effects (2.6%); 3) Cable and inverter losses (14%). The input data of the PV solar panel to the PVGIS are shown in Table 7.5.

Table 7.5: The input data to the PVGIS.

Property	Type / Value
Solar radiation database used	PVGIS-CMSAF
Daily normal power of the PV panel = (TE system power = 32.4 W) and (6 hrs TD system operation)	≈ 0.2 kWh
Panel Type	Crystalline silicon

The average daily and monthly electricity production and the global irradiation of the given PV solar panel are shown in Table 7.6.

Table 7.6: The output data (average electricity production E and the sum of global irradiation H) daily and monthly from the PVGIS.

Fixed system: inclination=30°, orientation=0° (Optimum at given orientation)				
Month	E_d	E_m	H_d	H_m
Jan	0.21	6.50	4.87	151
Feb	0.25	6.95	5.93	166
Mar	0.28	8.52	6.82	211
Apr	0.26	7.82	6.67	200
May	0.26	8.17	6.96	216
Jun	0.27	8.14	7.31	219
Jul	0.27	8.40	7.38	229
Aug	0.27	8.49	7.46	231
Sep	0.28	8.35	7.40	222
Oct	0.24	7.43	6.15	191
Nov	0.21	6.29	5.06	152
Dec	0.20	6.31	4.75	147
Yearly average	0.250	7.61	6.40	195
Total for year		91.4		2340

where E_d is the average daily electricity production from the fixed system (kWh), E_m is the average monthly electricity production from the fixed system (kWh), H_d is the average daily sum of global irradiation per square meter received by the panel of the fixed system (kWh/m^2) and H_m is the average monthly sum of global irradiation per square meter received by the panel of the fixed system (kWh/m^2). Initially, based on the electricity production values and the solar irradiation evaluations for a fixed panel system, the months from March to September are the best months of the year for power generation. The maximum monthly average of the electricity production and the solar irradiation for the summer period are 8.52 kWh and 231 kWh/m^2 respectively. The minimum monthly average of the electricity generation and solar irradiation for the winter months are 6.29 kWh and 147 kWh/m^2 , respectively. To illustrate these results, water production from the thermoelectric distillation system is plotted against the corresponding electricity generation from the PV solar panel.

At steady state condition, the thermoelectric distillation system produced 15.3 mL per hour at 0.0324 kWh the energy consumption of the system. Figure 7.3 shows the proportional relationship between the monthly average water production from the thermoelectric distillation system during steady state operation and the monthly average electricity production from the PV solar panel. It can be seen from Figure 7.3 that the relationship between the water and electricity production is directly proportional, the maximum average monthly water production is 4023.3 mL using 8.52 kWh of produced electricity (which occurs in March). The minimum the average monthly water production is 2970.3 mL using 6.29 kWh of produced electricity (which occurs in November). It is noted that this thermoelectric distillation system can also utilise the solar irradiation to heat the water in addition to heating from the thermoelectric hot side. This will further reduce the energy consumption of the system.

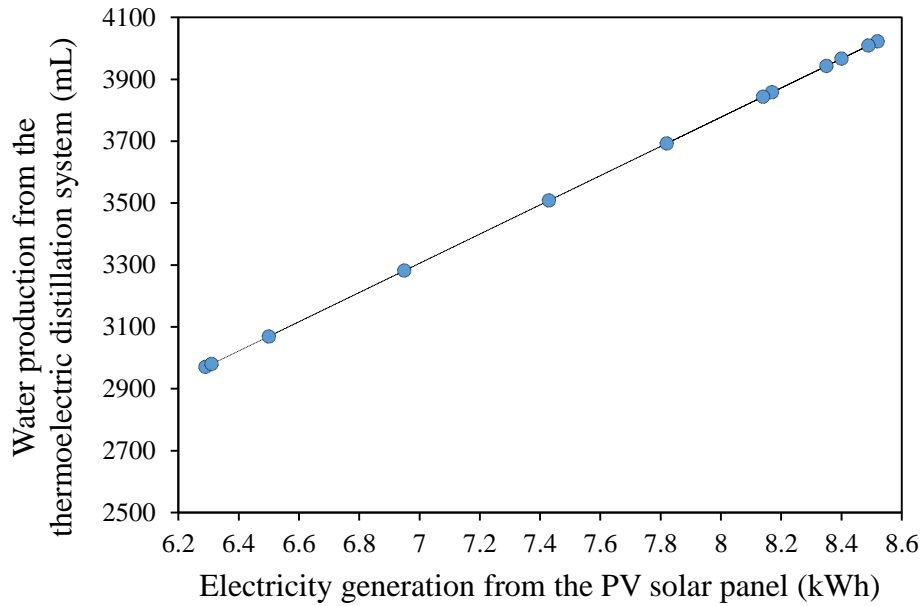


Figure 7.3: Average monthly water production from the thermoelectric distillation system versus electricity production from the PV solar panel.

Based on the PVGIS data and the daily normal power of the fixed system, a suitable solar panel can be selected commercially as shown in Table 7.7:

Table 7.7: Properties of some commercial solar panels can be used to power the TE system.

Solar panel	Efficiency	Power (W)	Type	Total area (m ²)	Price
Coleman	13 %	36	Crystalline Si	0.386	89 \$
Poly PV	17 %	36	Polycrystalline Si	0.235	105 \$
PV-MC4	20 %	36	Monocrystalline Si	0.324	179 \$

7.4 Conclusions

Measurements of the distilled water from the system shows that it has similar quality to drinkable tap water in terms of pH, total dissolved solids and electrical conductivity values. Assuming that the relationship between the water and electricity production is directly proportional, the maximum monthly average water production is 4023.3 mL when using 8.52 kWh of electricity produced during March at the chosen location. The minimum average monthly water production is 2970.3 mL using 6.29 kWh of electricity produced during November.

Chapter 8

Conclusions and Future Works

8.1 Conclusions

Despite huge global water resources, many parts of the world are faced with a growing challenge of access to fresh water for domestic and industrial purposes, particularly in developing countries. Water desalination removes salts and minerals from seawater and brackish water. It is playing an increasingly important role as a fresh water supply. However, current desalination technologies are limited by significant energy consumption. In addition, they are carbon intensive. These limitations make desalination technologies expensive and unsuitable for mass market, particularly for developing countries. The work embodied in this thesis describes a focus effort on improving the performance and economic viability of the thermal distillation process, by employing a thermoelectric device using an innovative concept. The main achievements are as follows:

A thermoelectric distillation system was designed, constructed and tested. The unique aspect of this design is to use the waste heat from the hot side of thermoelectric module for heating of the feed water, to improve the evaporation while using the cold side of the module to cool the condenser and improve the condensation process. Theoretical foundations associated with the evaporation and condensation processes were outlined to provide insights and guidelines for the design of the proposed thermoelectric distillation system. The major challenges faced during the design and construction of the developed thermoelectric distillation system are explained.

The developed thermoelectric distillation system produces 28.5 mL of distilled water (equivalent to 678 mL/m²) over a period of 1 hour. The corresponding electrical energy required for the water production is 0.0324 kWh, which gives a specific energy consumption of 0.00114 kWh/mL. This can be compared with the values ranging from 0.00122 to 0.05945 kWh/mL for a number of previously reported systems. It is noted that the reported values at low end were actually obtained from the systems where evaporation is assisted with solar heating, while the result obtained from this study is without solar heating. It is clear that the system developed in this research has significantly lower energy consumption than any of the existing thermoelectric distillation systems.

The quasi to steady state behaviour of the thermoelectric distillation system was investigated. It can be noted that the system reaches steady state after approximately three hours of system operation. The minimum *COP* of the thermoelectric module was 0.69, with a maximum temperature difference of 38 °C between hot and cold side of the thermoelectric module. The water temperature was increased from 22.3 °C to 47.8 °C. Similarly, the vapour temperature was increased moderately from 20.3 °C to 30.4 °C. The steady state water production, humidity, energy consumption and *COP* of the thermoelectric distillation system were 15.3 mL/h, 81%, 0.0324 kWh and 1.04, respectively.

Thermal models have been developed through water-vapour phase-change theory to interpret the evaporation and condensation processes involved in the fresh water production of a thermoelectric distillation system. The first model was related to the evaporation process to determine the vapour production in the system. The experimental results confirm the increase of the vapour produced has a direct effect on the increase of the water productivity due to the increase of the evaporation rate. Also, the water and vapour temperatures are increased, due to the heat transferred from the hot side of the

thermoelectric module to the circulating water and consequently, led to an increase in the water productivity. A theoretical distillation ratio of 12% was obtained, with a predicted water temperature of 42.7 °C. This is in reasonable agreement with the 9.5% value experimentally obtained. The second model has been developed for the water condensation process which uses a thermoelectric module. The developed model can be used for determining the key parameters that control the condensation processes and the system thermal performance. The model shows that the rate of water condensation is dependent upon the convection heat transfer coefficient of the cold-side heat exchanger. The fitted value of the convection heat transfer coefficient in the thermoelectric distillation system is 8 W/m².K.

The experimental setup of the thermoelectric distillation system is modified. Key factors that influence the total water production and water production rate have been investigated, including sample water temperature, vapour volume at sample water level, Peltier current and thermoelectric input power. The following conclusions were reached: the experimental data shows that an increase in sample water temperature from 30 °C to 60 °C gives a 47 % increase in total water production. Peltier current supply is demonstrated as a control factor in the design of an effective thermoelectric distillation system. The results show that the total water production increases by 61%, when reducing vapour volume from 600 cm³ to 400 cm³ by increasing sample water level from 10 mm to 30 mm in the system. The maximum water production is achieved by increasing sample water temperature and the corresponding optimised input power. In addition, the best performance of the modified thermoelectric distillation system is achieved when the condenser is working on the edge of ice formation.

Measurements of the distilled water show that it has similar quality to drinkable tap water in terms of pH, total dissolved solids and electrical conductivity values. PVGIS was

used to estimate the global irradiation per square meter and the solar electricity generation in kWh received by a solar panel in a specific region. The maximum monthly average water production is 4023.3 mL when using 8.52 kWh of electricity produced during March at the University of Kufa. The minimum average monthly water production is 2970.3 mL using 6.29 kWh of electricity produced during November.

8.2 Future works

Distillation is a physical process of complete or partial separating of the component substances from a liquid mixture by selective evaporation and condensation. There is a need to test the thermoelectric distillation system for various types of liquid, such as crude oil, alcohols and herbal oils. This requires the design of high corrosion resistance heat exchangers and pipes with complex flow arrangements. The calculations of the thermoelectric distillation system for multi liquid applications are algebraically complex and the solution requires a system and procedure which includes phase-change phenomena for different incompressible fluids.

Further work could be carried out by testing of different construction materials such as heat resistant plastics for the chamber and the pipes, and high thermal conductivity materials for the heat exchangers in order to obtain higher thermal performance. There is a need to carry out field trials for the system under different climatic conditions and also an investigation into the scalability of the technology for use in a village or town. This will help to further understand the behaviour of the system under practical conditions and also test the performance of the system against pollution and other operational challenges over long periods of time.

8.2.1 Suggestions

There are a number of suggestions, which have not been investigated due to the time constraint or outside the scope of this research, but worth of exploring in the future work. These include:

- Using the insulated Plexiglas walls around the system to reduce the water and vapour heat losses.
- Decreasing the angle of the inclined condenser from the vertical and reducing the collecting plate to enhance the motion of vapour around the condenser and to enhance the evaporation and condensation rates.
- Decreasing the condensation area and increasing evaporation area to enhance water evaporation.
- Increasing the temperature difference between the hot and cold sides of thermoelectric module to enhance the evaporation and condensation rates by using high-quality heat sinks which have a higher thermal conductivity values such as composite materials.

8.2.2 Large scale unit

Large scale evaluating could be carried out to ensure that the developed system operates reasonably under real life conditions and is scalable for commercial utilization. A larger scale unit could be designed for field trials based on theoretical and experimental research activity carried out in the laboratory. The thermoelectric distillation system had a 0.01 m² base (10 cm x 10 cm) with a steady state water production of 15.3 mL/h or (0.4 L/day), this could be scaled up to specify for larger scale units ranging from domestic to town size application. Typical numbers of occupiers in domestic, commercial, village and town categories are given in Table 8.1. The World Health Organisation (WHO) in its

“Guidelines for Drinking-Water Quality” [126], assumes an adult requires approximately two litres of drinking water per day. The unit fabrication cost was £45 (equal to 60 US Dollar, August 2017), based on the cost of components used during the research period and so does not include any cost saving which could be achieved via mass production. The daily energy consumption of the thermoelectric distillation system was 0.778 kWh (32.4 W in 24 hours). Standard electricity price in Iraq is 0.016 US Dollar per kWh (August 2017).

Table 8.1: Specification for large scale application.

Scale	Population	Water Need (L/day) W	No. of Systems Need Y	Total Fab. Cost (\$ *1000)	Total Area (m ²) (Y x 0.01 m ²)	Energy Consumption (kWh) Z	Energy Cost per day (US Dollar) (Z x \$0.016)
Formula	WHO Standard	(population x 2 L/day)	(W / 0.4 L/day)	(Y x \$60)	(Y x 0.01 m ²)	(Y x 0.778 daily kWh)	(Z x \$0.016)
Domestic	10	20	50	3	0.5	38.9	0.6
Commercial	100	200	500	30	5	388.5	6.2
Village	2500	5000	12500	750	125	9712.5	155.4
Town	25000	50000	125000	7500	1250	97125	1554

where, W is the population water needed (L/day), Y is the number of the thermoelectric distillation systems and Z is the total energy consumption of the systems.

8.2.3 Other applications

Distillation is a process that can be used to separate a pure liquid from a mixture of liquids. It works when the liquids have different boiling points. This type of distillation is known as fractional distillation. Here are some examples of solutions that could be used in the thermoelectric distillation system:

- Ethanol solution

The system could be used to separate ethanol from water at different concentrations for sterilization use. According to the solution concentration, the process requires varying amounts of energy to evaporate the solution (boiling temperature of the ethanol is less than the boiling temperature of water). This process is used in the medical industry.

- Herbs solutions

The system could be used to transfer all the volatiles from the source material to the distillate. The process requires less energy than that required to evaporate both the water and the herb mixture. This application is used in the perfumery industry.

Appendix

A.1 Steam Tables: Thermodynamic properties of water [106]

Properties of Saturated Water (Liquid–Vapor): Temperature Table

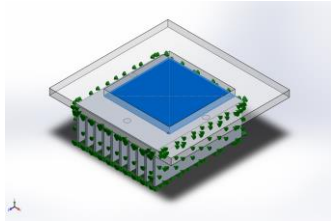
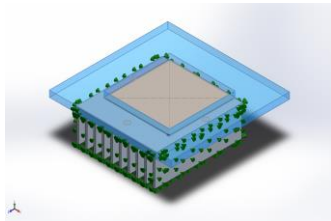
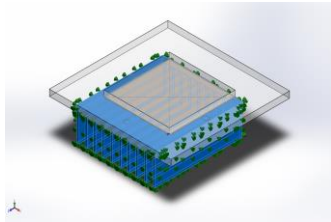
Specific Volume m ³ /kg		Internal Energy kJ/kg		Enthalpy kJ/kg			Entropy kJ/kg · K		Temp. °C
Sat. Liquid $v_f \times 10^3$	Sat. Vapor v_g	Sat. Liquid u_f	Sat. Vapor u_g	Sat. Liquid h_f	Evap. h_{fg}	Sat. Vapor h_g	Sat. Liquid s_f	Sat. Vapor s_g	
1.0002	206.136	0.00	2375.3	0.01	2501.3	2501.4	0.0000	9.1562	.01
1.0001	157.232	16.77	2380.9	16.78	2491.9	2508.7	0.0610	9.0514	4
1.0001	147.120	20.97	2382.3	20.98	2489.6	2510.6	0.0761	9.0257	5
1.0001	137.734	25.19	2383.6	25.20	2487.2	2512.4	0.0912	9.0003	6
1.0002	120.917	33.59	2386.4	33.60	2482.5	2516.1	0.1212	8.9501	8
1.0004	106.379	42.00	2389.2	42.01	2477.7	2519.8	0.1510	8.9008	10
1.0004	99.857	46.20	2390.5	46.20	2475.4	2521.6	0.1658	8.8765	11
1.0005	93.784	50.41	2391.9	50.41	2473.0	2523.4	0.1806	8.8524	12
1.0007	88.124	54.60	2393.3	54.60	2470.7	2525.3	0.1953	8.8285	13
1.0008	82.848	58.79	2394.7	58.80	2468.3	2527.1	0.2099	8.8048	14
1.0009	77.926	62.99	2396.1	62.99	2465.9	2528.9	0.2245	8.7814	15
1.0011	73.333	67.18	2397.4	67.19	2463.6	2530.8	0.2390	8.7582	16
1.0012	69.044	71.38	2398.8	71.38	2461.2	2532.6	0.2535	8.7351	17
1.0014	65.038	75.57	2400.2	75.58	2458.8	2534.4	0.2679	8.7123	18
1.0016	61.293	79.76	2401.6	79.77	2456.5	2536.2	0.2823	8.6897	19
1.0018	57.791	83.95	2402.9	83.96	2454.1	2538.1	0.2966	8.6672	20
1.0020	54.514	88.14	2404.3	88.14	2451.8	2539.9	0.3109	8.6450	21
1.0022	51.447	92.32	2405.7	92.33	2449.4	2541.7	0.3251	8.6229	22
1.0024	48.574	96.51	2407.0	96.52	2447.0	2543.5	0.3393	8.6011	23
1.0027	45.883	100.70	2408.4	100.70	2444.7	2545.4	0.3534	8.5794	24
1.0029	43.360	104.88	2409.8	104.89	2442.3	2547.2	0.3674	8.5580	25
1.0032	40.994	109.06	2411.1	109.07	2439.9	2549.0	0.3814	8.5367	26
1.0035	38.774	113.25	2412.5	113.25	2437.6	2550.8	0.3954	8.5156	27
1.0037	36.690	117.42	2413.9	117.43	2435.2	2552.6	0.4093	8.4946	28
1.0040	34.733	121.60	2415.2	121.61	2432.8	2554.5	0.4231	8.4739	29
1.0043	32.894	125.78	2416.6	125.79	2430.5	2556.3	0.4369	8.4533	30
1.0046	31.165	129.96	2418.0	129.97	2428.1	2558.1	0.4507	8.4329	31
1.0050	29.540	134.14	2419.3	134.15	2425.7	2559.9	0.4644	8.4127	32
1.0053	28.011	138.32	2420.7	138.33	2423.4	2561.7	0.4781	8.3927	33
1.0056	26.571	142.50	2422.0	142.50	2421.0	2563.5	0.4917	8.3728	34
1.0060	25.216	146.67	2423.4	146.68	2418.6	2565.3	0.5053	8.3531	35
1.0063	23.940	150.85	2424.7	150.86	2416.2	2567.1	0.5188	8.3336	36
1.0071	21.602	159.20	2427.4	159.21	2411.5	2570.7	0.5458	8.2950	38
1.0078	19.523	167.56	2430.1	167.57	2406.7	2574.3	0.5725	8.2570	40
1.0099	15.258	188.44	2436.8	188.45	2394.8	2583.2	0.6387	8.1648	45
1.0121	12.032	209.32	2443.5	209.33	2382.7	2592.1	.7038	8.0763	50
1.0146	9.568	230.21	2450.1	230.23	2370.7	2600.9	.7679	7.9913	55
1.0172	7.671	251.11	2456.6	251.13	2358.5	2609.6	.8312	7.9096	60
1.0199	6.197	272.02	2463.1	272.06	2346.2	2618.3	.8935	7.8310	65
1.0228	5.042	292.95	2469.6	292.98	2333.8	2626.8	.9549	7.7553	70
1.0259	4.131	313.90	2475.9	313.93	2321.4	2635.3	1.0155	7.6824	75
1.0291	3.407	334.86	2482.2	334.91	2308.8	2643.7	1.0753	7.6122	80
1.0325	2.828	355.84	2488.4	355.90	2296.0	2651.9	1.1343	7.5445	85
1.0360	2.361	376.85	2494.5	376.92	2283.2	2660.1	1.1925	7.4791	90
1.0397	1.982	397.88	2500.6	397.96	2270.2	2668.1	1.2500	7.4159	95
1.0435	1.673	418.94	2506.5	419.04	2257.0	2676.1	1.3069	7.3549	100

H₂O

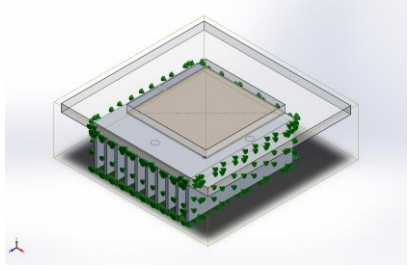
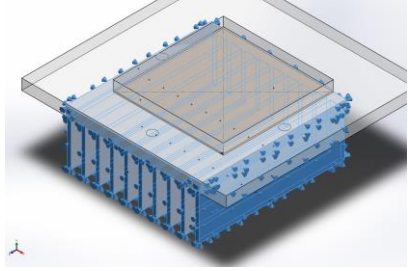
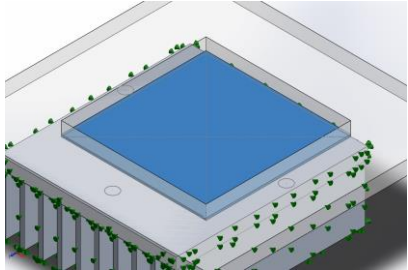
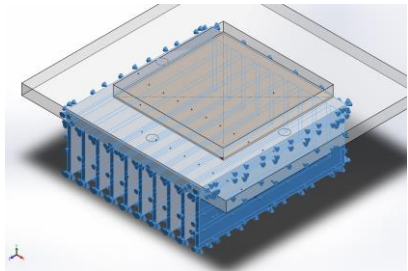
A.3 Thermal simulation study / Transient state of the cold side thermoelectric heat

sink

1. Material Properties:

Model Reference	Volumetric Properties	Properties
	Mass: 0.0137 kg Volume: 3.4596e-006 m ³ Density: 3960 kg/m ³ Weight: 0.13426 N	Name: Alumina Model type: Linear Elastic Isotropic Thermal conductivity: 30 W/(m.K) Specific heat: 850 J/(kg.K) Mass density: 3960 kg/m ³
	Mass: 0.0650592 kg Volume: 5.4216e-005 m ³ Density: 1200 kg/m ³ Weight: 0.63758 N	Name: Acrylic Model type: Linear Elastic Isotropic Thermal conductivity: 0.21 W/(m.K) Specific heat: 1500 J/(kg.K) Mass density: 1200 kg/m ³
	Mass: 0.194832 kg Volume: 7.216e-005 m ³ Density: 2700 kg/m ³ Weight: 1.90935 N	Name: Aluminum 6063-T4 Model type: Linear Elastic Isotropic Thermal conductivity: 200 W/(m.K) Specific heat: 900 J/(kg.K) Mass density: 2700 kg/m ³

2. Thermal Loads:

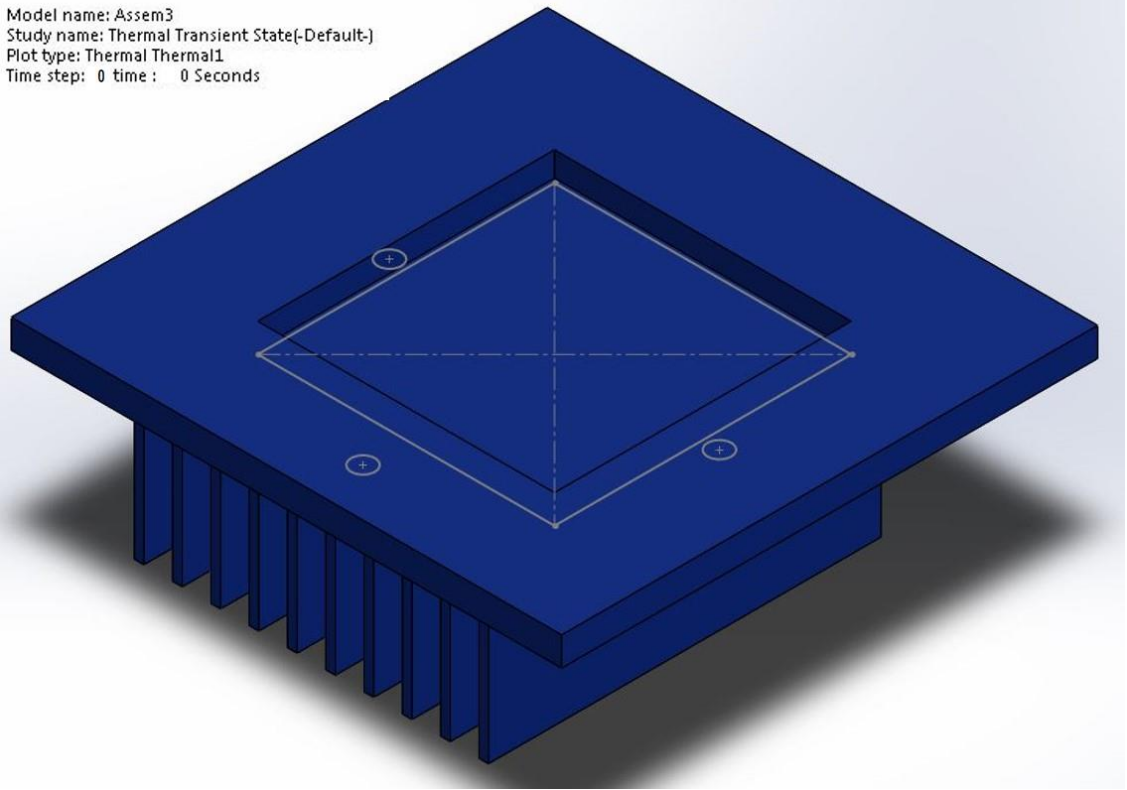
Load name	Load Image	Load Details
Temperature		Entities: 3 components Initial temperature: 295 Kelvin
Convection		Entities: 25 faces Convection Coefficient: 8 W/(m ² .K) Condenser Temperature: 295 Kelvin
Cooling		Entities: 1 component Cold side Temperature: -5 - 12 °C
Heating		Entities: 25 faces Latent heat: 2460 kJ/kg Vapour Temperature: 295 Kelvin

3. Study Results:

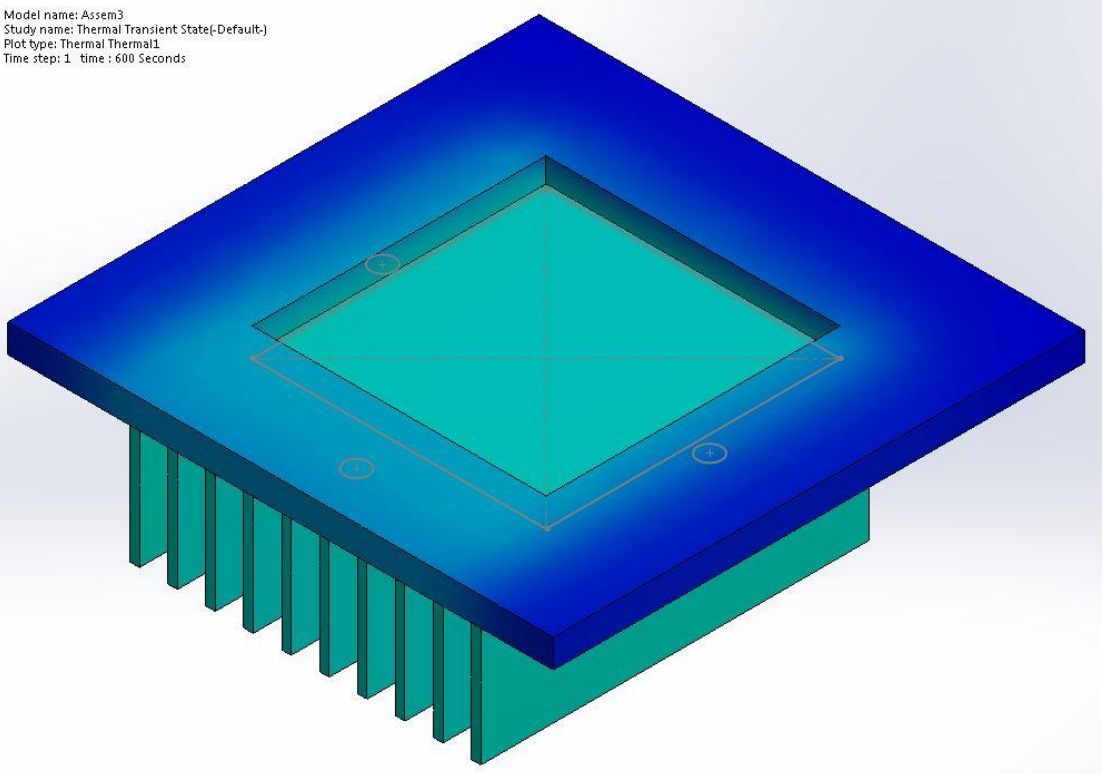
The temperature of the condenser is demonstrated as the below table and figures:

Time (s)	0	600	1200	1800	3600
T _{cond.} (°C)	21	6.2	9.4	14.9	16.3

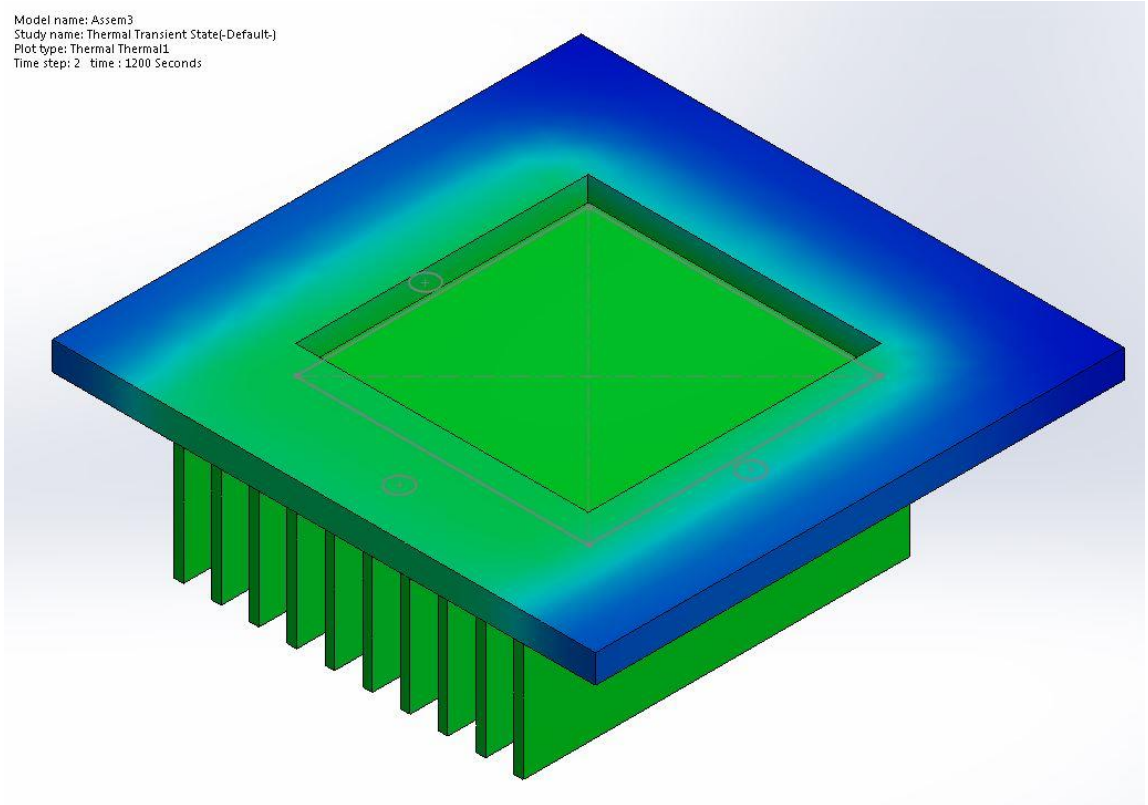
Model name: Assem3
Study name: Thermal Transient State(-Default-)
Plot type: Thermal Thermal1
Time step: 0 time : 0 Seconds



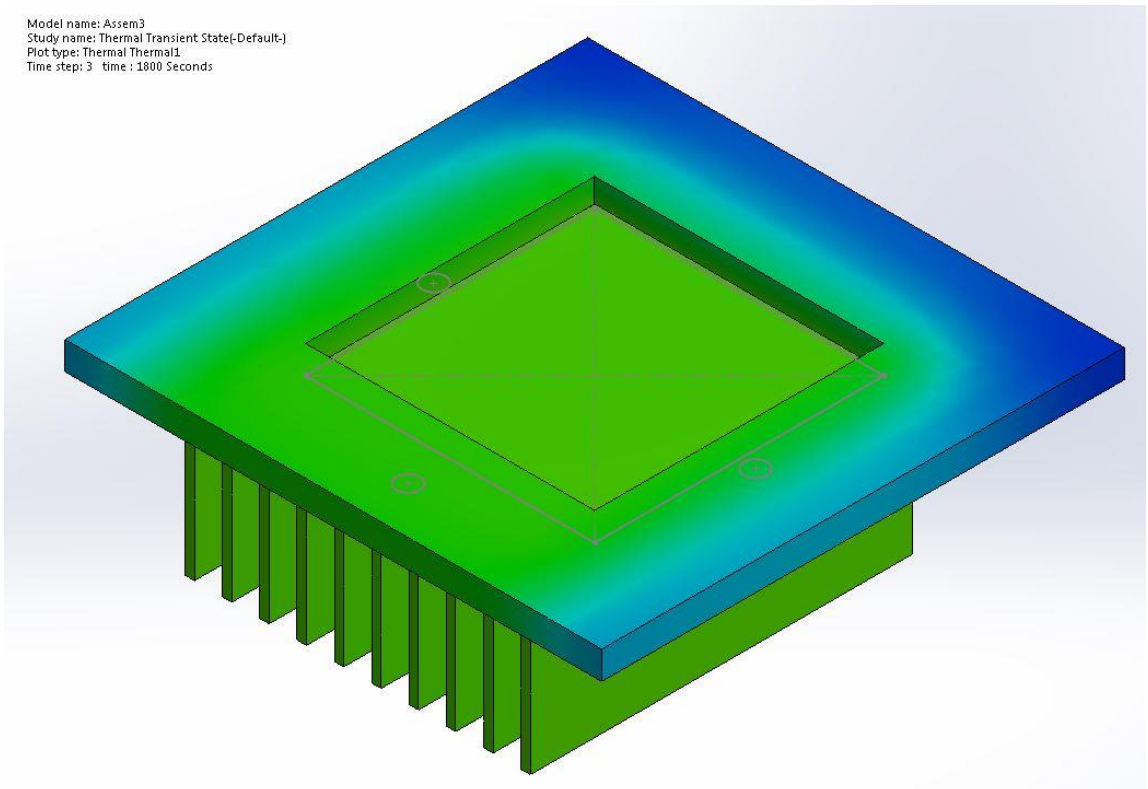
Model name: Assem3
Study name: Thermal Transient State(-Default-)
Plot type: Thermal Thermal1
Time step: 1 time : 600 Seconds



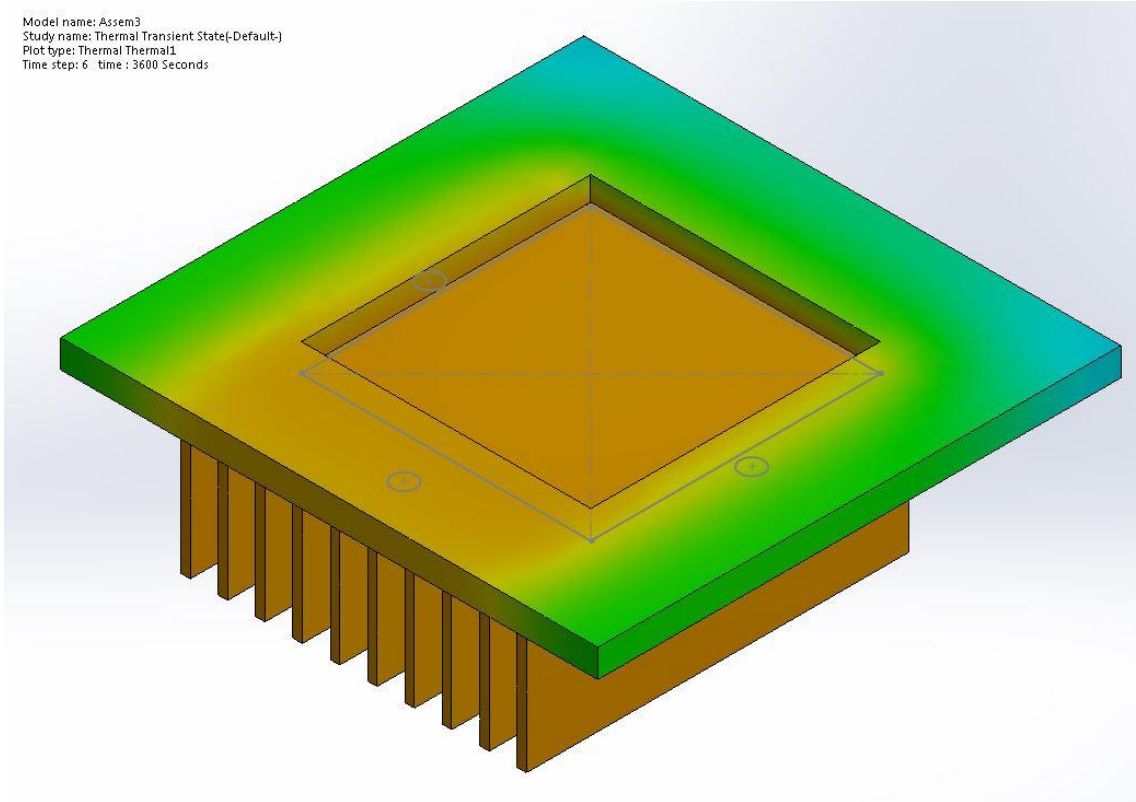
Model name: Assem3
Study name: Thermal Transient State(-Default-)
Plot type: Thermal Thermal1
Time step: 2 time : 1200 Seconds



Model name: Assem3
Study name: Thermal Transient State(-Default-)
Plot type: Thermal Thermal1
Time step: 3 time : 1800 Seconds



Model name: Assem3
 Study name: Thermal Transient State(-Default-)
 Plot type: Thermal Thermal1
 Time step: 6 time : 3600 Seconds



A.4 Thermal simulation study / Steady state of the cold side thermoelectric heat sink

Heat sink without thermoelectric area	Heat sink with thermoelectric area

A.5 The derivation of the heat balance of the straight fin of uniform cross section

$$q_x + dq_{conv} = q_{x+dx} \quad (1)$$

From Fourier's law:

$$q_x = k A_c \frac{dT}{dx} \quad (2)$$

The convection heat transfer rate expressed as

$$dq_{conv.} = h_c dA_s (T(x) - T_v) \quad (3)$$

The conduction heat rate at $(x + dx)$ expressed as

$$q_{x+dx} = q_x + \frac{dq_x}{dx} dx = k A_c \frac{dT}{dx} + k \frac{d}{dx} \left(A_c \frac{dT}{dx} \right) dx \quad (4)$$

Sub (2), (3) and (4) into (1)

$$k A_c \frac{dT}{dx} + h dA_s (T(x) - T_v) = k A_c \frac{dT}{dx} + k \frac{d}{dx} \left(A_c \frac{dT}{dx} \right) dx$$

$$k \frac{d}{dx} \left(A_c \frac{dT}{dx} \right) - h \frac{dA_s}{dx} (T(x) - T_v) = 0$$

$$\frac{d}{dx} \left(A_c \frac{dT}{dx} \right) + \frac{h}{k} \frac{dA_s}{dx} (T(x) - T_v) = 0$$

$$A_c \frac{d^2T}{dx^2} + \left(\frac{dA_c}{dx} \right) \frac{dT}{dx} - \left(\frac{h}{k} \frac{dA_s}{dx} \right) (T(x) - T_v) = 0$$

$$\frac{d^2T}{dx^2} + \left(\frac{1}{A_c} \frac{dA_c}{dx} \right) \frac{dT}{dx} - \left(\frac{1}{A_c} \frac{h}{k} \frac{dA_s}{dx} \right) (T(x) - T_v) = 0$$

Face Area is $A_c = w t$ So, $\frac{dA_c}{dx} = 0$

Surface Area is $A_s = P x$ So, $\frac{dA_s}{dx} = P$

$$\frac{d^2T}{dx^2} - \frac{P h}{A_c k} (T(x) - T_v) = 0 \quad (5)$$

To simplify the form of this equation, transform the dependent variable by defining an excess temperature

$$\theta(x) = T(x) - T_v \quad (6)$$

$$\frac{d^2\theta}{dx^2} - m^2 \theta = 0 \quad (7)$$

$$m^2 = \frac{P}{A_c} \frac{h}{k} \quad (8)$$

Equation (7) is a linear, homogeneous, second – order differential equation with constant coefficients. Its general solution is of the form:

$$\theta(x) = C_1 e^{mx} + C_2 e^{-mx} \quad (9)$$

To evaluate the constants C_1 and C_2 , it is necessary to specify two boundary conditions

At $x=0$

$$\theta(0) = T_b - T_v \quad (10)$$

$$\theta(0) = C_1 e^{m(0)} + C_2 e^{-m(0)}$$

$$\theta(0) = C_1 + C_2$$

$$C_2 = \theta(0) - C_1 \quad (11)$$

At $x=L$

At the tip of the fin, the rate of heat reached from the vapour by convection is equal to the rate of heat transferred by conduction:

$$h A_c (T(L) - T_v) = k A_c \frac{dT}{dx}$$

$$\theta(L) = \frac{k A_c}{h} \frac{d\theta}{dx} \quad (12)$$

$$\theta(L) = C_1 e^{m(L)} + C_2 e^{-m(L)} \quad (13)$$

Sub eq. (11) in eq. (13)

$$\theta(L) = C_1 e^{m(L)} + (\theta(0) - C_1) e^{-m(L)}$$

$$C_1 = \frac{\theta(L) - \theta(0) e^{-mL}}{e^{mL} - e^{-mL}} \quad (14)$$

Sub eq. (14) into (11)

$$C_2 = \frac{\theta(0) (e^{mL} - e^{-mL}) - \theta(L) - \theta(0) e^{-mL}}{e^{mL} - e^{-mL}} \quad (15)$$

Sub. eq. (12), (14) and (15) into eq. (9)

$$\theta(x) = \left(\frac{\theta(L) - \theta(0) e^{-mL}}{e^{mL} - e^{-mL}} \right) e^{mx} + \left(\frac{\theta(0) (e^{mL} - e^{-mL}) - \theta(L) - \theta(0) e^{-mL}}{e^{mL} - e^{-mL}} \right) e^{-mx}$$

$$\theta(x) = \theta(0) \left(\frac{(e^{m(L-x)} + e^{-mL-x}) + \left(\frac{h}{mk}\right)(e^{m(L-x)} - e^{-mL-x})}{(e^{mL} + e^{-mL}) + \left(\frac{h}{mk}\right)(e^{mL} - e^{-mL})} \right)$$

For Hyperbolic Functions

$$\sinh x = \frac{1}{2}(e^x - e^{-x})$$

$$\cosh x = \frac{1}{2}(e^x + e^{-x})$$

$$\theta(x) = \theta(0) \frac{\cosh m(L-x) + \left(\frac{h}{mk}\right) \sinh m(L-x)}{\cosh mL + \left(\frac{h}{mk}\right) \sinh mL} \quad (16)$$

$$q_{(x=0)} = k A_c \frac{d\theta}{dx}$$

$$q_{(0)} = \sqrt{hPkAc} \theta(0) \frac{\sinh mL + \left(\frac{h}{mk}\right) \cosh mL}{\cosh mL + \left(\frac{h}{mk}\right) \sinh mL} \quad (17)$$

To determine the total heat transfer Q_f

$$\frac{T(x) - T_v}{T_c - T_v} = \frac{\cosh n(L-x) + \left(\frac{h_c}{nk}\right) \sinh n(L-x)}{\cosh nL + \left(\frac{h_c}{nk}\right) \sinh nL} \quad (18)$$

$$Q_f = \sqrt{h_c P_f k A_c} (T_c - T_v) \frac{\sinh nL + \left(\frac{h_c}{nk}\right) \cosh nL}{\cosh nL + \left(\frac{h_c}{nk}\right) \sinh nL} \quad (19)$$

References

- [1] Green, P.A., Vörösmarty, C.J., Harrison, I., Farrell, T., Sáenz, L. and Fekete, B.M., 2015. Freshwater ecosystem services supporting humans: Pivoting from water crisis to water solutions. *Global Environmental Change*, 34, pp.108-118.
- [2] Gorjian, S. and Ghobadian, B., 2015. Solar desalination: A sustainable solution to water crisis in Iran. *Renewable and Sustainable Energy Reviews*, 48, pp.571-584.
- [3] Miller, S., Shemer, H. and Semiat, R., 2015. Energy and environmental issues in desalination. *Desalination*, 366, pp.2-8.
- [4] Priya, B.S.H., Kumari, R.S., Devi, V.S. and Tukaram, A.P.M., 2016. Review on Water Desalination using Renewable Solar Energy. *International Journal for Innovative Research in Science and Technology*, 2(7), pp.18-25.
- [5] Sharon, H. and Reddy, K.S., 2015. A review of solar energy driven desalination technologies. *Renewable and Sustainable Energy Reviews*, 41, pp.1080-1118.
- [6] Goldsmid, H.J., 2016. Review of Thermoelectric Materials. In *Introduction to Thermoelectricity* (pp. 153-195). Springer Berlin Heidelberg.
- [7] Enescu, D. and Virjoghe, E.O., 2014. A review on thermoelectric cooling parameters and performance. *Renewable and Sustainable Energy Reviews*, 38, pp.903-916.
- [8] He, W., Zhang, G., Zhang, X., Ji, J., Li, G. and Zhao, X., 2015. Recent development and application of thermoelectric generator and cooler. *Applied Energy*, 143, pp.1-25.
- [9] Riffat, S.B. and Ma, X., 2003. Thermoelectrics: a review of present and potential applications. *Applied thermal engineering*, 23(8), pp.913-935.
- [10] Elsheikh, M.H., Shnawah, D.A., Sabri, M.F.M., Said, S.B.M., Hassan, M.H., Bashir, M.B.A. and Mohamad, M., 2014. A review on thermoelectric renewable energy: Principle

parameters that affect their performance. *Renewable and Sustainable Energy Reviews*, 30, pp.337-355.

[11] Rowe, D.M. ed., 2005. *Thermoelectrics handbook: macro to nano*. CRC press.

[12] Goldsmid, H., 2013. *Thermoelectric refrigeration*. Springer.

[13] Gupta, B.A., Chand, S., Patel, N.K. and Soni, A., 2016. A Review on Thermoelectric Cooler. *International Journal for Innovative Research in Science and Technology*, 2(11), pp.674-679.

[14] Yilmazoglu, M.Z., 2016. Experimental and numerical investigation of a prototype thermoelectric heating and cooling unit. *Energy and Buildings*, 113, pp.51-60.

[15] Martinez, A., Astrain, D., Rodriguez, A. and Aranguren, P., 2016. Advanced computational model for Peltier effect based refrigerators. *Applied Thermal Engineering*, 95, pp.339-347.

[16] Ding, Z.M., Chen, L.G. and Sun, F.R., 2015. Optimum performance analysis of a combined thermionic-thermoelectric refrigerator with external heat transfer. *Journal of the Energy Institute*, 88(2), pp.169-180.

[17] Reddy, N.J.M., 2015. A low power, eco-friendly multipurpose thermoelectric refrigerator. *Frontiers in Energy*, pp.1-9.

[18] Hu, H.M., Ge, T.S., Dai, Y.J. and Wang, R.Z., 2016. Experimental study on water-cooled thermoelectric cooler for CPU under severe environment. *International Journal of Refrigeration*, 62, pp.30-38.

[19] Lu, Z., Zhang, H., Mao, C. and Li, C.M., 2016. Silk fabric-based wearable thermoelectric generator for energy harvesting from the human body. *Applied Energy*, 164, pp.57-63.

- [20] Jaworski, M., Bednarczyk, M. and Czachor, M., 2016. Experimental investigation of thermoelectric generator (TEG) with PCM module. *Applied Thermal Engineering*, 96, pp.527-533.
- [21] Gao, H.B., Huang, G.H., Li, H.J., Qu, Z.G. and Zhang, Y.J., 2016. Development of stove-powered thermoelectric generators: A review. *Applied Thermal Engineering*, 96, pp.297-310.
- [22] Nuwayhid, R.Y., Shihadeh, A. and Ghaddar, N., 2005. Development and testing of a domestic woodstove thermoelectric generator with natural convection cooling. *Energy Conversion and Management*, 46(9), pp.1631-1643.
- [23] Yu, S., Du, Q., Diao, H., Shu, G. and Jiao, K., 2015. Start-up modes of thermoelectric generator based on vehicle exhaust waste heat recovery. *Applied Energy*, 138, pp.276-290.
- [24] Zhao, D. and Tan, G., 2014. A review of thermoelectric cooling: materials, modeling and applications. *Applied Thermal Engineering*, 66(1), pp.15-24.
- [25] Bell, L.E., 2008. Cooling, heating, generating power, and recovering waste heat with thermoelectric systems. *Science*, 321(5895), pp.1457-1461.
- [26] Riffat, S.B. and Qiu, G., 2004. Comparative investigation of thermoelectric air-conditioners versus vapour compression and absorption air-conditioners. *Applied Thermal Engineering*, 24(14), pp.1979-1993.
- [27] Bansal, P.K. and Martin, A., 2000. Comparative study of vapour compression, thermoelectric and absorption refrigerators. *International Journal of Energy Research*, 24(2), pp.93-107.

- [28] Dai, Y.J., Wang, R.Z. and Ni, L., 2003. Experimental investigation and analysis on a thermoelectric refrigerator driven by solar cells. *Solar energy materials and solar cells*, 77(4), pp.377-391.
- [29] Field, R.L., 1980. Photovoltaic/thermoelectric refrigerator for medicine storage for developing countries. *Solar Energy*, 25(5), pp.445-447.
- [30] Min, G. and Rowe, D.M., 1999. Cooling performance of integrated thermoelectric microcooler. *Solid-State Electronics*, 43(5), pp.923-929.
- [31] Arora, C.P., 2000. *Refrigeration and air conditioning*. Tata McGraw-Hill Education.
- [32] Chein, R. and Huang, G., 2004. Thermoelectric cooler application in electronic cooling. *Applied Thermal Engineering*, 24(14), pp.2207-2217.
- [33] DiSalvo, F.J., 1999. Thermoelectric cooling and power generation. *Science*, 285(5428), pp.703-706.
- [34] Xi, H., Luo, L. and Fraisse, G., 2007. Development and applications of solar-based thermoelectric technologies. *Renewable and Sustainable Energy Reviews*, 11(5), pp.923-936.
- [35] Mei, V.C., Chen, F.C., Mathiprakasam, B. and Heenan, P., 1993. Study of solar-assisted thermoelectric technology for automobile air conditioning. *Journal of solar energy engineering*, 115(4), pp.200-205.
- [36] Zheng, X.F., Liu, C.X., Yan, Y.Y. and Wang, Q., 2014. A review of thermoelectrics research—Recent developments and potentials for sustainable and renewable energy applications. *Renewable and Sustainable Energy Reviews*, 32, pp.486-503.
- [37] Snyder, G.J. and Toberer, E.S., 2008. Complex thermoelectric materials. *Nature materials*, 7(2), pp.105-114.

- [38] Phelan, P.E., Chiriac, V.A. and Lee, T.Y., 2002. Current and future miniature refrigeration cooling technologies for high power microelectronics. *IEEE Transactions on Components and Packaging Technologies*, 25(3), pp.356-365.
- [39] Cai, Y., Liu, D., Zhao, F.Y. and Tang, J.F., 2016. Performance analysis and assessment of thermoelectric micro cooler for electronic devices. *Energy Conversion and Management*, 124, pp.203-211.
- [40] Sofrata, H., 1996. Heat rejection alternatives for thermoelectric refrigerators. *Energy Conversion and Management*, 37(3), pp.269-280.
- [41] Hara, T., Azuma, H., Shimizu, H., Obora, H. and Sato, S., 1998. Cooling performance of solar cell driven, thermoelectric cooling prototype headgear. *Applied Thermal Engineering*, 18(11), pp.1159-1169.
- [42] Benn, S.P., Poplaski, L.M., Faghri, A. and Bergman, T.L., 2016. Analysis of thermosyphon/heat pipe integration for feasibility of dry cooling for thermoelectric power generation. *Applied Thermal Engineering*, 104, pp.358-374.
- [43] Liu, D., Zhao, F.Y., Yang, H.X. and Tang, G.F., 2015. Thermoelectric mini cooler coupled with micro thermosiphon for CPU cooling system. *Energy*, 83, pp.29-36.
- [44] Kwan, T.H. and Wu, X., 2016. Power and mass optimization of the hybrid solar panel and thermoelectric generators. *Applied Energy*, 165, pp.297-307.
- [45] He, W., Zhou, J., Hou, J., Chen, C. and Ji, J., 2013. Theoretical and experimental investigation on a thermoelectric cooling and heating system driven by solar. *Applied energy*, 107, pp.89-97.
- [46] Abdul-Wahab, S.A., Elkamel, A., Al-Damkhi, A.M., Is' haq, A., Al-Rubai'ey, H.S., Al-Battashi, A.K., Al-Tamimi, A.R., Al-Mamari, K.H. and Chutani, M.U., 2009. Design

and experimental investigation of portable solar thermoelectric refrigerator. *Renewable Energy*, 34(1), pp.30-34.

[47] Dai, Y.J., Wang, R.Z. and Ni, L., 2003. Experimental investigation and analysis on a thermoelectric refrigerator driven by solar cells. *Solar energy materials and solar cells*, 77(4), pp.377-391.

[48] Chen, Y.L., Chien, Z.J., Lee, W.S., Jwo, C.S. and Cho, K.C., 2014. Experimental Investigation on Thermoelectric Chiller Driven by Solar Cell. *International Journal of Photoenergy*, 2014.

[49] Xi, H., Luo, L. and Fraisse, G., 2007. Development and applications of solar-based thermoelectric technologies. *Renewable and Sustainable Energy Reviews*, 11(5), pp.923-936.

[50] Pridasawas, W. and Lundqvist, P., 2004. An exergy analysis of a solar-driven ejector refrigeration system. *Solar energy*, 76(4), pp.369-379.

[51] Astrain, D., Vián, J.G. and Albizua, J., 2005. Computational model for refrigerators based on Peltier effect application. *Applied Thermal Engineering*, 25(17), pp.3149-3162.

[52] Demir, M.E. and Dincer, I., 2017. Performance assessment of a thermoelectric generator applied to exhaust waste heat recovery. *Applied Thermal Engineering*, 120, pp.694-707.

[53] Nuwayhid, R.Y., Rowe, D.M. and Min, G., 2003. Low cost stove-top thermoelectric generator for regions with unreliable electricity supply. *Renewable energy*, 28(2), pp.205-222.

- [54] Lertsatitthanakorn, C., 2007. Electrical performance analysis and economic evaluation of combined biomass cook stove thermoelectric (BITE) generator. *Bioresource technology*, 98(8), pp.1670-1674.
- [55] Mastbergen, D. and Willson, B., 2005. Generating light from stoves using a thermoelectric generator. In *ETHOS Int. Stove Res. Conference* (pp. 15-27).
- [56] Gude, V.G., 2016. Geothermal source potential for water desalination—Current status and future perspective. *Renewable and Sustainable Energy Reviews*, 57, pp.1038-1065.
- [57] Gude, V.G., 2015. Energy storage for desalination processes powered by renewable energy and waste heat sources. *Applied Energy*, 137, pp.877-898.
- [58] Gude, V.G., Nirmalakhandan, N. and Deng, S., 2010. Renewable and sustainable approaches for desalination. *Renewable and Sustainable Energy Reviews*, 14(9), pp.2641-2654.
- [59] Li, C., Goswami, Y. and Stefanakos, E., 2013. Solar assisted sea water desalination: A review. *Renewable and Sustainable Energy Reviews*, 19, pp.136-163.
- [60] Eltawil, M.A., Zhengming, Z. and Yuan, L., 2009. A review of renewable energy technologies integrated with desalination systems. *Renewable and Sustainable Energy Reviews*, 13(9), pp.2245-2262.
- [61] Khawaji, A.D., Kutubkhanah, I.K. and Wie, J.M., 2008. Advances in seawater desalination technologies. *Desalination*, 221(1), pp.47-69.
- [62] Gude, V.G., Nirmalakhandan, N. and Deng, S., 2010. Renewable and sustainable approaches for desalination. *Renewable and Sustainable Energy Reviews*, 14(9), pp.2641-2654.

- [63] Eltawil, M.A., Zhengming, Z. and Yuan, L., 2009. A review of renewable energy technologies integrated with desalination systems. *Renewable and Sustainable Energy Reviews*, 13(9), pp.2245-2262.
- [64] Avlonitis, S.A., Kouroumbas, K. and Vlachakis, N., 2003. Energy consumption and membrane replacement cost for seawater RO desalination plants. *Desalination*, 157(1), pp.151-158.
- [65] Al-Karaghoul, A. and Kazmerski, L.L., 2013. Energy consumption and water production cost of conventional and renewable-energy-powered desalination processes. *Renewable and Sustainable Energy Reviews*, 24, pp.343-356.
- [66] Eltawil, M.A., Zhengming, Z. and Yuan, L., 2009. A review of renewable energy technologies integrated with desalination systems. *Renewable and Sustainable Energy Reviews*, 13(9), pp.2245-2262.
- [67] Al-Karaghoul, A., Renne, D. and Kazmerski, L.L., 2010. Technical and economic assessment of photovoltaic-driven desalination systems. *Renewable Energy*, 35(2), pp.323-328.
- [68] Gabarrón, S., Gernjak, W., Valero, F., Barceló, A., Petrovic, M. and Rodríguez-Roda, I., 2016. Evaluation of emerging contaminants in a drinking water treatment plant using electrodialysis reversal technology. *Journal of hazardous materials*, 309, pp.192-201.
- [69] Goosen, M.F., Sablani, S.S., Shayya, W.H., Paton, C. and Al-Hinai, H., 2000. Thermodynamic and economic considerations in solar desalination. *Desalination*, 129(1), pp.63-89.

- [70] Sadineni, S.B., Hurt, R., Halford, C.K. and Boehm, R.F., 2008. Theory and experimental investigation of a weir-type inclined solar still. *Energy*, 33(1), pp.71-80.
- [71] Kumar, S. and Tiwari, A., 2008. An experimental study of hybrid photovoltaic thermal (PV/T) -active solar still. *International Journal of Energy Research*, 32(9), pp.847-858.
- [72] Gakkhar, N., Soni, M.S. and Jakhar, S., 2016. Second law thermodynamic study of solar assisted distillation system: A review. *Renewable and Sustainable Energy Reviews*, 56, pp.519-535.
- [73] Gordon, J.M. and Hui, T.C., 2016. Thermodynamic perspective for the specific energy consumption of seawater desalination. *Desalination*, 386, pp.13-18.
- [74] Aggarwal, S. and Tiwari, G.N., 1998. Convective mass transfer in a double-condensing chamber and a conventional solar still. *Desalination*, 115(2), pp.181-188.
- [75] Hongfei, Z., Xiaoyan, Z., Jing, Z. and Yuyuan, W., 2002. A group of improved heat and mass transfer correlations in solar stills. *Energy Conversion and Management*, 43(18), pp.2469-2478.
- [76] Tripathi, R. and Tiwari, G.N., 2005. Effect of water depth on internal heat and mass transfer for active solar distillation. *Desalination*, 173(2), pp.187-200.
- [77] Dwivedi, V.K. and Tiwari, G.N., 2009. Comparison of internal heat transfer coefficients in passive solar stills by different thermal models: an experimental validation. *Desalination*, 246(1), pp.304-318.
- [78] Rahbar, N. and Esfahani, J.A., 2012. Experimental study of a novel portable solar still by utilizing the heatpipe and thermoelectric module. *Desalination*, 284, pp.55-61.

- [79] Esfahani, J.A., Rahbar, N. and Lavvaf, M., 2011. Utilization of thermoelectric cooling in a portable active solar still—an experimental study on winter days. *Desalination*, 269(1), pp.198-205.
- [80] Haynes, W.M. ed., 2014. *CRC handbook of chemistry and physics*. CRC press.
- [81] Milani, D., Abbas, A., Vassallo, A., Chiesa, M. and Al Bakri, D., 2011. Evaluation of using thermoelectric coolers in a dehumidification system to generate freshwater from ambient air. *Chemical Engineering Science*, 66(12), pp.2491-2501.
- [82] Jradi, M., Ghaddar, N. and Ghali, K., 2012. Experimental and theoretical study of an integrated thermoelectric–photovoltaic system for air dehumidification and fresh water production. *International Journal of Energy Research*, 36(9), pp.963-974.
- [83] Atta, R.M., 2011. Solar water condensation using thermoelectric coolers. *The International Journal of Water Resources and Arid Environments*, 1(2), pp.142-145.
- [84] Yıldırım, C., Soylu, S.K., Atmaca, İ. and Solmuş, İ., 2014. Experimental investigation of a portable desalination unit configured by a thermoelectric cooler. *Energy Conversion and Management*, 85, pp.140-145.
- [85] Date, A., Gauci, L., Chan, R. and Date, A., 2015. Performance review of a novel combined thermoelectric power generation and water desalination system. *Renewable Energy*, 83, pp.256-269.
- [86] Fath, H.E., El-Samanoudy, M., Fahmy, K. and Hassabou, A., 2003. Thermal-economic analysis and comparison between pyramid-shaped and single-slope solar still configurations. *Desalination*, 159(1), pp.69-79.

- [87] Sathyamurthy, R., El-Agouz, S.A. and Dharmaraj, V., 2015. Experimental analysis of a portable solar still with evaporation and condensation chambers. *Desalination*, 367, pp.180-185.
- [88] Samee, M.A., Mirza, U.K., Majeed, T. and Ahmad, N., 2007. Design and performance of a simple single basin solar still. *Renewable and Sustainable Energy Reviews*, 11(3), pp.543-549.
- [89] Sadineni, S.B., Hurt, R., Halford, C.K. and Boehm, R.F., 2008. Theory and experimental investigation of a weir-type inclined solar still. *Energy*, 33(1), pp.71-80.
- [90] Wade, N.M., 2001. Distillation plant development and cost update. *Desalination*, 136(1), pp.3-12.
- [91] Hammond, R.P., Eissenberg, D.M., Emmermann, D.K., Jones, J.E., Sephton, H.H., Standiford, F.C., Scott, R.F., Rider, W.J. and Dean, D.W., 1994. Seawater desalination plant for southern California. *Desalination*, 99(2-3), pp.483-508.
- [92] Darwish, M.A., Al Asfour, F. and Al-Najem, N., 2003. Energy consumption in equivalent work by different desalting methods: case study for Kuwait. *Desalination*, 152(1), pp.83-92.
- [93] Maheshwari, G.P., Al-Ramadhan, M. and Al-Abdulhadi, M., 1995. Energy requirement of water production in dual-purpose plants. *Desalination*, 101(2), pp.133-140.
- [94] Hinge, S. and Salemsen, M., 1996. Seawater desalination wins in Denmark. Why? Preservation of resources and lowest cost. *International Desalination & Water Reuse*, 6(2), pp.52-54.

- [95] Duong, H.C., Cooper, P., Nelemans, B., Cath, T.Y. and Nghiem, L.D., 2016. Evaluating energy consumption of air gap membrane distillation for seawater desalination at pilot scale level. *Separation and Purification Technology*, 166, pp.55-62.
- [96] Carta, J.A., González, J., Cabrera, P. and Subiela, V.J., 2015. Preliminary experimental analysis of a small-scale prototype SWRO desalination plant, designed for continuous adjustment of its energy consumption to the widely varying power generated by a stand-alone wind turbine. *Applied Energy*, 137, pp.222-239.
- [97] Semiat, R., 2008. Energy issues in desalination processes. *Environmental science & technology*, 42(22), pp.8193-8201.
- [98] Hernández-Gaona, C.G. and Hernandez, S., 2004. Comparison of energy consumptions and total annual costs between heats integrated and thermally linked distillation sequences. *Chemical and biochemical engineering quarterly*, 18(2), pp.137-144.
- [99] Miller, S., Shemer, H. and Semiat, R., 2015. Energy and environmental issues in desalination. *Desalination*, 366, pp.2-8.
- [100] Gude, V.G., 2015. Energy storage for desalination processes powered by renewable energy and waste heat sources. *Applied Energy*, 137, pp.877-898.
- [101] Ang, W.L., Mohammad, A.W., Hilal, N. and Leo, C.P., 2015. A review on the applicability of integrated/hybrid membrane processes in water treatment and desalination plants. *Desalination*, 363, pp.2-18.
- [102] Semiat, R., 2008. Energy issues in desalination processes. *Environmental science & technology*, 42(22), pp.8193-8201.

- [103] Arunkumar, T., Jayaprakash, R., Denkenberger, D., Ahsan, A., Okundamiya, M.S., Tanaka, H. and Aybar, H.Ş., 2012. An experimental study on a hemispherical solar still. *Desalination*, 286, pp.342-348.
- [104] Al-Karaghoul, A. and Kazmerski, L.L., 2013. Energy consumption and water production cost of conventional and renewable-energy-powered desalination processes. *Renewable and Sustainable Energy Reviews*, 24, pp.343-356.
- [105] Ayhan, T. and Al-Madani, H., 2016. Combined effects of evaporation and cavitation on the performance of a renewable energy powered natural vacuum desalination unit in Bahrain. *Desalination and Water Treatment*, 57(28), pp.12929-12940.
- [106] Shavit, A. and Gutfinger, C., 2008. *Thermodynamics: from concepts to applications*. CRC Press.
- [107] Moran, M.J., Shapiro, H.N., Boettner, D.D. and Bailey, M.B., 2010. *Fundamentals of engineering thermodynamics*. John Wiley & Sons.
- [108] Chen, S.L., Gerner, F.M. and Tien, C.L., 1987. General film condensation correlations. *Experimental Heat Transfer An International Journal*, 1(2), pp.93-107.
- [109] Hidouri, K., Slama, R.B. and Gabsi, S., 2010. Hybrid solar still by heat pump compression. *Desalination*, 250(1), pp.444-449.
- [110] Bergman, T.L., Incropera, F.P., DeWitt, D.P. and Lavine, A.S., 2011. *Fundamentals of heat and mass transfer*. John Wiley & Sons.
- [111] Atreya, A., 2016. Convection heat transfer. In *SFPE Handbook of Fire Protection Engineering* (pp. 53-101). Springer New York.

- [112] Goldsmid, H.J., 2016. Theory of Thermoelectric Refrigeration and Generation. In *Introduction to Thermoelectricity* (pp. 9-24). Springer Berlin Heidelberg.
- [113] Gurevich, Y.G. and Logvinov, G.N., 2005. Physics of thermoelectric cooling. *Semiconductor science and technology*, 20(12), p.R57.
- [114] Harby, K., Gebaly, D.R., Koura, N.S. and Hassan, M.S., 2016. Performance improvement of vapor compression cooling systems using evaporative condenser: An overview. *Renewable and Sustainable Energy Reviews*, 58, pp.347-360.
- [115] Benganem, M., Al-Mashraqi, A.A. and Daffallah, K.O., 2016. Performance of solar cells using thermoelectric module in hot sites. *Renewable Energy*, 89, pp.51-59.
- [116] Zhou, Y. and Yu, J., 2012. Design optimization of thermoelectric cooling systems for applications in electronic devices. *International journal of refrigeration*, 35(4), pp.1139-1144.
- [117] Keenan, J.H. and Keenan, J.H., 1969. *Steam tables: thermodynamic properties of water, including vapour, liquid, and solid phases (English units)*.
- [118] Panchal, H.N. and Patel, S., 2016. Effect of Various Parameters on Augmentation of Distillate Output of Solar Still: A Review. *Technology and Economics of Smart Grids and Sustainable Energy*, 1(1), pp.1-8.
- [119] Panchal, H.N. and Patel, S., 2017. An extensive review on different design and climatic parameters to increase distillate output of solar still. *Renewable and Sustainable Energy Reviews*, 69, pp.750-758.
- [120] Prakash, P. and Velmurugan, V., 2015. Parameters influencing the productivity of solar stills—A review. *Renewable and Sustainable Energy Reviews*, 49, pp.585-609.

- [121] Manokar, A.M., Murugavel, K.K. and Esakkimuthu, G., 2014. Different parameters affecting the rate of evaporation and condensation on passive solar still—A review. *Renewable and Sustainable Energy Reviews*, 38, pp.309-322.
- [122] Sharshir, S.W., Yang, N., Peng, G. and Kabeel, A.E., 2016. Factors affecting solar stills productivity and improvement techniques: A detailed review. *Applied Thermal Engineering*, 100, pp.267-284.
- [123] Ahsan, A., Imteaz, M., Thomas, U.A., Azmi, M., Rahman, A. and Daud, N.N., 2014. Parameters affecting the performance of a low cost solar still. *Applied energy*, 114, pp.924-930.
- [124] Sharshir, S.W., Peng, G., Wu, L., Yang, N., Essa, F.A., Elsheikh, A.H., Mohamed, S.I. and Kabeel, A.E., 2017. Enhancing the solar still performance using nanofluids and glass cover cooling: Experimental study. *Applied Thermal Engineering*, 113, pp.684-693.
- [125] Abujazar, M.S.S., Fatihah, S., Rakmi, A.R. and Shahrom, M.Z., 2016. The effects of design parameters on productivity performance of a solar still for seawater desalination: A review. *Desalination*, 385, pp.178-193.
- [126] Edition, F., 2011. Guidelines for drinking-water quality. *WHO chronicle*, 38, pp.104-108.
- [127] Al-Shohani, W.A., 2013. Performance of photovoltaic module for different sites in Iraq. *Arabian Journal for Science and Engineering*, 38(2), pp.277-283.
- [128] the Image Permanence Institute. 2017. Dew Point Calculator [Online]. Available at: <http://www.dpcalc.org/> [Accessed: 10 August 2017].